GRID EQUIDISTRIBUTION METHOD FOR NUMERICAL SOLUTIONS TO A CLASS OF SINGULARLY PERTURBED INTEGRO-DIFFERENTIAL EQUATIONS

Wubeshet Seyoum Manebo

A Dissertation Submitted to the Department of Applied Mathematics
School of Applied Natural Science

Presented in Partial Fulfillment of the Requirement for the Degree of Doctor of Philosophy in Applied Mathematics (Numerical Analysis)

Office of Graduate Studies
Adama Science and Technology University

June, 2024
Adama, Ethiopia

GRID EQUIDISTRIBUTION METHOD FOR NUMERICAL SOLUTIONS TO A CLASS OF SINGULARLY PERTURBED INTEGRO-DIFFERENTIAL EQUATIONS

Wubeshet Seyoum Manebo

Supervisor: Prof. Gemechis File Duressa

Co-supervisor: Dr. Mesfin Mekuria Woldaregay
Dr. Tekle Gemechu Dinka

A Dissertation Submitted to the Department of Applied Mathematics
School of Applied Natural Science

Presented in Partial Fulfillment of the Requirement for the Degree of Doctor of Philosophy in Applied Mathematics (Numerical Analysis)

Office of Graduate Studies
Adama Science and Technology University

June, 2024
Adama, Ethiopia

Declaration

I hereby declare that this dissertation entitled "**Grid equidistribution method for numerical solutions to a class of singularly perturbed integro-differential equations**" is my original work. That is, it has not been submitted for the award of any academic degree, diploma, or certificate in any other university. All sources of materials used for this dissertation have been duly acknowledged through appropriate citations.

Name of Student	Signature	Date

Recommendation

We, the supervisors of this dissertation, hereby certify that we have read and revised the dissertation entitled "**Grid equidistribution method for numerical solutions to a class of singularly perturbed integro-differential equations**" prepared under our guidance by **Wubeshet Seyoum** submitted in partial fulfillment of the requirements for the degree of Doctor of Philosophy in Applied Mathematics. Therefore, we recommend the submission of the dissertation to the department for further review and defense.

______________________	____________	______________
Major Supervisor	Signature	Date
______________________	____________	______________
Co-supervisor	Signature	Date
______________________	____________	______________
Co-supervisor	Signature	Date

Approval Sheet

We hereby certify that the recommendations and suggestions made by the board of examiners are appropriately incorporated into the final version of the dissertation entitled "**Grid equidistribution method for numerical solutions to a class of singularly perturbed integro-differential equations**" by **Wubeshet Seyoum**.

Major Supervisor	Signature	Date
Co-supervisor	Signature	Date
Co-supervisor	Signature	Date

We, the undersigned, members of the Board of Examiners of the dissertation open defense by **Wubeshet Seyoum** have read and evaluated the dissertation entitled "**Grid equidistribution method for numerical solutions to a class of singularly perturbed integro-differential equations**" and examined the candidate during open defense. This is, therefore, to certify that the dissertation is accepted for partial fulfillment of the requirement of the degree of Doctor of Philosophy in Applied Mathematics.

Chairperson	Signature	Date
Internal Examiner 1	Signature	Date
Internal Examiner 2	Signature	Date
External Examiner 1	Signature	Date
External Examiner 2	Signature	Date

Finally, approval and acceptance of the dissertation is contingent upon submission of its final copy to the Office of Postgraduate Studies (OPGS) through the candidate's Department Graduate Council (DGC) and School Graduate Committee (SGC).

Department Head	Signature	Date
School Dean	Signature	Date
Office of Postgraduate Studies, Dean	Signature	Date

ACKNOWLEDGMENTS

First and foremost, I wholeheartedly express my gratitude to Almighty God for granting me unwavering strength to complete this dissertation. His abundant blessings, including patience, health, and wisdom, nourished my growth and guided me toward this achievement.

With heartfelt appreciation, I sincerely thank my esteemed supervisor, Professor Gemechis File, for introducing me to this research area and for his invaluable guidance, constructive criticism, and encouragement which shaped my academic journey.

I would like to express my utmost gratitude to my co-supervisor, Dr. Mesfin Mekuria, whose invaluable insights, knowledge, unwavering support, and expert guidance significantly facilitated the conceptualization of this work. I extend my appreciation to my co-supervisor, Dr. Tekle Gemechu, for motivating and encouraging me to pursue a path of diligent learning and proper study.

Moreover, I am profoundly grateful to Adama Science and Technology University for their financial support and to the Department of Applied Mathematics for their invaluable assistance throughout my doctoral studies. I am particularly grateful to all my distinguished lecturers for their dedication and perseverance in imparting knowledge and fostering my understanding. I extend my appreciation to Wachemo University for sponsoring this PhD fellowship.

Finally, to my beloved family, my dear mother, sisters, and brothers, my heart is filled with gratitude for your support. Your prayers were a soothing balm during challenging moments, and your encouragement was a vibrant chorus that cheered me. With a family like yours, I would not dream of wishing for anything different.

TABLE OF CONTENTS

*

LIST OF TABLES

LIST OF FIGURES

LIST OF ACRONYMS AND ABBREVIATIONS

The next list describes several acronyms and abbreviations that will be later used within the body of the document

$\bar{\Omega}$	Given domain
$\bar{\Omega}_N, \Omega_N^-, \Omega_N^+$	Set of mesh points
ℓ_ε	differential operator
ℓ_ε^N	difference operator
λ	A real parameter
$\|\|f\|\|_\infty, \|\|f\|\|_{\infty,\bar{\Omega}}$	$Sup\{\|f(x)\| : x \in \bar{\Omega}\}$
$\mathcal{L}_\varepsilon$	Combined operator (differential and integral)
$\mathcal{L}_\varepsilon^N$	Combined operator (difference and quadrature)
τ	A constant delay
ε	Singular perturbation parameter
C	Generic constant, independent of ε
$C^k(\bar{\Omega})$	Space of k-times continuously differentiable functions in $\bar{\Omega}$.
D^-, D^+, D, δ^2	Difference quotients
e^N, e_ε^N	Maximum absolute error
h, h_i	Mesh size
K	Kernel function

r^N	Rate of convergence
u, U	Solutions to the continuous and discrete problems, respectively
FDM	Finite Difference Method
FIDE	Fredholm Integro-Differential Equation
FMFDM	Fitted Mesh Finite Difference Method
FOFDM	Fitted Operator Finite Difference Method
IDE	Iintegro-Differential Equation
NSFD	Nonstandard Finite Difference
RPP	Regular Perturbation Problem
SPFIDE	Singularly Perturbed Fredholm Integro-Differential Equation
SPIDE	Singularly Perturbed Integro-Differential Equation
SPP	Singularly Perturbed Problem
SPVDIDE	Singularly Perturbed Volterra Delay-Integro-Differential Equation
SPVFIDE	Singularly Perturbed Volterra-Fredholm Integro-Differential Equation
SPVIDE	Singularly Perturbed Volterra Integro-Differential Equation
VDIDE	Volterra Delay-Integro-Differential Equation
VIDE	Volterra Integro-Differential Equation

ABSTRACT

Numerical solutions to singular perturbation problems are well known to be difficult due to the inherent presence of a small parameter ε, which drastically amplifies errors. These errors are highly dependent on the mesh distribution, which demands extremely fine discretizations in specific regions, leading to a significant computational burden. This study resolved this challenge by presenting numerical schemes for a class of singularly perturbed integro-differential equations that emancipate their solutions from the effect of ε. These schemes demonstrated remarkable accuracy, irrespective of the perturbation parameter's value. This work focused on three classes of integro-differential equations: Fredholm, Volterra, and the hybrid Volterra-Fredholm type. Each equation presents a unique challenge, as they are all not only singularly perturbed but also exhibit a variety of complexities. These complexities include discontinuities present in the source term for some equations, and the presence of a delay parameter in another. To construct the required parameter uniform numerical schemes, the finite difference method was used for the differential component and the composite trapezoidal rule for the integral portion of the equations. To mitigate the perturbation parameter's influence, the grid equidistribution method was primarily relied upon, an adaptive mesh technique that strategically positions grid nodes to achieve uniform error distribution within the domain. Additionally, for problems with discontinuities, a novel grid distribution technique was introduced that demonstrated superior performance. Rigorous convergence and stability analysis were employed to establish the theoretical foundation for the effectiveness of the proposed schemes. Compelling numerical simulations strongly endorse the accuracy and stability of the proposed schemes. A comparative analysis with existing approaches revealed their distinct advantages in terms of accuracy, as illustrated by compelling numerical examples.

keyword: *Singular perturbation, Parameter uniform convergence, Grid equidistribution, Mesh generation algorithm, Adaptive grid, Discontinuous source term, Finite difference method, Integro-differential equation.*

CHAPTER ONE

INTRODUCTION

1.1 Background of study

The inception of singular perturbations is widely acknowledged to have taken place at the Third International Congress of Mathematicians held in Heidelberg in 1904, during Ludwig Prandtl's engaging discourse titled "On fluid motion with minimal friction". Although a few preliminary mathematical papers discussing singularly perturbed boundary value problems emerged in the 1930s, their long-term influence remained limited. However, in 1946, the term singular perturbations was first introduced in Friedrichs and Wasow's publication, which stemmed from an intellectually productive seminar on nonlinear vibrations at New York University. Since the mid-1960s, this field of study has undergone remarkable growth and development (O'Malley, 2012).

The study of singular perturbation problems (SPPs) has often stemmed from their practical applications in various fields. These problems often arise in systems with multiple time scales, where one scale is much slower or faster than the others. Notable instances include the identification of the boundary layer in hydrodynamics, the advancements in computing devices, and the theories of automatic control, nonlinear oscillations, gas dynamics, quantum mechanics, and chemical kinetics. In the realm of mathematics, certain problems relating to the exploration of underground hydromechanics and the determination of hydrodynamic parameters of formations can be simplified to singularly perturbed boundary value problems (Miller et al., 1996).

1.1.1 Singularly perturbed problems

In various scientific disciplines, perturbation theory delves into how slight modifications or disruptions to a system influence its solution. These perturbation problems can be broadly categorized into two distinct classes: regular and singular. Regular perturbation problems (RPPs) involve small perturbations that do not drastically alter the behavior of the system, or the solution can be approximated easily. In contrast, SPPs involve small perturbations that can lead to significant changes in the system behavior or the solution, making them more challenging to solve and requiring advanced techniques to accurately approximate the solution.

In distinguishing between RPPs and SPPs, the critical factor lies in the behavior of the solution as ε approaches zero and at $\varepsilon = 0$. In RPPs, the solution for a small but nonzero perturbation smoothly approaches the unperturbed solution (solution when $\varepsilon = 0$) as ε tends to zero. Unlike RPPs, for SPPs, the solution for $\varepsilon = 0$ has a qualitatively different character from the solutions obtained in the limit $\varepsilon \to 0$. In simpler terms, even with a tiny perturbation (small ε), the solution behaves very differently from the solution without any perturbation ($\varepsilon = 0$). In essence, RPPs involve minor alterations that incrementally influence the result, whereas SPPs can demonstrate significant changes in behavior even with tiny variations (Hunter, 2004; Vasil'Eva et al., 1995).

Singularly perturbed differential equations are commonly distinguished by the inclusion of a small parameter ε that multiplies one or more of the highest-order terms in the differential equation. Generally, the solutions of these equations exhibit phenomena that occur on multiple scales. Within certain regions that are exceptionally narrow, known as boundary or interior layers, there is a significant discrepancy in the scale of certain derivatives compared to others. The difficulty in solving SPPs lies in their multiscale nature, the rapidly changing nature of the solution, the lack of uniform convergence, and the need for schemes specifically designed to handle boundary layers effectively. Overcoming these challenges requires a combination of analytical insights, advanced numerical techniques, and careful selection of appropriate methods for the specific problem at hand (Kopteva & O'Riordan, 2010; Shishkin & Shishkina, 2008).

In addressing SPPs, two main approaches are utilized: numerical analysis and asymptotic analysis. Asymptotic methods, although they apply only to certain subsets of problems, provide valuable insight into the qualitative behavior of the solution. Among the asymptotic methods, analytical estimates of the exact solution can be obtained through the application of matched asymptotic expansions, which serve as the primary tool for solving SPPs. By employing these asymptotic approximations, one can discern the underlying nature of the solution across the various scales. Constructing asymptotic expansions can be challenging, and even when successful, they may not simplify the problem, especially for complex problems with multiple parameters or dimensions. Numerical methods might be more practical in such cases (Roos et al., 2008).

Numerical methods, while popular, face challenges when applied to SPPs. The application of classical numerical methods to SPPs often results in errors in the solution, which are influenced by the value of the parameter ε. This highlights the need for methods that exhibit consistent and reliable performance, regardless of the specific value of the singular perturbation parameter. These methods are commonly referred to as $\varepsilon-$uniform methods, with ε representing the singular perturbation parameter. The underlying concept is that the convergence properties, accuracy, and computational cost should remain unaffected by the value chosen for ε. For SPPs, $\varepsilon-$uniformly convergent difference schemes are constructed using two main approaches: Fitted operator finite difference methods (FOFDM) and Fitted mesh finite difference methods (FMFDM). Both methods aim to tackle the challenges of solving SPPs using finite difference methods (FDMs). However, they do so in fundamentally different ways. The choice between them depends on the specific characteristics of the problem, the desired accuracy, and the computational resources available. For relatively simple SPPs, FOFDM might be more efficient. For complex geometries or multidimensional problems, FMFDM might be necessary. Additionally, hybrid approaches combining elements of both methods are also explored in advanced cases. For details concerning numerical methods for solving SPPs, refer to Kadalbajoo and Reddy (1989), Kadalbajoo and Patidar (2002) and Kadalbajoo and Gupta (2010).

1.1.2 Integro-differential equations

Integro-differential equations (IDEs) are equations that combine differential and integral operators. They are used in various scientific fields, including physics, biology, and engineering, and are essential tools in mathematical modeling. Finding a solution to these equations can be challenging as they involve a combination of differential and integral equations, which requires a function that satisfies both simultaneously. The problem can become even more complex with the inclusion of additional initial or boundary conditions. However, IDEs remain a valuable tool for modeling complex systems (Lakshmikantham, 1995; Wazwaz, 2011).

This dissertation investigates three types of IDEs: Fredholm, Volterra, and Volterra-Fredholm. The key difference lies in the limits of integration. Fredholm integro-differential equations (FIDEs) are characterized by definite integration limits, meaning both bounds are fixed values. In contrast, Volterra integro-differential equations (VIDEs) exhibit indefinite integrals. Volterra-Fredholm integro-differential equations (VFIDEs) blend both, with one fixed and one variable limit. VIDEs may be observed when converting an initial value problem to an integral equation. The VIDE appeared after its establishment by Volterra. It then appeared in many physical applications such as the glass forming process, nanohydrodynamics, heat transfer, diffusion process in general, and biological species coexisting together with increasing and decreasing rates of generating, and wind ripple in the desert. FIDE appears in various scientific and engineering fields. Its name derives from Ivar Fredholm, a Swedish mathematician who originally introduced this equation during the late 1800s. FIDEs, as a kind of IDE, appear when converting boundary value problems with given boundary conditions to integral equations and are often used to study scientific applications such as the theory of signal processing and neural networks (Jackiewicz et al., 2006, 2008).

Several analytic and numerical methods have been used to handle the IDEs. This includes the Adomian decomposition method (ADM) and its refined variant, the modified ADM. In addition, the Laplace transform method, the series solution method, and the direct computation method have all been utilized (Wazwaz, 2011). The critical theorems on the existence and uniqueness are well established and documented within the relevant scientific literature (Hamoud et al., 2020; Lakshmikantham, 1995).

Singularly perturbed integro-differential equations (SPIDEs) are hybrid equations that combine features of both differential and integral equations, with an added twist: a small parameter multiplying some of the highest-order terms. This smallness introduces unique challenges and fascinating behaviors in their solutions. SPIDEs arise in models describing diffusion-dissipation processes, epidemic dynamics, synchronous control systems, renewal processes, and filament stretching (Angell & Olmstead, 1985). As is typical with SPPs, obtaining accurate solutions for SPIDEs is difficult. Interest in accurately approximating the solutions of IDEs involving small parameters motivates research in this area. This study focuses on achieving accurate approximations for Solutions of SPIDEs that contain a diminutive parameter multiplied by the highest derivative term. Due to the inherent challenges of SPIDEs, a significant research effort has been focused on developing accurate and efficient methods for approximating their solutions.

1.1.3 Fitted operator finite difference methods

FOFDMs are numerical methods that are specifically designed to overcome the limitations of traditional methods when dealing with SPPs. This can be achieved by introducing a fitted operator, customized for the specific problem at hand. This fitted operator accurately captures the solution's behavior in both the interior and boundary layer regions of the domain. Once the fitted operator is constructed, it replaces the exact operator in a standard finite difference scheme. This modified scheme can then be used to solve the SPP numerically on a uniform mesh.

FOFDMs have been proven effective in solving various SPPs. They offer higher accuracy compared to traditional FDMs. Key advantages of FOFDMs include their ability to achieve high accuracy even for small perturbation parameter values. However, FOFDMs have some limitations. Determining the fitting operator in FOFDMs can be computationally expensive. This is due to the need to solve large systems of equations, which can be time-consuming and resource-intensive, especially for complex or non-linear problems. Additionally, FOFDMs have difficulty accurately representing boundary layers unless the mesh is adjusted to properly resolve them. Without this adaptation, the solution near the boundary may be unreliable (Miller et al., 1996;

Shishkin & Shishkina, 2008)

Overall, FOFDMs are powerful and versatile numerical methods for solving SPPs. They offer significant advantages in terms of accuracy and efficiency over traditional FDMs and can be applied to a wide range of problems.

1.1.4 Fitted mesh finite difference methods

FMFDMs constitute a robust set of numerical techniques specifically designed to solve SPPs. These methods are based on the concept of employing a mesh specifically tailored to solve the specific problem. The mesh is adjusted and refined in regions where the solution is changing rapidly, particularly in boundary and interior layers. This adaptive approach enables FMFDMs to achieve high levels of accuracy, even when dealing with extremely small singular perturbation parameters.

FMFDMs extend traditional FDMs that use a uniform mesh with consistent spacing throughout the domain. The lack of adaptivity in this conventional approach can yield inaccurate results when solving SPPs, as the solution may exhibit significant gradients in certain areas. To address this limitation, FMFDMs employ a mesh that is specifically designed to fit the solution. The mesh is condensed in regions with rapid variations in the solution. This adaptation allows FMFDMs to accurately capture sharp gradients in the solution and achieve high levels of accuracy.

FMFDMs offer several advantages. One is their ability to handle problems with small singular perturbation parameters by accurately resolving boundary layers. Additionally, these methods are relatively straightforward to implement by utilizing standard FDMs and incorporating a unique mesh generation algorithm. However, there are some drawbacks associated with FMFDMs. Implementing these methods can be more complex and intricate in comparison to standard FDMs. This increased complexity may require a greater level of expertise and effort to effectively utilize these methods. Additionally, fitted mesh FDMs might necessitate more computational resources, such as processing power and memory, than standard FDMs. Therefore, careful consideration of available resources and the complexity of the problem is essential when deciding to implement these methods (Miller et al., 2012)

Various types of FMFDMs exist, but they all share the fundamental principle of employing a mesh adapted to the solution. The specific approach of mesh adaptation may vary depending on the particular type of SPP being solved. Among fitted mesh techniques, the most fundamental type is the piecewise uniform mesh, also known as a Shishkin mesh. While various mesh adaptation methods exist, none match the simplicity of piecewise uniform meshes. Examples include Bakhvalov meshes and Vulanović meshes, which offer more complex adaptations.

1.1.5 Grid equidistribution method

Grid equidistribution refers to a mesh fitting technique used in numerical methods to distribute grid points within a computational domain based on a specific mesh density function. This is particularly relevant for solving SPPs where the solution exhibits rapid changes in certain regions, like boundary and interior layers. This dissertation relies mainly on this technique to generate adaptive meshes, thereby effectively mitigating the influence of the perturbation parameter.

The grid equidistribution method is a highly effective technique to reduce numerical errors. In this method, the grid nodes are placed in a way that uniformly distributes the error of the numerical solution (Huang & Russell, 2010; Liseikin, 2010). Various scholars have implemented this technique to address SPPs with different mesh density functions, resulting in improved numerical outcomes (Beckett & Mackenzie, 2000, 2001; Chadha & Kopteva, 2011; De Boor, 2006; Kopteva, 2001, 2007; Kopteva & Stynes, 2001; Linß, 2001; Pereyra & Sewell, 1974; Russell & Christiansen, 1978; White, 1979). This method effectively captures sharp transitions and steep gradients in the solution, reducing numerical errors. It relies on a mesh density function that determines the density of nodes in different regions, with layer regions having densely packed nodes and smoother regions having sparsely distributed nodes. Although many researchers have relied on the arc length of the solution as a mesh density function, it has been proven insufficient for solving reaction-diffusion problems. This dissertation focuses on utilizing grid equidistribution using a mesh density function described in (Kopteva et al., 2005) to achieve highly accurate numerical results.

1.2 Statement of the problem

The desired characteristic for a numerical solution of a SPP is insensitivity of its accuracy to the size of the perturbation parameter. However, existing numerical methods designed for regular problems introduce errors in the solution that exhibit dependence on the value of the perturbation parameter. These errors are influenced by the arrangement of mesh points and only diminish when the effective mesh size within the layer is significantly smaller than the perturbation parameter. Consequently, these numerical methods are inappropriate for solving SPPs.

This research addresses the issue by employing a numerical scheme that provides error estimates that are independent of the perturbation parameter for a class of SPIDEs. To accomplish this, the grid equidistribution method is implemented. Additionally, a combination of FOFDM and FMFDM is utilized.

1.3 Objectives

1.3.1 General objective

The main objective of this dissertation is to accurately solve a class of singularly perturbed integro-differential equations using fitted numerical methods, particularly the grid equidistribution method.

1.3.2 Specific objectives

The specific objectives of the study are:

- To formulate parameter uniform numerical schemes for a class of SPIDEs.
- To conduct a stability analysis of the proposed numerical schemes to guarantee reliable and robust solutions.
- To analyze the $\varepsilon-$uniform convergence of the proposed numerical schemes, ensuring that the solutions converge to the exact solution of the equations uniformly.
- To design adaptive grid generation algorithms based on appropriate mesh density functions to enhance the performance of the numerical schemes.

1.4 Significance of the study

This study holds substantial importance as it introduces new approaches to solving SPPs, which will lead to further advancements and analysis of efficient numerical methods. Specifically, the study aims to contribute to the development of parameter uniformly convergent methods for solving a particular class of SPIDEs. By addressing these unsolved problems, this research will contribute to the ongoing research in the field of singular perturbations, thereby enhancing the existing body of knowledge.

1.5 Delimitation of the study

The realm of SPIDEs is a vast and intricate landscape, encompassing a diverse array of mathematical phenomena. The following SPIDEs will be the focus of this dissertation.

(1) A linear second-order reaction-diffusion type singularly perturbed Fredholm integro-differential equation (SPFIDE) of the form:

$$-\varepsilon u''(x) + b(x)u(x) + \lambda \int_0^1 K(x,\xi)u(\xi)d\xi = f(x), \quad x \in (0,1) \tag{1.1}$$

subject to the boundary conditions

$$u(0) = A, \quad u(1) = B, \tag{1.2}$$

where $0 < \varepsilon \ll 1$ is a perturbation parameter and λ is a real parameter. It is assumed, furthermore, that $b(x)$ is a function in $C^2(\bar{\Omega} = [0,1])$ that satisfies

$$b(x) \geq \beta > 0, \quad x \in \bar{\Omega}.$$

Similarly, $f(x)$ and $K(x,\xi)$ are functions in $C^2(\bar{\Omega})$ and $C^2(\bar{\Omega} \times \bar{\Omega})$, respectively. Typically, a boundary layer appears at both ends of the interval $[0,1]$ when solving (1.1) subject to the boundary conditions (1.2). The problem in (1.1)-(1.2) is extended with a discontinuous source term. Thus,

$$-\varepsilon u''(x) + b(x)u(x) + \lambda \int_0^1 K(x,\xi)u(\xi)d\xi = F(x), \quad \text{for all } x \in \Omega^- \cup \Omega^+ \tag{1.3}$$

with

$$F(x) = \begin{cases} F_1(x), & x \in \Omega^-, \\ F_2(x), & x \in \Omega^+, \end{cases} \qquad u(0) = A \quad \text{and} \quad u(1) = B, \tag{1.4}$$

where $\Omega^- = (0,d)$, $\Omega^+ = (d,1)$, and $\bar{\Omega} = [0,1]$. d is a point within the domain $\Omega = (0,1)$ where the discontinuity in the source term $F(x)$ emerges. A boundary layer appears at both ends of $\bar{\Omega}$ and an interior layer at the point $x = d$ when solving (1.3) subject to the boundary conditions given by (1.4).

(2) A second-order linear convection-diffusion type SPFIDE of the form:

$$\varepsilon^2 u''(x) + \varepsilon a(x)u'(x) - b(x)u(x) + \lambda \int_0^1 K(x,\xi)u(\xi)d\xi = F(x), x \in \Omega^- \cup \Omega^+ \tag{1.5}$$

and conditions (1.4). The function $b(x)$ belongs to the class $C^2(\bar{\Omega})$ and satisfies the condition $b(x) \geq \beta > 0$. Similarly, the function $K(x,\xi)$ is also in $C^2(\bar{\Omega} \times \bar{\Omega})$. Boundary layers appear at $x = 0$ and $x = 1$, while an interior layer arises at $x = d$.

(3) A linear second-order singularly perturbed Volterra-Fredholm integro-differential equation (SPVFIDE) of the reaction-diffusion type:

$$-\varepsilon u''(x) + b(x)u(x) + \lambda_1 \int_0^x K_1(x,\xi)u(\xi)d\xi + \lambda_2 \int_0^1 K_2(x,\xi)u(\xi)d\xi = f(x), x \in \Omega \tag{1.6}$$

and boundary condition (1.2), where $\Omega = (0,1)$, λ_1 and λ_2 are real parameters. It is assumed that the functions $b(x)$ and $f(x)$ belong to the class $C^2(\bar{\Omega})$, and the functions $K_1(x,\xi)$ and $K_2(x,\xi)$ belong to the class $C^2(\bar{\Omega} \times \bar{\Omega})$. Furthermore, $b(x)$ satisfies the condition $b(x) \geq \beta > 0$. The boundary layers appear in $x = 0$ and $x = 1$.

(4) Linear first-order singularly perturbed Volterra delay integro-differential equation (SPVDIDE) of the form:

$$\varepsilon u'(t) + a(t)u(t) + \int_{t-\tau}^{t} K(t,\xi)u(\xi)d\xi = f(t), \quad t \in \Omega = (0,T], \tag{1.7}$$

subject to

$$u(t) = \varphi(t), \quad t \in \Omega_0 = [-\tau, 0], \tag{1.8}$$

where $\bar{\Omega} = [0, T]$, $\Omega = \bigcup_{r=1}^{p} \Omega_r, \Omega_r = \{t : (r-1)\tau < t \leq r\tau\}$, for $1 \leq r \leq p$ and $a(t) \geq \alpha > 0$, $f(t)(t \in \bar{\Omega}), \varphi(t)(t \in \Omega_0)$ and $K(t,\xi)((t,\xi) \in \bar{\Omega} \times \bar{\Omega})$ are assumed to be twice continuously differentiable functions. Under these conditions, the solution of problem (1.7)-(1.8) has an initial layer at $t = 0$ for small values of ε.

1.6 Preliminaries

This section presents basic facts and definitions that are relevant to the ongoing discussion in this dissertation. Since the schemes considered rely on the finite difference method for approximating differential terms and the composite trapezoidal rule for approximating integral terms, an introduction to these concepts is provided first. Tools for measuring the accuracy of the proposed schemes and operational definitions will then be provided.

Finite difference methods: FDMs are a class of numerical techniques for solving differential equations by approximating derivatives with finite differences. They involve dividing a continuous domain into a finite number of discrete points and approximating the derivatives at those points using algebraic equations.

Unless specified otherwise, the finite difference scheme will be considered on an arbitrary nonuniform mesh on $[0, 1]$:

$$\bar{\Omega}_N = \{0 = x_0 < x_1 < \cdots < x_{N-1} < x_N = 1; h_i = x_i - x_{i-1}\},$$

where N represents the total number of intervals. To obtain the forward difference approximations for the first derivative of $\nu(x)$, $\nu(x + h_{i+1})$ is expanded in Taylor series, resulting in:

$$\nu(x + h_{i+1}) = \nu(x) + h_{i+1}\nu'(x) + \frac{h_{i+1}^2}{2}\nu''(x) + \frac{h_{i+1}^3}{6}\nu'''(x) + \cdots. \tag{1.9}$$

From which it follows that

$$\nu'(x) = \frac{\nu(x+h_{i+1}) - \nu(x)}{h_{i+1}} + O(h_{i+1}).$$

Similarly, expansion of $\nu(x-h_i)$ in Taylor's series gives backward difference approximations for the first derivative of ν.

$$\nu(x-h_i) = \nu(x) - h_i\nu'(x) + \frac{h_i^2}{2}\nu''(x) - \frac{h_i^3}{6}\nu'''(x) + \dots \tag{1.10}$$

Solving for $\nu'(x)$:

$$\nu'(x) = \frac{\nu(x) - \nu(x-h_i)}{h_i} + O(h_i).$$

For the second derivative $\nu''(x)$, a central difference approximation can be obtained by multiplying (1.9) by h_i and (1.10) by h_{i+1} and adding the two. This yields

$$\nu''(x) \approx \frac{2}{h_i + h_{i+1}} \left(\frac{\nu(x+h_{i+1}) - \nu(x)}{h_{i+1}} - \frac{\nu(x) - \nu(x-h_i)}{h_i} \right).$$

Assuming a discrete setting, for a given mesh function ν_i on the mesh $\bar{\Omega}_N$, the discrete difference operators are defined as

$$D^+\nu_i = \frac{\nu_{i+1} - \nu_i}{h_{i+1}}, \quad D^-\nu_i = \frac{\nu_i - \nu_{i-1}}{h_i}, \quad D\nu_i = \frac{\nu_{i+1} - \nu_i}{\hbar_i}$$

and

$$\delta^2\nu_i = \frac{2}{h_i + h_{i+1}} \left(\frac{\nu_{i+1} - \nu_i}{h_{i+1}} - \frac{\nu_i - \nu_{i-1}}{h_i} \right) = DD^-\nu_i,$$

where $\hbar_i = (h_i + h_{i+1})/2$.

Composite trapezoidal rule: The composite trapezoidal rule is a numerical integration method used to approximate the definite integral of a function $\nu(x)$ over an interval $[a,b]$. It works by dividing the interval of integration into smaller subintervals and approximating the integral over each subinterval using the trapezoidal rule. The formula for the composite trapezoidal rule with N subintervals is:

$$\int_a^b \nu(x)dx \approx \sum_{j=1}^{N} \frac{h_j}{2} (\nu_{j-1} + \nu_j).$$

The accuracy of the proposed schemes is measured in terms of the pointwise maximum errors and the order of convergence of the scheme. The maximum absolute error e_ε^N and the $\varepsilon-$uniform maximum point-wise error e^N are defined as follows:

$$e_\varepsilon^N = \|U_\varepsilon - u_\varepsilon\|_{\infty,\bar{\Omega}} \quad \text{and} \quad e^N = \max_{\varepsilon} e_\varepsilon^N,$$

where U_ε is the numerical approximation to u_ε. The experimental rate of uniform convergence r^N is computed as

$$r^N = \log_2(e^N/e^{2N}).$$

As the analytical solution is not readily accessible, the double mesh principle is employed to measure the maximum absolute error.

Double mesh principle: The double mesh principle is used to measure pointwise error in situations where finding the exact solution is difficult or impossible. This technique is particularly useful for problems with singularly perturbed differential equations, where the solution exhibits rapid changes in specific regions of the domain. the double mesh differences are defined as

$$e_\varepsilon^N = \max_{0\le i\le N} \left| U_i^N - U_i^{2N} \right|,$$

where U^{2N} is the numerical approximation of the exact solution u_ε on the finer mesh

$$\Omega_{2N} = \left\{ x_{\frac{i}{2}} : i = 0,1,2,\ldots,2N \right\} \text{ with } x_{i+\frac{1}{2}} = \frac{x_i + x_{i+1}}{2} : i = 0,1,2,\ldots,N-1.$$

Definition 1.1. ***Mesh density function***

A mesh density function $\rho(x)$ is an arbitrary nonnegative function defined on $\bar{\Omega}$.

Definition 1.2. ***Equidistribution principle***

A mesh $\{x_i\}_{i=0}^N$ is said to equidistribute $\rho(\cdot)$ if

$$\int_{x_{i-1}}^{x_i} \rho(\xi) d\xi = \frac{1}{N} \int_0^l \rho(\xi) d\xi \qquad i = 1,2,\ldots N.$$

If N is given, the efficiency of an equidistributing mesh depends on the choice of $\rho(\cdot)$.

Definition 1.3. $\varepsilon-$***uniform numerical method*** *(Miller et al., 2012)*

Consider a family of mathematical problems parameterized by a singular perturbation parameter ε, $0 < \varepsilon \leq 1$. Assume that each problem in the family has a unique solution denoted by u_ε and that each u_ε is approximated by a sequence of numerical solutions $\left\{\left(U_\varepsilon, \bar{\Omega}^N\right)\right\}_{N=1}^{\infty}$, where U_ε is defined on the mesh $\bar{\Omega}^N$ and N is a discretization parameter. Then, the numerical solutions U_ε are said to converge $\varepsilon-$uniformly to the exact solution u_ε, if there exist a positive integer N_0, and positive numbers C and p, where N_0, C and p are all independent of N and ε, such that, for all $N \geq N_0$,

$$\sup_{0<\varepsilon\leq 1} ||U_\varepsilon - u_\varepsilon||_{\bar{\Omega}^N} \leq CN^{-p}$$

Here p is called the $\varepsilon-$uniform rate of convergence and C is called the $\varepsilon-$uniform error constant.

1.7 Organization of the study

The dissertation is structured to provide a clear roadmap, with each chapter building upon the previous one. Chapter 1 is the introductory chapter, which contains a background, statement of the problem, objectives, significance of the study, delimitation of the study, and preliminaries. Chapter 2 provides a comprehensive overview of relevant and previous literature related to the topic. The methodologies employed in conducting this research are detailed in Chapter 3. Chapters 4-8 form the main work of the dissertation, encompassing two distinct parts. In the first part (Chapters 4-7), the FDM combined with the composite trapezoidal rule on an equidistributed mesh is applied to effectively address SPFIDEs and SPVFIDE. The main ingredients of these chapters are the behavior of solutions, convergence, and stability analysis. The second part (Chapter 8) incorporates the integration of nonstandard finite difference with uniform and Shishkin-type mesh to solve a SPVDIDE. Ultimately, the dissertation culminates with a conclusive summary, along with recommendations.

CHAPTER TWO

LITERATURE REVIEW

The dissertation investigates three classes of IDEs: Fredholm, Volterra, and Volterra-Fredholm. A separate literature review for each class will be presented, with a particular focus on SPIDEs. These equations are characterized by a small highest derivative scaling parameter causing sudden changes and steep gradients in their solutions. Traditional numerical methods struggle to handle these situations, necessitating the development of new analytical and numerical techniques to accurately estimate the solutions.

2.1 Singularly perturbed Fredholm integro-differential equations

This section delves into an in-depth exploration of the existing literature on the three SPFIDEs, subject to the boundary conditions $u(0) = A$ and $u(1) = B$. Currently, there are three fitting schemes for SPFIDEs of the form (1.1) discussed in the literature. The first approach, developed by Amiraliyev et al. (2021), employed an exponentially fitted method on a uniform mesh. This scheme demonstrates first-order convergence. Durmaz and Amiraliyev (2021) proposed a second scheme using an exponentially fitted approach on a Shishkin mesh, which achieves a second-order convergence rate. Badeye et al. (2023) improved on this scheme by combining an exact finite difference technique with a composite Simpsons 1/3 rule, resulting in a more accurate scheme that almost achieves second-order convergence. However, both the first and second schemes have limitations in terms of accuracy. Furthermore, the latter scheme does not adequately resolve the layer problem. Therefore, there is a need for more accurate and layer-resolving approaches to address these limitations.

For second-order SPFIDEs of the form

$$-\varepsilon u'' + b(x)u + \lambda \int_0^1 K(x,\xi)u(\xi)d\xi = \begin{cases} F_1(x), & x \in \Omega^-, \\ F_2(x), & x \in \Omega^+, \end{cases}$$

a fitted scheme has been developed by (Rathore et al., 2023). This scheme, based on a first-order exponentially-fitted numerical scheme on a Shishkin mesh, stands as the sole approach documented in the literature for this specific problem. However, its reliance on a first-order scheme restricts its accuracy potential. Therefore, the development of alternative methods with enhanced accuracy becomes crucial for achieving more reliable and precise solutions to such problems.

The currently available literature lacks a suitable numerical scheme for solving the convection-diffusion type SPFIDE of the form

$$\varepsilon^2 u''(x) + \varepsilon a(x)u'(x) - b(x)u(x) + \lambda \int_0^1 K(x,\xi)u(\xi)d\xi = \begin{cases} F_1(x), & x \in \Omega^-, \\ F_2(x), & x \in \Omega^+. \end{cases}$$

This absence underscores the critical need for a parameter-uniform scheme to effectively address this challenging problem. This dissertation aims to bridge this gap by developing a novel numerical approach tailored to the specific characteristics of this problem.

To address the computational challenges posed by the aforementioned problems, this dissertation utilizes the grid equidistribution technique introduced by (Kopteva et al., 2005), which enables the generation of highly accurate numerical solutions. The approach involves combining the central finite difference and composite trapezoidal rule.

2.2 Singularly perturbed Volterra-Fredholm integro-differential equations

Previous works have aimed to develop numerical schemes for solving SPVFIDEs. In one study by Cakir and Güneş (2022), a numerical scheme for first-order linear SPVFIDEs was proposed using implicit difference rules and composite numerical quadrature rules on a Shishkin mesh. They demonstrated nearly first-order uniform convergence for this scheme. A later study by Durmaz et al. (2023) introduced a more advanced scheme that achieved almost second-order uniform convergence. This scheme used a fitted operator finite difference approach on a piecewise uniform mesh.

For second-order SPVFIDEs of the reaction-diffusion type (1.6), there are currently two existing schemes in the literature. The first scheme, described in (Cakir & Gunes, 2022)), is a first-order numerical scheme applied to a Boglaev-Bakhvalov-type mesh. This approach utilizes interpolating quadrature rules and linear basis functions. A recent modification of this scheme, presented in (Durmaz, 2023), uses a FDM on a Shishkin mesh. However, despite significant progress in numerical methods for SPVFIDEs, challenges still remain in developing more accurate, parameter-uniformly convergent, and higher-order schemes. The proposed approach utilizes the FDM and composite trapezoidal rule on an equidistributed grid, resulting in a uniformly convergent scheme that provides accurate and reliable numerical solutions.

2.3 Singularly perturbed Volterra delay-integro-differential equations

Volterra delay-integro-differential equations (VDIDEs) are used to model various scientific phenomena in fields such as ecology, medicine, and biology (Bocharov & Rihan, 2000; Gaetano & Arino, 2000; Marino et al., 2007; Rihan, 2021). These equations have also been applied to different mathematical problems (Brunner & Zhang, 1999; Burton, 2005). Due to their significance in modeling engineering and science problems, researchers have focused on developing theory and numerical analysis for VDIDEs involving small parameters, known as SPPs.

To gain an understanding of previous work on singularly perturbed Volterra integro-differential equations (SPVIDEs), Kauthen (1997) provides a comprehensive survey. In recent decades, various effective numerical methods have been developed to solve this class of equations: Exponential type schemes, collocation methods, fitted difference schemes, implicit Runge-Kutta methods, the coupled method, and non-standard FDMs have all been successful approaches (Amiraliyev et al., 2018; Amiraliyev & Şevgin, 2006;

Horvat & Rogina, 2002; Mbroh et al., 2020; Parand & Rad, 2011; Ramos, 2007, 2008; Salama & Bakr, 2007; Salama & Evans, 2001; Şevgin, 2014; Tao & Zhang, 2019; Ömer Yapman & Amiraliyev, 2019).

While there have been several studies on solving SPVIDEs without delay argument, limited efforts have been made in solving SPVDIDEs. Wu and Gan (2009) investigated the error behavior of linear multistep methods for SPVDIDEs. Amiraliyev et al. (2019) explored a fitted scheme using exponential basis functions and interpolating quadrature rules for a VDIDE with an initial layer. Amiraliyev and Yapman (2019) developed a first-order accurate scheme based on the method of integral identities with the use of interpolating quadrature rules with a remainder term in integral form in combination with fitted mesh for SPVDIDEs. They also studied convergence analysis of the homogeneous second-order difference method for a SPVDIDE using exponentially fitted schemes on Shishkin-type meshes (Yapman & Amiraliyev, 2021).

In this dissertation, a nonstandard finite difference (NSFD) scheme combined with integral identities is proposed for the first-order linear SPVDIDE in (1.7). The scheme is initially implemented on a uniform mesh. Then, the results are extended to Shishkin-type meshes. The NSFD method aims to enhance general finite-difference schemes by incorporating exact forms, resulting in improved efficiency and accuracy (Manning & Margrave, 2006; Mickens, 2002).

This review aimed to identify critical gaps in the research on a class of SPIDEs. Two key shortcomings were revealed by an analysis of the existing research. Firstly, a lack of $\varepsilon-$uniform convergence schemes was evident for a subset of these problems. Secondly, even when such schemes exist, their accuracy often proves inadequate. Consequently, further research is imperative. This research directly addresses these shortcomings by developing high-accuracy numerical schemes for problems with low-accuracy schemes and, of even greater significance, establishing $\varepsilon-$uniform convergence schemes where none currently exist.

CHAPTER THREE

METHODOLOGY

This chapter details the systematic implementation steps of the study. It will include study design and mathematical procedure.

3.1 Study design

The study began by meticulously reviewing relevant, current sources and supplementary documents on the problem at hand. After a thorough analysis, a numerical scheme was proposed. The next step involved applying these proposed computational schemes to the problem to assess their effectiveness in finding a solution. Subsequently, efforts were directed towards establishing the stability and convergence of the developed numerical schemes. Finally, the newly developed approach was rigorously tested through comprehensive numerical experiments.

3.2 Study procedures

The study procedure is the blueprint that the researcher will follow to conduct the study. The following mathematical procedures were employed in this study to achieve the stated objectives.

1) **Describing the problems:** The problem to be investigated was described unambiguously along with the necessary initial and boundary conditions, ensuring smooth progression through all consequential research steps. The conditions imposed on the problem's data, necessary for ensuring solution smoothness and designing and justifying $\varepsilon-$uniformly convergent schemes, were also described.

2) **Analyzing the properties of continuous problem:** The difference schemes are constructed and investigated based on estimates for the solution of the problem and its derivatives. Estimates of the solutions and derivatives depend on the value of the parameter ε, and the behavior of the derivatives in a neighborhood of the layer. Using these estimates, finite difference schemes are constructed that converge $\varepsilon-$uniformly.

3) **Formulating numerical schemes:** The numerical schemes were formulated for the problem using FDM and composite trapezoidal rule. These schemes were developed to maintain $\varepsilon-$uniform convergence and were constructed using FOFDM and FMFDM difference schemes.

4) **Establishing the stability and ε-uniform convergence:** The $\varepsilon-$uniform stability of the finite difference operator is established using a maximum principle. The convergence of discrete schemes is considered in norms corresponding to the applied numerical method.

5) **Developing an algorithm and writing code:** The development of efficient computational algorithms often requires an understanding of the basic properties of the solutions to the equations to be solved numerically. This procedure involves two steps:

   - Expressing the numerical problem to be solved and the methods to be used in a complete algorithm.
   - Translating the algorithm into a computer code using a specific programming language or implementing the numerical schemes in a computer program.

   The numerical experiments in this study are conducted on Matlab.

6) **Validating the schemes with numerical examples:** Numerical examples are given to show that the numerical results found and conclusions reached are consistent with the theoretical analysis. To demonstrate the performance and efficiency of the techniques developed, comparisons are made with earlier research findings

which have been duly validated, documented, and communicated through appropriate media. The accuracy of the schemes is measured in terms of the pointwise maximum errors.

7) **Presenting the results:** The results of numerical tests on stability, convergence, and accuracy properties are presented using tables and graphs.

CHAPTER FOUR

SINGULARLY PERTURBED REACTION DIFFUSION TYPE FREDHOLM INTEGRO-DIFFERENTIAL EQUATION

This chapter presents a numerical solution for a second-order FIDE with two boundary layers using a central finite difference approximation combined with a trapezoidal rule on an adaptive grid generated using the equidistribution principle. The grid equidistribution method creates meshes that adapt to physical quantities, allowing discrete solutions to represent those quantities as accurately as possible. This approach is particularly fruitful for solving SPPs, where classical numerical techniques often fail due to sharp boundary layers. The proposed scheme achieves second-order uniform convergence. In two numerical experiments, the applicability and efficiency of the scheme are compared to known schemes in the literature.

4.1 Description of the problem

The following second-order SPFIDE is considered:

$$\begin{cases} \mathcal{L}_\varepsilon u(x) := \ell_\varepsilon u(x) + \lambda \int\limits_0^1 K(x,\xi)u(\xi)d\xi = f(x), \quad x \in \Omega = (0,1), \\ u(0) = A, \quad u(1) = B, \end{cases} \tag{4.1}$$

where $\ell_\varepsilon u(x) = -\varepsilon u''(x) + b(x)u(x)$, $0 < \varepsilon \ll 1$ is the perturbation parameter and λ is a real parameter. A and B are given constants. Moreover, $b(x)$, $f(x) \in C^4(\bar{\Omega} = [0,1])$ and $K(x,\xi) \in C^2(\bar{\Omega} \times \bar{\Omega})$. It is assumed, furthermore, that the coefficient function satisfies the condition

$$b(x) \geq \beta > 0, \quad \text{for all } x \in \bar{\Omega}.$$

A singular perturbation phenomenon occurs in (4.1). This arises when the solution's properties for $\varepsilon > 0$ differ significantly from those for $\varepsilon = 0$. Substituting $\varepsilon = 0$ into (4.1) yields the reduced equation

$$b(x)u(x) + \lambda \int_0^1 K(x,\xi)u(\xi)d\xi = f(x)$$

which is a Fredholm integral equation of the second kind. Particular interest lies in problems where such a discrepancy manifests in the behavior of $u(x)$ near $x = 0$ and $x = 1$. This suggests the presence of a boundary layer close to these boundaries, where the solution exhibits a rapid change. This is supported by the analysis of prior estimates on the solution and its derivatives presented in the subsequent section. While a priori estimates don't directly prove the existence of a boundary layer, they provide strong evidence for its presence by highlighting the regions where the solution deviates significantly from its behavior in the bulk of the domain. These insights can then be used alongside other analytical techniques or numerical simulations to conclusively demonstrate the existence and properties of the boundary layer.

4.2 A priori bounds on the solution and its derivatives

An estimate of the analytical solution to problem (4.1) and its derivatives is presented here to facilitate the analysis of error estimates in later sections. The proofs of these bounds are based on the work of Miller et al. (1996) and Amiraliyev et al. (2021). The maximum principle can be used to estimate the solution and its derivative. The differential operator ℓ_ε in (4.1) for all $\Psi \in C^2(\bar{\Omega})$ satisfies the following maximum principle.

Lemma 4.2.1. ***(Maximum principle)*** *(Miller et al., 2012) Assume that $\Psi(0) \geq 0$ and $\Psi(1) \geq 0$. Then, $\ell_\varepsilon \Psi(x) \geq 0$ for all $x \in \Omega$ implies that $\Psi(x) \geq 0$ for all $x \in \bar{\Omega}$.*

Proof. Let s be such that $\Psi(s) = \min_{x \in \bar{\Omega}} \Psi(x)$ and suppose that $\Psi(s) < 0$. It is clear that $s \notin \{0, 1\}$. Therefore $\Psi'(s) = 0$, $\Psi''(s) \geq 0$ and $\ell_\varepsilon \Psi(s) = -\varepsilon \Psi''(s) + b(s)\Psi(s) < 0$ which is a contradiction with the given conditions. It follows that $\Psi(s) \geq 0$ and thus that $\Psi(x) \geq 0$ for all $x \in \bar{\Omega}$. $\square$

Lemma 4.2.2. *(Amiraliyev et al., 2021) Let u be the solution of (4.1). Assume that $b, f \in C^4(\bar{\Omega})$, $\frac{\partial^n K}{\partial x^n}, \frac{\partial^n K}{\partial \xi^n} \in C(\bar{\Omega} \times \bar{\Omega})$, n=0,1,2 and*

$$|\lambda| < \frac{\beta}{\max\limits_{0 \leq x \leq 1} \int_0^1 |K(x,\xi)| d\xi}. \tag{4.2}$$

Then $u(x)$ satisfies

$$\|u\|_\infty \leq C, \tag{4.3}$$

$$\left|u^{(k)}(x)\right| \leq C\left\{1 + \varepsilon^{-\frac{k}{2}} e(x,\beta)\right\}, \quad 1 \leq k \leq 4, \tag{4.4}$$

where $e(x,\beta) = e^{-\sqrt{\frac{\beta}{\varepsilon}}x} + e^{-\sqrt{\frac{\beta}{\varepsilon}}(1-x)}$.

Proof. To proof (4.3) consider the functions

$$\Psi^{\pm}(x) = \frac{1}{\beta}\|F\| + max\{|A|, |B|\} \pm u(x), \tag{4.5}$$

where

$$F(x) = f(x) - \lambda \int_0^1 K(x,\xi) u(\xi) d\xi. \tag{4.6}$$

It is easy to see that $\Psi^{\pm}(0) \geq 0$, $\Psi^{\pm}(1) \geq 0$ and that $\ell_\varepsilon \Psi^{\pm}(x) \geq 0$. Applying the maximum principle then gives $\Psi^{\pm}(x) \geq 0$, and so

$$\|u\|_\infty \leq \frac{1}{\beta}\|F\| + max\{|A|, |B|\}. \tag{4.7}$$

Using (4.6) in the expression (4.7) gives

$$\|u\|_\infty \leq |A| + |B| + \beta^{-1}\left(\|f\|_\infty + |\lambda| \max_{0 \leq x \leq 1} \int_0^1 |K(x,\xi)||u(\xi)| d\xi\right). \tag{4.8}$$

When combined with (4.2), this leads to (4.3).

It remains to establish (4.4). Note, from (4.1), that

$$|u''(x)| = \frac{1}{\varepsilon}\left|b(x)u(x) + \lambda \int\limits_0^1 K(x,\xi) u(\xi) d\xi - f(x)\right|,$$

and so, using (4.3) above,

$$|u''(x)| \leq \frac{C}{\varepsilon}. \tag{4.9}$$

Next, $u'(0)$ and $u'(1)$ are estimated as follows. In this case, the following relation is used, which is valid for any function $\varrho \in C^2(\Omega)$:

$$\varrho'(x) = \frac{\varrho(\alpha_1) - \varrho(\alpha_0)}{\alpha_1 - \alpha_0} - \int_{\alpha_0}^{\alpha_1} \kappa(x,\xi)\varrho''(\xi)d\xi, \tag{4.10}$$

where

$$\kappa(x,\xi) = T_0(\xi - x) - \frac{\xi - \alpha_0}{\alpha_1 - \alpha_0}$$

with

$$T_0(s) = \begin{cases} 1, & s \geq 0, \\ 0, & s < 0. \end{cases}$$

Taking $\varrho(x) = u(x)$, $x = 0$, $\alpha_0 = 0$, and $\alpha_1 = \sqrt{\varepsilon}$ in (4.10) and using (4.9) gives

$$|u'(0)| \leq \frac{C}{\sqrt{\varepsilon}}. \tag{4.11}$$

Similarly, taking $\varrho(x) = u(x)$, $x = 1$, $\alpha_0 = 1 - \sqrt{\varepsilon}$, and $\alpha_1 = 1$ in (4.10) and using (4.9) leads to

$$|u'(1)| \leq \frac{C}{\sqrt{\varepsilon}}. \tag{4.12}$$

Differentiating (4.1) gives

$$\begin{aligned} -\varepsilon\tilde{u}'' + b(x)\tilde{u} = \Phi(x), \quad x \in \Omega, \\ \tilde{u}(0) = O(\varepsilon^{-\frac{1}{2}}), \quad \tilde{u}(1) = O(\varepsilon^{-\frac{1}{2}}), \end{aligned} \tag{4.13}$$

with

$$\begin{aligned} \tilde{u}(x) =& u'(x), \\ \Phi(x) =& f'(x) - b'(x)u(x) - \lambda \int_0^1 \frac{\partial}{\partial x} K(x,\xi)u(\xi)d\xi, \end{aligned}$$

and, using (4.3), it follows that, $|\Phi(x)| \leq C$. In order to find the bounds, the solution

$\tilde{u}$ is decomposed as follows:

$$\tilde{u} = v + w,$$

where v, w are defined as the solutions of the problems

$$\ell_\varepsilon v = -\varepsilon v'' + \beta v = \Phi(x), \quad v(0) = v(1) = 0, \tag{4.14}$$

$$\ell_\varepsilon w = -\varepsilon w'' + \beta w = 0, \qquad w(0) = \tilde{u}(0), \quad w(1) = \tilde{u}(1). \tag{4.15}$$

Then the maximum principle for ℓ_ε on $\bar{\Omega}$ gives, for all $x \in \bar{\Omega}$,

$$|v(x)| \leq C \tag{4.16}$$

and for problem (4.15) it follows that $|w(x)| \leq \bar{w}$, where the function $w(x)$ is the solution of the following problem:

$$\ell_\varepsilon w = -\varepsilon w'' + \beta w = 0, \quad w(0) = \tilde{u}(0), \quad w(1) = \tilde{u}(1). \tag{4.17}$$

For (4.17), the solution is given by

$$w(x) = csch\left(\sqrt{\frac{\beta}{\varepsilon}}\right)\left\{w(0)sinh\left(\sqrt{\frac{\beta}{\varepsilon}}(1-x)\right) + w(1)sinh\left(\sqrt{\frac{\beta}{\varepsilon}}x\right)\right\}. \tag{4.18}$$

Using the bounds on $w(0)$ and $w(1)$ in (4.18), the function w satisfies the following bound:

$$w(x) \leq C\varepsilon^{-\frac{1}{2}}\left(e^{-\sqrt{\frac{\beta}{\varepsilon}}x} + e^{-\sqrt{\frac{\beta}{\varepsilon}}(1-x)}\right). \tag{4.19}$$

Combining (4.16) and (4.19) proves (4.4) for k=1. The bounds on the higher derivatives are obtained from the bounds on u and u' using an analogous approach. □

4.3 The numerical scheme

This section focused on the two main components of the proposed numerical scheme: the discretization scheme, which translates the continuous equations into a discrete form, and the adaptive mesh generation, which ensures the accuracy of the solution by adjusting the mesh distribution.

4.3.1 The discrete scheme

An arbitrary non-uniform mesh $\bar{\Omega}_N = \{0 = x_0 < x_1 < \cdots < x_{N-1} < x_N = 1\}$ with $h_i = x_i - x_{i-1},\ 1 \leq i \leq N$ is considered to discritize (4.1). Applying the centered finite difference scheme yields the difference approximation

$$u_i'' \approx \frac{2}{h_i + h_{i+1}} \left(\frac{u_{i+1} - u_i}{h_{i+1}} - \frac{u_i - u_{i-1}}{h_i} \right), \quad 1 \leq i \leq N-1.$$

The composite trapezoidal rule is applied for the numerical approximation of the integral, resulting in

$$\int_0^1 K(x_i, \xi) u(\xi) d\xi \approx \sum_{j=1}^{N} \frac{h_j}{2} \left(K_{i,j-1} u_{j-1} + K_{i,j} u_j \right), \quad 1 \leq i \leq N-1.$$

The resulting discrete problem becomes:

$$\begin{cases} \mathcal{L}_\varepsilon u_i := -\varepsilon \delta^2 u_i + b_i u_i + \lambda \sum_{j=1}^{N} \frac{h_j}{2} \left(K_{i,j-1} u_{j-1} + K_{i,j} u_j \right) + \mathcal{R}_i = f_i, 1 \leq i \leq N-1 \\ u_0 = A, \quad u_N = B, \end{cases} \tag{4.20}$$

where $\mathcal{R}_i$ is the truncation error given by

$$\mathcal{R}_i = -\varepsilon \left(u_i'' - \delta^2 u_i \right) + \lambda \int_0^1 K(x_i, \xi) u(\xi) d\xi - \lambda \sum_{j=1}^{N} \frac{h_j}{2} \left(K_{i,j-1} u_{j-1} + K_{i,j} u_j \right). \tag{4.21}$$

From (4.20), the following scheme is obtained for approximating (4.1):

$$\begin{cases} \mathcal{L}_\varepsilon^N U_i := -\varepsilon \delta^2 U_i + b_i U_i + \lambda \sum_{j=1}^{N} \frac{h_j}{2} \left(K_{i,j-1} U_{j-1} + K_{i,j} U_j \right) = f_i, 1 \leq i \leq N-1 \\ U_0 = A, \quad U_N = B. \end{cases} \tag{4.22}$$

4.3.2 Adaptive grid generation via equidistribution

The adaptive grids used in this study are generated using the equidistribution principle, which prioritizes equal distribution of solution errors by increasing the density of mesh points within the boundary layer, where solution errors are most likely to occur. This approach enables achievement of improved accuracy with a fixed number of mesh points. To obtain such a mesh, a positive mesh density function is equidistributed.

The mesh density function $\rho(u(\xi),\xi)$ from (Kopteva et al., 2005) is used here, given by

$$\rho(u(\xi),\xi) = 1 + \frac{|u''(\xi)|^{\frac{1}{2}} + |(bu)''(\xi)|^{\frac{1}{2}}}{2\,\|u\|_{\infty}^{\frac{1}{2}}}. \tag{4.23}$$

This function controls mesh concentration through the equidistribution principle, i.e.,

$$\int_{x_{i-1}}^{x_i} \rho(u(\xi),\xi)d\xi = \frac{1}{N}\int_0^1 \rho(u(\xi),\xi)d\xi, \quad i = 1,2,\ldots N. \tag{4.24}$$

Lemma 4.3.1. *Let $u(\xi)$ be the solution to (4.1) and $\rho(u(\xi),\xi)$ be the mesh density function in (4.23). Then,*

$$\int_0^1 \rho(u(\xi),\xi)d\xi \le C, \tag{4.25}$$

and, for $i = 1,2,\ldots,N$, h_i satisfies

$$h_i \le CN^{-1}. \tag{4.26}$$

Proof. Integrating the mesh density function $\rho(\xi,u(\xi))$ over $[0,1]$ gives

$$\begin{aligned}\int_0^1 \rho(u(\xi),\xi)d\xi =& \int_0^1 \left(1 + \frac{|u''(\xi)|^{\frac{1}{2}} + |(bu)''(\xi)|^{\frac{1}{2}}}{2\,\|u\|_{\infty}^{\frac{1}{2}}}\right) d\xi \\ \le& 1 + C\int_0^1 \left(|u''(\xi)|^{\frac{1}{2}} + |(bu)''(\xi)|^{\frac{1}{2}}\right) d\xi. \end{aligned}\tag{4.27}$$

From the bounds in Lemma 4.2.2, it follows that

$$\begin{aligned}\int_0^1 \left|u''(\xi)\right|^{\frac{1}{2}} d\xi \le& C\int_0^1 \left(1+\varepsilon^{-1}\left(e^{-\sqrt{\frac{\beta}{\varepsilon}}s} + e^{-\sqrt{\frac{\beta}{\varepsilon}}(1-\xi)}\right)\right)^{\frac{1}{2}} d\xi \\ \le& C\int_0^1 \left(1+\varepsilon^{-\frac{1}{2}}e^{-\sqrt{\frac{\beta}{\varepsilon}}\frac{s}{2}} + \varepsilon^{-\frac{1}{2}}e^{-\sqrt{\frac{\beta}{\varepsilon}}\frac{(1-\xi)}{2}}\right) d\xi = C\left(1+\frac{4}{\beta}\left(1-e^{-\sqrt{\frac{\beta}{\varepsilon}}\frac{1}{2}}\right)\right),\end{aligned}$$

which implies that $\int_0^1 |u''(\xi)|^{\frac{1}{2}} d\xi \le C$. A similar argument yields $\int_0^1 |(bu)''(\xi)|^{\frac{1}{2}} d\xi \le C$. The two inequalities, when used in (4.27), give (4.25). Furthermore, on the the grid $\{x_i\}_{i=0}^N$ satisfying (4.24), for all $1 \le i \le N$,

$$h_i = x_i - x_{i-1} \le \int_{x_{i-1}}^{x_i} \rho(u(\xi),\xi)d\xi = \frac{1}{N}\int_0^1 \rho(u(\xi),\xi)d\xi \le CN^{-1}$$

as required. □

To compute the grid $\{x_i\}_{i=0}^N$ and the numerical solution $\{U_i\}_{i=0}^N$ of (4.22), the discrete forms of (4.23) and (4.24) are utilized. These equations can be expressed in their discrete form as

$$\rho_i = 1 + \frac{\left|\delta^2 U_i^{(k)}\right|^{\frac{1}{2}} + \left|\delta^2 b_i U_i^{(k)}\right|^{\frac{1}{2}}}{2\max_i \left|U_i^{(k)}\right|^{\frac{1}{2}}}, \quad i = 1,2,\dots,N, \tag{4.28}$$

and

$$h_j \rho_j = \frac{1}{N}\sum_{i=1}^{N} h_i \rho_i, \quad 1 \le j \le N. \tag{4.29}$$

The equidistribution problem aims to find $\{x_i, U_i\}_{i=0}^N$ as a simultaneous solution of the difference scheme (4.22) and the relation (4.29), where ρ_i is given in (4.28). The algorithm below (Algorithm 1) is constructed by referencing the algorithms in (Kopteva et al., 2005; Kopteva & Stynes, 2001).

Algorithm 1 Adaptive mesh generation

Input $N \in \mathbb{Z}^+$, $0 < \varepsilon \le 1$ and a user-chosen constant $C_0 > 1$.
Output Adaptive mesh Ω_N^* and corresponding solution $\{U_i^*\}_{i=0}^N$
Step 1. Initialization
Take initial uniform mesh $\Omega_N^{(0)} = \{x_i^{(0)}\}_{i=0}^N$ with N intervals.
Step 2. Solution construction
Obtain $\{U_i^{(k)}\}_{i=0}^N$ by solving (4.22) on $\Omega_N^{(k)} = \{x_i^{(k)}\}_{i=0}^N$.
Step 3. Mesh density function
Let $h_i^{(k)} = x_i^{(k)} - x_{i-1}^{(k)}$ for $i = 1,2,\dots,N$ and compute
$\rho_i^{(k)} = 1 + \frac{|\delta^2 U_i^{(k)}|^{\frac{1}{2}} + |\delta^2 b_i U_i^{(k)}|^{\frac{1}{2}}}{2\max_i |U_i^{(k)}|^{\frac{1}{2}}}, \quad i = 1,2,\dots,N-1.$
Set $\rho_0^{(k)} := \rho_1^{(k)}$ and $\rho_N^{(k)} := \rho_{N-1}^{(k)}$. Then $\mathcal{M}_i = \frac{\rho_{i-1}+\rho_i}{2}, i = 1,2,\dots,N$.
Step 4. Terminating condition
Set $L_0^{(k)} := 0$. For $1 \le i \le N$, let $l_i^{(k)} = h_i^{(k)} \mathcal{M}_i^{(k)}$, $L_i^{(k)} = \sum_{j=1}^{i} l_j^{(k)}$ and $C_*^{(k)} = \frac{N}{L_N^{(k)}} \max_i l_i^{(k)}$.
If $C_*^{(k)} \le C_0$, then go to the sixth step, otherwise continue with next step.
Step 5. Equidistribution
Set $\omega_i := iL_N^{(k)}/N$ for $i = 0,1,\dots,N$. Interpolate to the points $(L_i^{(k)}, x_i^{(k)})$. Generate $\{x^{(k+1)}\}$ by evaluating the interpolant at $\{\omega_i\}_{i=0}^N$. Update $k = k+1$ and get back to the second step.
Step 6. Set $\Omega_N^* := \{x_i^{(k)}\}_{i=0}^N$ and $\{U^*\} := \{U_i^{(k)}\}_{i=0}^N$, then stop.

4.4 Stability and uniform convergence

This section presents a stability analysis of the proposed scheme, followed by an error analysis to demonstrate its $\varepsilon-$uniform convergence.

The difference operator in (4.22), $\ell_\varepsilon^N := -\varepsilon\delta^2 + b_i$, satisfies the following discrete maximum principle on $\bar{\Omega}_N$.

Lemma 4.4.1. *(**Discrete maximum principle**) (Miller et al., 2012) Assume that the mesh function ψ_i satisfies $\psi_0 \geq 0$ and $\psi_N \geq 0$. Then, $\ell_\varepsilon^N \psi_i \geq 0$ for all $1 \leq i \leq N-1$ implies that $\psi_i \geq 0$ for all $0 \leq i \leq N$.*

Proof. Let s be such that $\psi_s = \min\limits_{1\leq i\leq N-1} \psi_i$ and suppose that $\psi_s < 0$. It is clear that $s \notin \{0, N\}$, $\psi_{s+1} - \psi_s \geq 0$, and $\psi_s - \psi_{s-1} \leq 0$. Therefore,

$$\ell_\varepsilon^N \psi_s = \frac{-2\varepsilon}{h_s + h_{s+1}} \left(\frac{\psi_{s+1} - \psi_s}{h_{s+1}} - \frac{\psi_s - \psi_{s-1}}{h_s} \right) + b_s \psi_s < 0,$$

which is false. It follows that $\psi_s \geq 0$ and thus that $\psi_i \geq 0$ for all $0 \leq i \leq N$. $\square$

The following stability result is an immediate consequence of this discrete maximum principle.

4.4.1 A stability result

Lemma 4.4.2. *Suppose the conditions of Lemma 4.2.2 are satisfied and*

$$|\lambda| < \frac{\beta}{\max\limits_{0\leq i\leq N} \sum\limits_{j=1}^{N} \frac{h_j}{2} \left(|K_{i,j-1}| + |K_{i,j}|\right)}. \tag{4.30}$$

Then, the solution of (4.22) satisfies the estimate

$$\max_{0\leq i\leq N} |U_i| \leq \frac{|A| + |B| + \beta^{-1} \|f\|_\infty}{1 - |\lambda|\beta^{-1} \max\limits_{0\leq i\leq N} \sum\limits_{j=1}^{N} \frac{h_j}{2} \left(|K_{i,j-1}| + |K_{i,j}|\right)}. \tag{4.31}$$

Proof. Consider (4.22) in the form

$$\begin{cases} \ell_\varepsilon^N U_i := -\varepsilon\delta^2 U_i + b_i U_i = f_i - \lambda \sum\limits_{j=1}^{N} \frac{h_j}{2} \left(K_{i,j-1} U_{j-1} + K_{i,j} U_j\right), 1 \leq i \leq N-1, \\ U_0 = A, \quad U_N = B \end{cases}$$

and apply the maximum principle. The maximum principle on $\bar{\Omega}_N$ for the finite difference operator $\ell_\varepsilon^N := -\varepsilon\delta^2 + b_i$ gives,

$$\begin{aligned}\max_{0\le i\le N}|U_i| &\le |A|+|B|+\beta^{-1}\max_{0\le i\le N}\left|f_i-\lambda\sum_{j=1}^{N}\frac{h_j}{2}\left(K_{i,j-1}U_{j-1}+K_{i,j}U_j\right)\right|\\ &\le |A|+|B|+\beta^{-1}\left(\|f\|_\infty+|\lambda|\max_{0\le i\le N}\sum_{j=1}^{N}\frac{h_j}{2}\left(|K_{i,j-1}|+|K_{i,j}|\right)|U_i|\right).\end{aligned}$$

This simplifies to

$$\max_{0\le i\le N}|U_i|\left(1-\frac{|\lambda|}{\beta}\max_{0\le i\le N}\sum_{j=1}^{N}\frac{h_j}{2}\left(|K_{i,j-1}|+|K_{i,j}|\right)\right)\le |A|+|B|+\beta^{-1}\|f\|_\infty.$$

Under the condition (4.30), this leads to

$$\max_{0\le i\le N}|U_i|\le\frac{|A|+|B|+\beta^{-1}\|f\|_\infty}{1-\frac{|\lambda|}{\beta}\max_{0\le i\le N}\sum_{j=1}^{N}\frac{h_j}{2}\left(|K_{i,j-1}|+|K_{i,j}|\right)}.$$

This completes the proof. □

4.4.2 Error analysis

The parameter uniform convergence of the scheme (4.22) on an equidistributed grid is analyzed here. Let $e_i = U_i - u(x_i)$ be the approximate solution error. From (4.20) and (4.22), it follows that

$$\mathcal{L}_\varepsilon^N e_i = \mathcal{R}_i, \quad 1\le i\le N-1, \tag{4.32}$$

$$e_0 = e_N = 0, \tag{4.33}$$

where $\mathcal{R}_i$ is given by (4.21).

Lemma 4.4.3. *For $i = 1,2,\ldots,N-1$, the truncation error $\mathcal{R}_i$, satisfies the estimate*

$$\max_i|\mathcal{R}_i|\le C\left\{\max_i h_i^2+\max_i\max_{x\in[x_{i-1/2},x_i]}\sqrt{\varepsilon}h_i^2|u'''(x)|+\max_i\max_{x\in[x_{i-1/2},x_{i+1/2}]}\varepsilon\hbar_i^2|u^{(4)}(x)|\right\}. \tag{4.34}$$

Proof. From (4.21), for $1\le i\le N-1$,

$$\mathcal{R}_i = -\varepsilon\left(u_i''-\delta^2 u_i\right)+r_i, \tag{4.35}$$

where r_i is the error in the composite trapezoidal rule approximation defined by

$$r_i = \frac{\lambda}{2}\sum_{j=1}^{N}\int\limits_{x_{j-1}}^{x_j}(x_{j-1}-\xi)(x_j-\xi)\frac{\partial^2}{\partial t^2}\left(K(x_i,\xi)u(\xi)\right)d\xi. \tag{4.36}$$

To demonstrate the validity of (4.36), consider the following relation for any $\nu \in C^2[a,b]$,

$$\int\limits_a^b \nu(\xi)d\xi = \left(\frac{b-a}{2}(\nu(a)+\nu(b))\right) + \left[\frac{1}{2}\int\limits_a^b (a-\xi)(b-\xi)\nu''(\xi)d\xi\right].$$

Applying twice integration by part to the right-hand term in the closed bracket proves the equality. The right-hand term inside the open bracket is the trapezoidal rule approximation. Therefore,

$$\left[\frac{1}{2}\int\limits_a^b (a-\xi)(b-\xi)\nu''(\xi)d\xi\right]$$

represents the error in the approximation. The relation (4.36) is based on this and the composite trapezoidal rule. For the first term on the right in (4.35),

$$-\varepsilon\left(u_i''-\delta^2 u_i\right) = \frac{-\varepsilon}{2\hbar_i}\left(\frac{1}{h_i}\int\limits_{x_{i-1}}^{x_i}(\xi-x_{i-1})^2 u'''(\xi)d\xi - \frac{1}{h_{i+1}}\int\limits_{x_i}^{x_{i+1}}(x_{i+1}-\xi)^2 u'''(\xi)d\xi\right).$$

It follows that

$$-\varepsilon\left(u_i''-\delta^2 u_i\right) = \frac{\varepsilon}{6}\left(\frac{h_{i+1}^2-h_i^2}{\hbar_i}\right)u_i''' + \frac{\varepsilon}{24}\left(\frac{h_i^3+h_{i+1}^3}{\hbar_i}\right)u_i^{(4)} + O\left(h_i^4\right) + O\left(h_{i+1}^4\right), \tag{4.37}$$

in which the following relations are used:

$$\frac{1}{h_i}\int\limits_{x_{i-1}}^{x_i}(\xi-x_{i-1})^2 u'''(\xi)d\xi = \frac{h_i^2}{3}u_i''' - \frac{h_i^3}{12}u_i^{(4)} + O\left(h_i^4\right)$$

and

$$\frac{1}{h_{i+1}}\int\limits_{x_i}^{x_{i+1}}(x_{i+1}-\xi)^2 u'''(\xi)d\xi = \frac{h_{i+1}^2}{3}u_i''' + \frac{h_{i+1}^3}{12}u_i^{(4)} + O\left(h_{i+1}^4\right).$$

Set $x_{i-1/2} = (x_{i-1}+x_i)/2$ for $i = 1,2,\ldots,N$. Then, considering

$$u_i''' = u_{i-1/2}''' + O(h_i/2) \text{ and } u_i''' = u_{i+1/2}''' + O(h_{i+1}/2)$$

in (4.37),

$$-\varepsilon\left(u_i'' - \delta^2 u_i\right) = \varepsilon\left(\frac{h_{i+1}^2 u_{i+1/2}''' - h_i^2 u_{i-1/2}'''}{6\hbar_i}\right) + \varepsilon \bar{M}\hbar_i^2 u_i^{(4)}(\eta_i), \tag{4.38}$$

where $\eta_i \in (x_{i-1/2}, x_{i+1/2})$ and $\bar{M}$ is a positive value which depends on the mesh, but its magnitude is bounded. It follows, from (4.38), that

$$-\varepsilon\left(u_i'' - \delta^2 u_i\right) = \frac{\varepsilon}{6} D\left(h_i^2 u_{i-1/2}'''\right) + \varepsilon \bar{M}\hbar_i^2 u_i^{(4)}(\eta_i). \tag{4.39}$$

Evaluating the first term on the right in (4.39) using a negative norm yields

$$\left| -\varepsilon\left(u_i'' - \delta^2 u_i\right)\right| \le C\left(\max_{x\in[x_{i-1/2},x_i]} \sqrt{\varepsilon} h_i^2 |u'''(x)| + \max_{x\in[x_{i-1/2},x_{i+1/2}]} \varepsilon \hbar_i^2 |u_i^{(4)}(x)|\right). \tag{4.40}$$

For the term r_i, it follows from (4.36) that

$$\begin{aligned}
|r_i| \le & C\sum_{i=1}^{N} \int_{x_{i-1}}^{x_i} (\xi - x_{i-1})(x_i - \xi)(1 + |u'(\xi)| + |u''(\xi)|)d\xi \\
\le & C\left\{\sum_{i=1}^{N} \frac{h_i^3}{6} + \sum_{i=1}^{N} h_i \int_{x_{i-1}}^{x_i} (\xi - x_{i-1})|u''(\xi)|d\xi\right\} \\
\le & C\left\{\max_i h_i^2 + \sum_{i=1}^{N} h_i \left(\int_{x_{i-1}}^{x_i} |u''(\xi)|^{\frac{1}{2}} d\xi\right)^2\right\},
\end{aligned}$$

where C is chosen to be sufficiently large so that

$$\int_{x_{i-1}}^{x_i} (\xi - x_{i-1})|u''(\xi)|d\xi \le C\left\{\int_{x_{i-1}}^{x_i} |u''(\xi)|^{\frac{1}{2}} d\xi\right\}^2.$$

Then, noting that

$$2\|u\|_\infty^{\frac{1}{2}} \int_{x_{i-1}}^{x_i} \frac{|u''(\xi)|^{\frac{1}{2}}}{2\|u\|_\infty^{\frac{1}{2}}} d\xi \le C\int_{x_{i-1}}^{x_i} \rho(u(\xi),\xi)d\xi,$$

it follows that, for all i, $1 \leq i \leq N$,

$$|r_i| \leq C \left\{ \max_i h_i^2 + \left(\frac{1}{N} \int_0^1 \rho(u(\xi),\xi) d\xi \right)^2 \sum_{i=1}^{N} h_i \right\}.$$

From (4.25) and observing that $\frac{1}{N} \leq \max_i h_i$, it follows

$$|r_i| \leq C \left\{ \max_i h_i^2 \right\}. \tag{4.41}$$

Using (4.40) and (4.41) in (4.35) then leads to (4.34). □

Remark 1. *The estimate in (4.39) shows that the first term on the right is zero on an equidistant grid, and the approximation error is of order two on the maximum norm. On a non-equidistant grid, the error appears to be of order one and affects the theoretical analysis, but it still retains second-order accuracy in the negative norm. Therefore, it is possible to derive an approximation error of second-order on a non-equidistant grid using a negative norm*

$$\|\nu\|_{-1,\infty} = \min_{C \in R} \max_i \left| \sum_{j=i}^{N-1} \nu_j \hbar_j - C \right|.$$

According to Tikhonov and Samarskii (1963), the maximum norm is inadequate for determining the actual order of accuracy when evaluating the accuracy of difference schemes on non-equidistant grids. Instead, Samarskii (2001) suggested using a negative norm for non-equidistant grids, and Kopteva et al. (2005) and Andreev (2004) applied this norm to establish second-order convergence for $\lambda = 0$.

The following lemma serves as the cornerstone for the subsequent analysis. It allows us to evaluate the last two terms on the right side of (4.34).

Lemma 4.4.4. *For each i, $1 \leq i \leq N-1$,*

$$\max_{x \in [x_{i-1/2}, x_i]} \sqrt{\varepsilon} h_i^2 |u'''(x)| \leq CN^{-2} \tag{4.42}$$

and

$$\max_{x \in [x_{i-1/2}, x_{i+1/2}]} \varepsilon \hbar_i^2 |u_i^{(4)}(x)| \leq CN^{-2}. \tag{4.43}$$

Proof. Using the estimate in (4.4), it follows that

$$\begin{aligned}\max_{x\in[x_{i-1/2},x_i]}\sqrt{\varepsilon}h_i^2|u'''(x)| \leq &\sqrt{\varepsilon}h_i^2\left\{C\left[1+\varepsilon^{-\frac{3}{2}}\left(e^{-\sqrt{\frac{\beta}{\varepsilon}}x_{i-1/2}}+e^{-\sqrt{\frac{\beta}{\varepsilon}}(1-x_i)}\right)\right]\right\}\\ \leq &C\left\{h_i^2+\frac{h_i^2}{\varepsilon}\left(e^{-\sqrt{\frac{\beta}{\varepsilon}}x_{i-1/2}}+e^{-\sqrt{\frac{\beta}{\varepsilon}}(1-x_i)}\right)\right\}\\ \leq &C\left\{h_i^2+\frac{1}{\varepsilon}\left(\int_{x_{i-1}}^{x_i} e^{-\sqrt{\frac{\beta}{\varepsilon}}\frac{\xi}{2}}d\xi\right)^2+\frac{1}{\varepsilon}\left(\int_{x_i}^{x_i+1} e^{-\sqrt{\frac{\beta}{\varepsilon}}\frac{(1-\xi)}{2}}d\xi\right)^2\right\}.\end{aligned}$$

This implies

$$\begin{aligned}&\max_{x\in[x_{i-1/2},x_i]}\sqrt{\varepsilon}h_i^2|u'''(x)|\\ &\qquad\leq C\left\{h_i^2+\frac{1}{\varepsilon}\left(\sqrt{\varepsilon}\int_{x_{i-1}}^{x_i}\rho(u(\xi),\xi)d\xi\right)^2+\frac{1}{\varepsilon}\left(\sqrt{\varepsilon}\int_{x_i}^{x_i+1}\rho(u(\xi),\xi)d\xi\right)^2\right\}.\end{aligned}$$

Using (4.24) and Lemma 4.3.1, then gives

$$\begin{aligned}\max_{x\in[x_{i-1/2},x_i]}\sqrt{\varepsilon}h_i^2|u'''(x)| \leq &C\left\{N^{-2}+\left(\frac{1}{N}\int_0^1\rho(u(\xi),\xi)d\xi\right)^2+\left(\frac{1}{N}\int_0^1\rho(u(\xi),\xi)d\xi\right)^2\right\}\\ \leq &CN^{-2},\end{aligned}$$

which is the first result. One can use analogous arguments to establish the bound in (4.43). □

The above results lead to the following $\varepsilon-$uniform error estimates.

Theorem 4.1. *Let the conditions of Lemma 4.2.2 hold. Let u_i be the exact solution of (4.1) and U_i be the solution of (4.22) on the equidistributed grid $\bar{\Omega}_N$ satisfying (4.24). Then*

$$\max_{0\leq i\leq N}|U_i-u_i| \leq CN^{-2}. \tag{4.44}$$

Proof. Applying Lemma 4.4.2 to (4.32)-(4.33) yields

$$\max_{0\leq i\leq N}|U_i-u_i| = \max_{0\leq i\leq N}|e_i| \leq C\max_{0\leq i\leq N}|\mathcal{R}_i|. \tag{4.45}$$

Then, using the estimates from Lemma 4.4.4 in (4.34),

$$\max_{0\le i\le N}|\mathcal{R}_i| \le CN^{-2}. \tag{4.46}$$

Combining (4.45)-(4.46) then leads to

$$\max_{0\le i\le N}|U_i - u_i| \le CN^{-2},$$

which completes the proof. □

4.5 Numerical results and discussion

This section provides a comprehensive insight into the efficacy of the proposed scheme by presenting examples that confirm the theoretical analysis. Moreover, the efficiency and accuracy of the scheme are compared with other existing schemes. The accuracy of the scheme is measured through the maximum absolute errors e^N and convergence rate r^N. Due to the absence of an exact solution for the given problems, the double mesh principle is used to determine the values of e^N and r^N.

The maximum absolute error and approximate order of convergence are obtained using

$$e^N = \max_{\varepsilon} e_\varepsilon^N, \quad e_\varepsilon^N = \max_{0\le i\le N}\left|U_i^N - U_i^{2N}\right|$$

and

$$r^N = \log_2^{(e^N/e^{2N})},$$

respectively.

Example 4.1. *Consider the SPFIDE in (Amiraliyev et al., 2021),*

$$-\varepsilon u''(x) + u(x) + \frac{1}{2}\int_0^1 xu(\xi)d\xi = x - \varepsilon + \varepsilon e^{-\frac{x}{\varepsilon}}, \quad x \in (0,1)$$

and boundary conditions

$$u(0) = 1, \quad u(1) = 2 - \varepsilon + \varepsilon e^{-\frac{1}{\varepsilon}}.$$

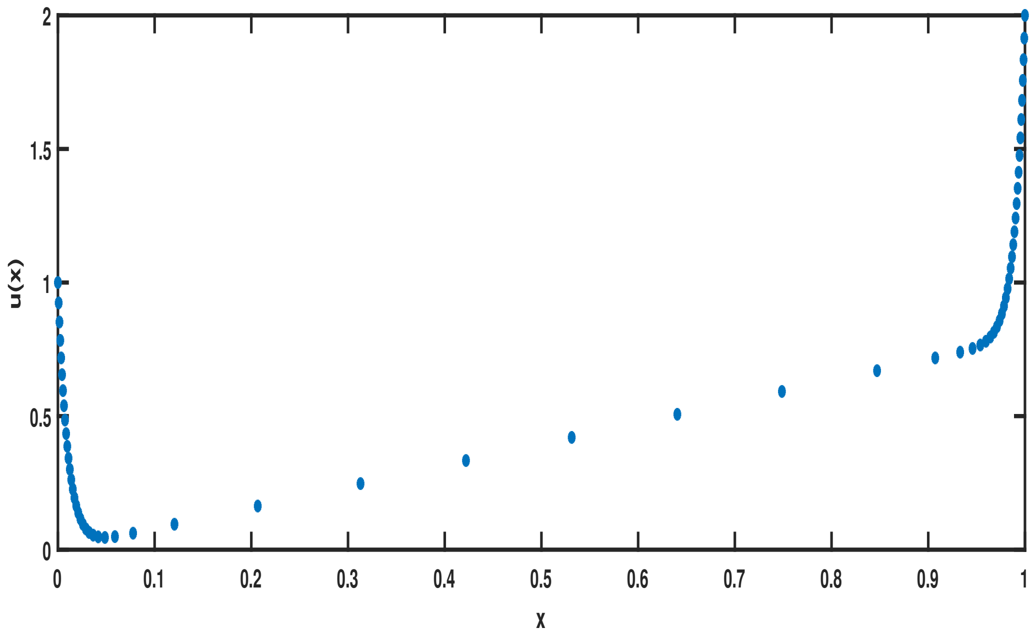

Figure 4.1: Numerical solution of Example 4.1 for $N = 64$ and $\varepsilon = 10^{-4}$.

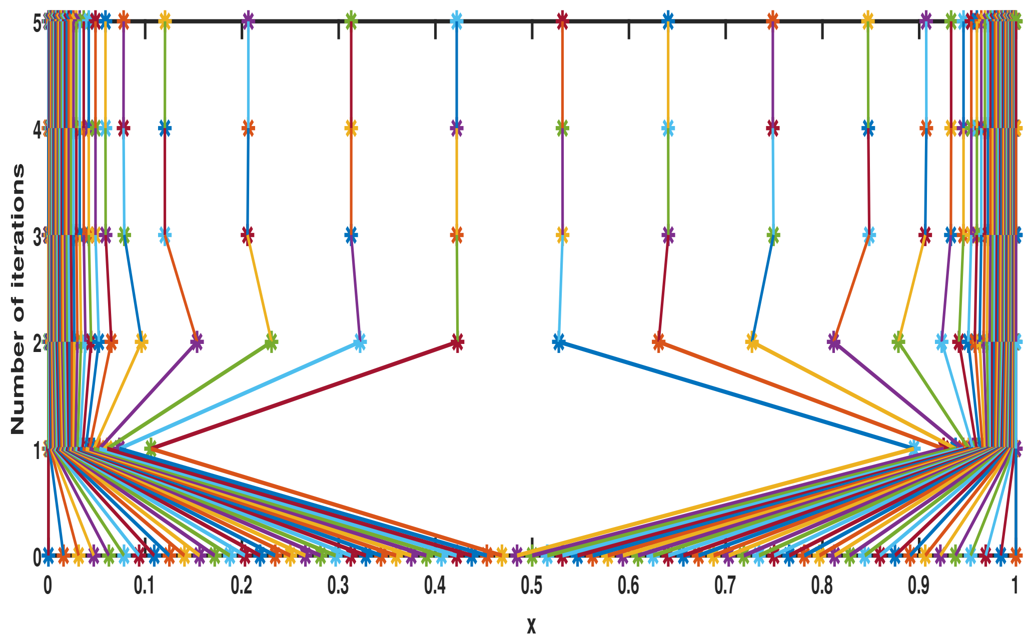

Figure 4.2: Mesh movement of Example 4.1 for $N = 64$ and $\varepsilon = 10^{-4}$.

Table 4.1: Maximum absolute error and rate of convergence of Example 4.1 for varying values of N and ε.

ε	N=32	N=64	N=128	N=256	N=512	N=1024
10^{-0}	1.0730e-06	2.8556e-07	7.3409e-08	1.8594e-08	4.6530e-09	9.0036e-10
	1.91	1.96	1.98	2.00	2.37	
10^{-1}	7.2711e-05	1.7858e-05	4.4356e-06	1.1061e-06	2.7622e-07	6.9048e-08
	2.03	2.01	2.00	2.00	2.00	
10^{-2}	6.8147e-04	1.7113e-04	4.2845e-05	1.0713e-05	2.6784e-06	6.6960e-07
	1.99	2.00	2.00	2.00	2.00	
10^{-3}	1.1059e-03	2.6820e-04	6.6455e-05	1.6577e-05	4.1419e-06	1.0359e-06
	2.04	2.01	2.00	2.00	2.00	
10^{-4}	1.3250e-03	3.1942e-04	7.8090e-05	1.9440e-05	4.8465e-06	1.2108e-06
	2.05	2.03	2.01	2.00	2.00	
10^{-5}	1.5231e-03	3.6034e-04	8.5843e-05	2.1223e-05	5.2760e-06	1.3178e-06
	2.08	2.07	2.02	2.01	2.00	
10^{-6}	1.5710e-03	3.7714e-04	9.1657e-05	2.2309e-05	5.5219e-06	1.3761e-06
	2.06	2.04	2.04	2.01	2.00	
10^{-7}	1.6435e-03	3.9262e-04	9.5210e-05	2.3161e-05	5.6601e-06	1.4076e-06
	2.07	2.04	2.04	2.03	2.01	
10^{-8}	1.6644e-03	4.0095e-04	9.7588e-05	2.4485e-05	5.9779e-06	1.4248e-06
	2.05	2.03	2.01	2.03	2.07	
10^{-9}	1.6857e-03	4.1206e-04	9.7622e-05	2.4029e-05	6.0075e-06	1.4649e-06
	2.03	2.08	2.02	2.00	2.04	
10^{-10}	1.6923e-03	4.0766e-04	9.7812e-05	2.4203e-05	5.9607e-06	1.4850e-06
	2.05	2.06	2.01	2.02	2.01	
10^{-11}	1.7050e-03	4.0892e-04	9.7885e-05	2.4144e-05	5.9446e-06	1.4887e-06
	2.06	2.06	2.02	2.02	2.00	
e^N	1.7050e-03	4.1206e-04	9.7885e-05	2.4485e-05	6.0075e-06	1.4887e-06
r^N	2.05	2.07	2.00	2.03	2.01	

Table 4.2: Comparison of the proposed scheme and the scheme in (Amiraliyev et al., 2021) using Example 4.1.

Scheme		N=128	N=256	N=512	N=1024
Scheme in	e^N	3.6884e-03	2.0181e-03	1.0303e-03	5.1622e-04
(Amiraliyev et al., 2021)	r^N	0.87	0.97	0.99	
Proposed scheme	e^N	9.7885e-05	2.4485e-05	6.0075e-06	1.4887e-06
	r^N	2.00	2.03	2.01	

Example 4.2. *Consider the SPFIDE in (Durmaz & Amiraliyev, 2021),*

$$-\varepsilon u''(x)+(2-e^{-x})u(x)+\frac{1}{2}\int_0^1 (e^{x\cos(\pi\xi)}-1)u(\xi)d\xi=\frac{1}{1+x},\quad x\in(0,1),$$

$$u(0)=1,\quad u(1)=0.$$

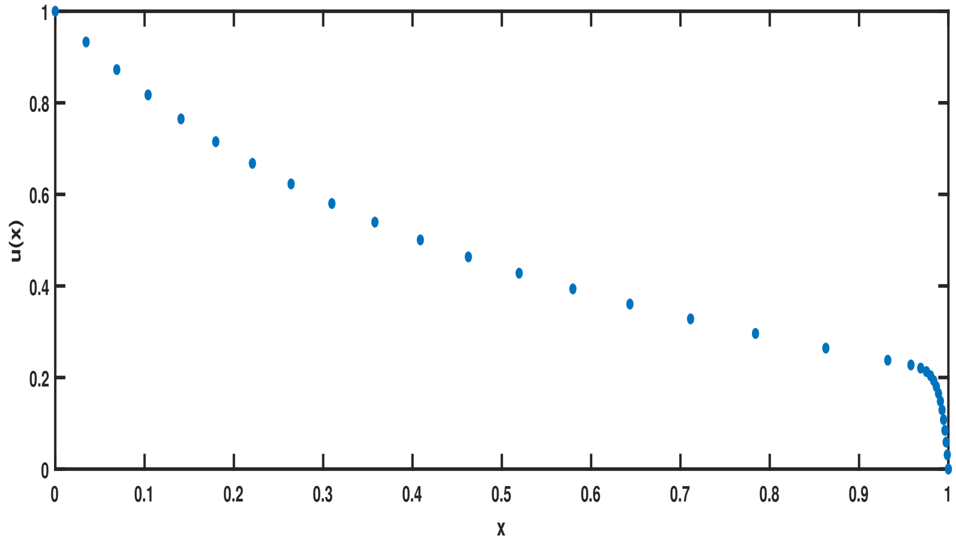

Figure 4.3: Numerical solution of Example 4.2 for $N=32$ and $\varepsilon=10^{-4}$.

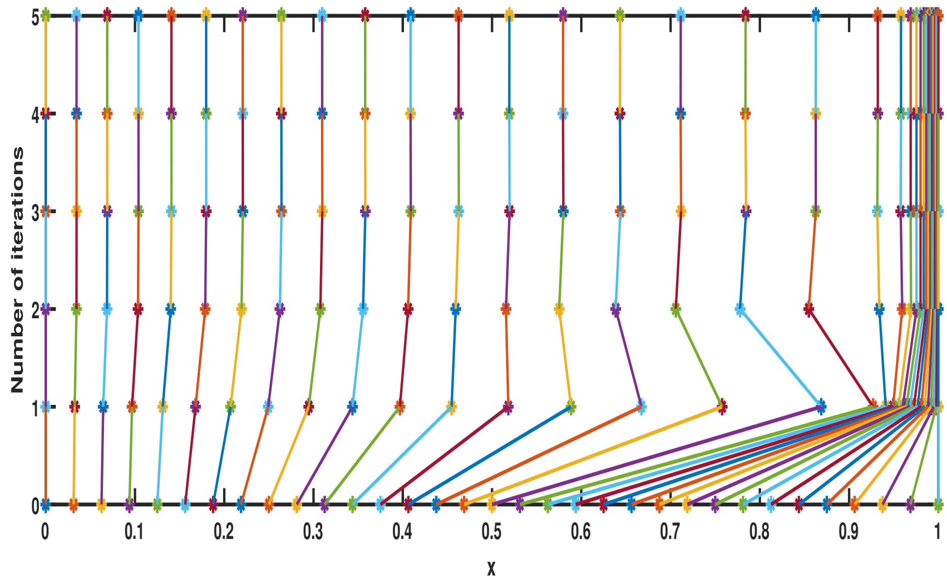

Figure 4.4: Mesh movement of Example 4.2 for $N=32$ and $\varepsilon=10^{-4}$.

Table 4.3: Maximum absolute error and rate of convergence of Example 4.2 for varying values of N and ε.

ε	N=32	N=64	N=128	N=256	N=512	N=1024
10^{-0}	1.9548e-05	4.8909e-06	1.2231e-06	3.0588e-07	7.6458e-08	1.8974e-08
10^{-1}	6.9679e-05	1.7580e-05	4.4200e-06	1.1057e-06	2.7648e-07	6.9115e-08
10^{-2}	9.5765e-05	2.6078e-05	6.8501e-06	1.7353e-06	4.3470e-07	1.0892e-07
10^{-3}	1.6747e-04	4.2945e-05	1.1274e-05	2.7925e-06	7.0332e-07	1.7663e-07
10^{-4}	2.4181e-04	5.7470e-05	1.4936e-05	3.7433e-06	9.4511e-07	2.3641e-07
10^{-5}	2.6261e-04	6.5429e-05	1.6830e-05	4.1767e-06	1.0604e-06	2.6483e-07
10^{-6}	2.8182e-04	7.0186e-05	1.7125e-05	4.3710e-06	1.0912e-06	2.7482e-07
10^{-7}	2.8997e-04	7.0766e-05	1.7717e-05	4.3633e-06	1.0959e-06	2.7615e-07
10^{-8}	2.9320e-04	7.1368e-05	1.7728e-05	4.3725e-06	1.0911e-06	2.7704e-07
$\vdots$	$\vdots$	$\vdots$	$\vdots$	$\vdots$	$\vdots$	$\vdots$
10^{-12}	2.9938e-04	7.3031e-05	1.7812e-05	4.4399e-06	1.1009e-06	2.7380e-07
10^{-13}	3.0088e-04	7.3118e-05	1.7816e-05	4.4440e-06	1.1019e-06	2.7391e-07
10^{-14}	3.0453e-04	7.3266e-05	1.7820e-05	4.4417e-06	1.1009e-06	2.7401e-07
10^{-15}	3.0660e-04	7.3155e-05	1.7824e-05	4.4423e-06	1.1001e-06	2.7510e-07
10^{-16}	3.0910e-04	7.3410e-05	1.7833e-05	4.4387e-06	1.0999e-06	2.7611e-07
10^{-17}	3.1198e-04	7.3172e-05	1.7859e-05	4.4406e-06	1.0995e-06	2.7613e-07
e^N	3.1198e-04	7.3410e-05	1.7859e-05	4.4440e-06	1.1019e-06	2.7704e-07
r^N	2.09	2.04	2.01	2.01	1.99	2.00

Table 4.4: Comparison of the proposed scheme and the scheme in (Durmaz & Amiraliyev, 2021) using Example 4.2.

Scheme		N=128	N=256	N=512	N=1024
Scheme in	e^N	2.8042e-03	7.1231e-04	1.8094e-04	4.5930e-05
(Durmaz & Amiraliyev, 2021)	r^N	1.977	1.977	1.978	
Proposed scheme	e^N	1.7859e-05	4.4440e-06	1.1019e-06	2.7704e-07
	r^N	2.01	2.01	1.99	2.00

Figures 4.1 and 4.3 depict the numerical solutions obtained through the application of the equidistribution technique (based on the mesh density function in equation (4.23)) for Examples 4.1 and 4.2, respectively. Figures 4.2 and 4.4 correspondingly illustrate the resulting adaptive mesh behavior. Furthermore, the plots confirm the existence of boundary layers at $x = 0$ and $x = 1$.

From Tables 4.1 and 4.3, it can be deduced that the maximum pointwise errors remain uniform and do not depend on ε. Additionally, it can be observed that the solution converges with second-order accuracy, aligning with what was estimated in

Theorem 4.1. It is worth mentioning that the proposed scheme produces more accurate approximations, as evident from the results in Tables 4.2 and 4.4, in comparison to the outcomes mentioned in (Amiraliyev et al., 2021) and (Durmaz & Amiraliyev, 2021).

4.6 Summary

In this chapter, a demanding problem involving a singularly perturbed FIDE of the reaction-diffusion type, with the complexity of two boundary layers, has been successfully tackled. To effectively address this problem, a centered finite difference scheme was employed in combination with the composite trapezoidal rule on adaptive meshes. Grid equidistribution was used to generate the adaptive mesh. The proposed scheme has been shown to produce superior numerical results compared to existing numerical schemes. Numerical experiments are performed and results are presented for validation of the theoretical error estimates. It is also shown that the scheme exhibits uniform convergence independent of the perturbation parameter in the discrete maximum norm, and it is second-order uniformly accurate.

CHAPTER FIVE

SINGULARLY PERTURBED REACTION DIFFUSION TYPE FREDHOLM INTEGRO-DIFFERENTIAL EQUATION WITH AN INTERIOR LAYER

Building upon the foundation established in Chapter 4, this chapter tackles a more complex scenario by introducing a discontinuity to the source term. The previously discussed numerical scheme is utilized, but with strategic modifications to effectively handle the discontinuity. This enhanced approach surpasses existing schemes in terms of accuracy, demonstrably achieving second-order uniform convergence.

5.1 Description of the problem

A numerical scheme is investigated to solve a SPFIDE that contains a discontinuous source term f. The discontinuity in f is assumed to occur at a point d in the domain $\Omega = (0,1)$. Additionally, the jump in any function ν at d is defined as $[\nu](d) = \nu(d+) - \nu(d-)$. The corresponding SPFIDE is

$$\begin{cases} \mathcal{L}_\varepsilon u := \ell_\varepsilon u + \lambda \int\limits_0^1 K(x,\xi)u(\xi)d\xi = f(x), \quad x \in \Omega^- \cup \Omega^+, \\ u(0) = A, \quad u(1) = B, \\ f(d-) \neq f(d+), \end{cases} \tag{5.1}$$

where $\ell_\varepsilon u = -\varepsilon u'' + b(x)u$, $0 < \varepsilon \ll 1$ is the perturbation parameter and λ is a real parameter. Moreover, $\Omega^- = (0,d)$, $\Omega^+ = (d,1)$, $\bar{\Omega} = [0,1]$, $b \in C^2(\bar{\Omega})$ such that $0 < \beta \leq b(x)$ and $K \in C^2(\bar{\Omega} \times \bar{\Omega})$. Typically, a boundary layer appears at both ends of $\bar{\Omega}$ and an interior layer at the point $x = d$ when solving equations (5.1).

5.2 A priori bounds on the solution and its derivatives

To formally establish the convergence of the proposed scheme, the following qualitative result is presented for the solution to the problem (5.1) and its derivatives in this section. The maximum principle guarantees a priori bounds for the solution. The differential operator ℓ_ε in (5.1) for all $\Psi \in C^0(\bar{\Omega}) \cap C^2(\Omega^- \cup \Omega^+)$ satisfies the following maximum principle on $\bar{\Omega}$.

Lemma 5.2.1. *(**Maximum principle**) (Farrell et al., 2000) Assume that a function $\Psi \in C^0(\bar{\Omega}) \cap C^2(\Omega^- \cup \Omega^+)$ satisfies*

$$
\begin{aligned}
\Psi(0) \geq 0, &\quad \Psi(1) \geq 0 \\
\ell_\varepsilon \Psi(x) \geq 0, &\quad \textit{for all}\, x \in \Omega^- \cup \Omega^+ \\
[\Psi](d) = 0, &\quad [\Psi'](d) \leq 0. \\
\textit{Then} \quad \Psi(x) \geq 0, &\quad \textit{for all}\, x \in \bar{\Omega}.
\end{aligned}
$$

Lemma 5.2.2. *(Rathore et al., 2023) Let u be the solution of (5.1). Assume that $b \in C^2(\bar{\Omega})$, $f \in C^2(\Omega^- \cup \Omega^+)$, $\frac{\partial^n K}{\partial x^n}, \frac{\partial^n K}{\partial \xi^n} \in C(\bar{\Omega} \times \bar{\Omega})$, n=0,1,2 and*

$$
|\lambda| < \frac{\beta}{\max\limits_{0 \leq x \leq 1} \int_0^1 |K(x,\xi)|\, d\xi}. \tag{5.2}
$$

Then u(x) satisfies

$$
\|u\|_\infty \leq C, \quad x \in \bar{\Omega} \tag{5.3}
$$

and, for all k, $1 \leq k \leq 4$,

$$
\left| u^{(k)}(x) \right| \leq \begin{cases} C\left(1 + \varepsilon^{-\frac{k}{2}} e_1(x,\beta)\right), & x \in \Omega^-, \\ C\left(1 + \varepsilon^{-\frac{k}{2}} e_2(x,\beta)\right), & x \in \Omega^+, \end{cases} \tag{5.4}
$$

where

$$
e_1(x,\beta) = e^{-\sqrt{\frac{\beta}{\varepsilon}}x} + e^{-\sqrt{\frac{\beta}{\varepsilon}}(d-x)} \quad \textit{and} \quad e_2(x,\beta) = e^{-\sqrt{\frac{\beta}{\varepsilon}}(x-d)} + e^{-\sqrt{\frac{\beta}{\varepsilon}}(1-x)}.
$$

Proof. The proof for (5.3) is an immediate consequence of the maximum principle satisfied by the operator ℓ_ε, and is derived by applying the maximum principle to the functions

$$\Psi_{\pm}(x) = max\{|A|,|B|\} + \frac{1}{\beta}\|F\|_{\Omega^-\cup\Omega^+} \pm u(x),$$

where

$$F(x) = f(x) - \lambda\int_0^1 K(x,\xi)u(\xi)d\xi, \quad x \in \Omega^- \cup \Omega^+. \tag{5.5}$$

Clearly $\Psi_{\pm}(0) \geq 0$, $\Psi_{\pm}(1) \geq 0$ and for each $x \in \Omega^- \cup \Omega^+$ that $\ell_\varepsilon \Psi_{\pm}(x) \geq 0$. Furthermore

$$[\Psi_{\pm}](d) = \pm[u_\varepsilon](d) = 0 \quad \text{and} \quad [\Psi'_{\pm}](d) = \pm[u'](d) = 0.$$

Applying the maximum principle then gives $\Psi_{\pm} \geq 0$, and so

$$\|u\|_\infty \leq \max\{|A|,|B|\} + \frac{1}{\beta}\|F\|_{\Omega^-\cup\Omega^+}. \tag{5.6}$$

Using (5.5) in the expression (5.6) gives

$$\|u\|_\infty \leq |A| + |B| + \beta^{-1}\left(\|f\|_{\Omega^-\cup\Omega^+} + |\lambda| \max_{0\leq x\leq 1}\int_0^1 |K(x,\xi)|d\xi\,\|u\|_\infty\right).$$

This simplifies to

$$\|u\|_\infty \leq \frac{|A| + |B| + \beta^{-1}\|f\|_{\Omega^-\cup\Omega^+}}{1 - \beta^{-1}|\lambda| \max_{0\leq x\leq 1}\int_0^1 |K(x,\xi)|d\xi}.$$

When combined with (5.2), this leads to (5.3). The estimates in (5.4) can be derived similarly to Lemma 4.2.2 in Chapter 4. □

5.3 The numerical scheme

This section delves into the process of discretizing the governing continuous equations, transforming them into a tractable, discrete format. The application of an adaptive mesh, which dynamically concentrates mesh points in regions where the solution exhibits intricate characteristics, is explored. This targeted approach refines the computational grid, thereby significantly enhancing the accuracy of the results in these critical areas.

5.3.1 The discrete scheme

To form the adaptive mesh $\bar{\Omega}_N$, the domain $\bar{\Omega}$ is first divided into two subdomains using the point of discontinuity d as the transition point. The adaptive mesh can be defined as

$$\bar{\Omega}_N = \{0 = x_0 < x_1 < \cdots < x_{n-1} < x_n = d < x_{n+1} < \cdots < x_N = 1; h_i = x_i - x_{i-1}\},$$

where $n = N/2$ is the index number at which discontinuity occurs. The interior points of the mesh are denoted by

$$\Omega_N = \{x_i : 1 \le i \le N/2-1\} \cup \{x_i : N/2+1 \le i \le N-1\} = \Omega_N^- \cup \Omega_N^+.$$

For any mesh function ν_i on mesh $\bar{\Omega}_N$, define

$$\begin{aligned}\mathcal{D}_2^-\nu_i =& \frac{h_i}{2h_{i-1}\hbar_{i-1}}\nu_{i-2} - \left(\frac{1}{h_{i-1}} + \frac{1}{h_i}\right)\nu_{i-1} + \left(\frac{1}{2\hbar_{i-1}} + \frac{1}{h_i}\right)\nu_i \quad \text{and}\\ \mathcal{D}_2^+\nu_i =& -\left(\frac{1}{2\hbar_{i+1}} + \frac{1}{h_{i+1}}\right)\nu_i + \left(\frac{1}{h_{i+1}} + \frac{1}{h_{i+2}}\right)\nu_{i+1} - \frac{h_{i+1}}{2\hbar_{i+1}h_{i+2}}\nu_{i+2},\end{aligned}$$

where $\hbar_i = (h_i + h_{i+1})/2$ for $1 \le i \le N-1$. The expressions $\mathcal{D}_2^+\nu_i$ and $\mathcal{D}_2^-\nu_i$ approximate the first derivative using forward and backward difference formulas, respectively. It's important to note that these approximations have second-order accuracy.

The central FDM is used to approximate the derivative part of (5.1), leading to a finite difference approximation:

$$-\varepsilon u_i'' = -\frac{2\varepsilon}{h_i + h_{i+1}}\left(\frac{u_{i+1} - u_i}{h_{i+1}} - \frac{u_i - u_{i-1}}{h_i}\right) + \mathcal{R}_i^{(1)}, \quad 1 \le i \le N-1, i \ne \tfrac{N}{2},$$

where

$$\mathcal{R}_i^{(1)} = -\varepsilon\left(u_i'' - \delta^2 u_i\right). \tag{5.7}$$

By numerically approximating the integral part using the composite trapezoidal rule, it follows that

$$\lambda\int_0^1 K(x_i,\xi)u(\xi)d\xi = \lambda\sum_{j=1}^{N}\frac{h_j}{2}\left(K_{i,j-1}u_{j-1} + K_{i,j}u_j\right) + \mathcal{R}_i^{(2)}, \quad x_i \in \Omega_N^- \cup \Omega_N^+,$$

where

$$\mathcal{R}_i^{(2)} = \frac{\lambda}{2} \sum_{j=1}^{N} \int_{x_{j-1}}^{x_j} (x_{j-1} - \xi)(x_j - \xi) \frac{\partial^2}{\partial \xi^2} \left(K(x_i, \xi) u(\xi) \right) d\xi. \tag{5.8}$$

The resulting discrete problem becomes:

$$\begin{cases} \mathcal{L}_\varepsilon u_i := -\varepsilon \delta^2 u_i + b_i u_i + \lambda \sum_{j=1}^{N} \frac{h_j}{2} \left(K_{i,j-1} u_{j-1} + K_{i,j} u_j \right) = f_i - \mathcal{R}_i, \, 1 \le i \le N-1, i \ne \frac{N}{2}, \\ u_0 = A, \quad u_N = B, \\ \mathcal{D}_2^- u_{N/2} = \mathcal{D}_2^+ u_{N/2}. \end{cases} \tag{5.9}$$

The error term $\mathcal{R}_i$ is given by

$$\mathcal{R}_i = \mathcal{R}_i^{(1)} + \mathcal{R}_i^{(2)} + \mathcal{R}_i^{(3)}, \tag{5.10}$$

where $\mathcal{R}_i^{(1)}$ and $\mathcal{R}_i^{(2)}$ are defined by (5.7) and (5.8) respectively, and

$$\mathcal{R}_i^{(3)} = \left(\mathcal{D}_2^- - \frac{d}{dx} \right) u(x_{N/2}) - \left(\mathcal{D}_2^+ - \frac{d}{dx} \right) u(x_{N/2}), \tag{5.11}$$

which is an error due to the condition $\mathcal{D}_2^- u_{N/2} = \mathcal{D}_2^+ u_{N/2}$.

When the remainder term in (5.9) is omitted, the following scheme for approximating (5.1) is obtained:

$$\begin{cases} \mathcal{L}_\varepsilon^N U_i := -\varepsilon \delta^2 U_i + b_i U_i + \lambda \sum_{j=1}^{N} \frac{h_j}{2} \left(K_{i,j-1} U_{j-1} + K_{i,j} U_j \right) = f_i, \quad 1 \le i \le N-1, i \ne \frac{N}{2}, \\ U_0 = A, \quad U_N = B, \\ \mathcal{D}_2^- U_{N/2} = \mathcal{D}_2^+ U_{N/2}. \end{cases} \tag{5.12}$$

5.3.2 Adaptive grid generation via equidistribution

The equidistribution principle is employed to generate adaptive grids. This principle ensures an even distribution of solution errors by concentrating grid nodes within the boundary layer. This is achieved by equidistributing a positive mesh density function,

$$\rho(u(\xi),\xi) = 1 + \frac{|u''(\xi)|^{\frac{1}{2}} + |(bu)''(\xi)|^{\frac{1}{2}}}{\|u\|_{\infty}^{\frac{1}{2}}} \tag{5.13}$$

over the domain $\bar{\Omega}_N$. Kopteva et al. (2005) suggested this mesh density function for solving reaction-diffusion problems. Since the domain $\bar{\Omega}_N$ is divided using the point of discontinuity d as a transition point, equidistribution is independently applied to both sides. Consequently, the relations are as follows:

$$\int_{x_{i-1}}^{x_i} \rho(u(\xi),\xi)d\xi = \frac{2}{N}\int_0^d \rho(u(\xi),\xi)d\xi, \quad i = 1,2,\ldots,N/2 \tag{5.14}$$

and

$$\int_{x_{i-1}}^{x_i} \rho(u(\xi),\xi)d\xi = \frac{2}{N}\int_d^1 \rho(u(\xi),\xi)d\xi, \quad i = N/2+1, N/2+2,\ldots,N. \tag{5.15}$$

Lemma 5.3.1. *Let $\rho(u(\xi),\xi)$ be the mesh density function in (5.13). Then,*

$$\int_0^d \rho(u(\xi),\xi)d\xi \leq C \tag{5.16}$$

and

$$\int_d^1 \rho(u(\xi),\xi)d\xi \leq C. \tag{5.17}$$

Proof. Integrating (5.13) over $[0,d]$ gives

$$\begin{aligned}\int_0^d \rho(u(\xi),\xi)d\xi &= \int_0^d \left(1 + \frac{|u''(\xi)|^{\frac{1}{2}} + |(bu)''(\xi)|^{\frac{1}{2}}}{\|u\|_{\infty}^{\frac{1}{2}}}\right) d\xi \\ &\leq d + C\int_0^d \left(\left|u''(\xi)\right|^{\frac{1}{2}} + \left|(bu)''(\xi)\right|^{\frac{1}{2}}\right) d\xi. \end{aligned} \tag{5.18}$$

From Lemma 5.2.2, it follows that

$$\begin{aligned}\int_0^d \left|u''(\xi)\right|^{\frac{1}{2}} d\xi &\leq C\int_0^d \left(1 + \varepsilon^{-1}\left(e^{-\sqrt{\frac{\beta}{\varepsilon}}s} + e^{-\sqrt{\frac{\beta}{\varepsilon}}(d-\xi)}\right)\right)^{\frac{1}{2}} d\xi \\ &\leq C\int_0^d \left(1 + \varepsilon^{-\frac{1}{2}} e^{-\sqrt{\frac{\beta}{\varepsilon}}\frac{s}{2}} + \varepsilon^{-\frac{1}{2}} e^{-\sqrt{\frac{\beta}{\varepsilon}}\frac{(d-\xi)}{2}}\right) d\xi \\ &= C\left(d + \frac{4}{\beta}\left(1 - e^{-\sqrt{\frac{\beta}{\varepsilon}}\frac{d}{2}}\right)\right).\end{aligned}$$

It follows that

$$\int_0^d \left|u''(\xi)\right|^{\frac{1}{2}} d\xi \le C.$$

A similar argument yields

$$\int_0^d \left|(bu)''(\xi)\right|^{\frac{1}{2}} d\xi \le C.$$

The two inequalities, when used in (5.18), give

$$\int_0^d \rho(u(\xi),\xi) d\xi \le C.$$

This completes the proof of the first result of the lemma. The proof can be extended to the interval $[d,1]$ with similar steps. □

A solution algorithm for the problem (5.1) is introduced utilizing the discrete scheme (5.12) and equidistribution of the mesh density function

$$\rho_i = 1 + \frac{\left|\delta^2 U_i^{(k)}\right|^{\frac{1}{2}} + \left|\delta^2 b_i U_i^{(k)}\right|^{\frac{1}{2}}}{\max\limits_i \left|U_i^{(k)}\right|^{\frac{1}{2}}}, \quad i = 1, 2, \ldots, N,$$

which is the discrete equivalent of (5.13). Since grid $\{x_i\}_{i=0}^N$ and solution $\{U_i\}_{i=0}^N$ are unknown a priori, the equidistribution problem requires the simultaneous solution of (5.12) and the relations

$$h_j \rho_j = \frac{2}{N} \sum_{i=1}^{N/2} h_i \rho_i, \quad 1 \le j \le N/2$$

and

$$h_j \rho_j = \frac{2}{N} \sum_{i=N/2+1}^{N} h_i \rho_i, \quad N/2 \le j \le N$$

to find $\{x_i, U_i\}$.

Here, a mesh-generation algorithm similar to the one presented in Chapter 4 is used, but with modifications detailed in Algorithm 2.

Algorithm 2 Adaptive mesh generation

Input $N \in \mathbb{Z}^+$, $0 < \varepsilon \le 1$, point of discontinuity d, & a user-chosen constant $C_0 > 1$.
Output Adaptive mesh Ω_N^* and corresponding solution $\{U_i^*\}_{i=0}^N$
Step 1. Initialization

Take the initial piecewise uniform mesh $\Omega_N^{(0)} = \left\{x_0^{(0)}, x_1^{(0)}, \ldots, x_{N/2}^{(0)}, \ldots, x_N^{(0)}\right\}$, where $x_{N/2}^{(0)} = d$ is the transition point.

Step 2. Solution construction

Obtain $\left\{U_i^{(k)}\right\}_{i=0}^N$ by solving (5.12) on $\Omega_N^{(k)} = \left\{x_i^{(k)}\right\}_{i=0}^N$.

Step 3. Mesh density function

Let $h_i^{(k)} = x_i^{(k)} - x_{i-1}^{(k)}$ for $i = 1, 2, \ldots, N$ and compute

$$\rho_i^{(k)} = 1 + \frac{\left|\delta^2 U_i^{(k)}\right|^{\frac{1}{2}} + \left|\delta^2 b_i U_i^{(k)}\right|^{\frac{1}{2}}}{\tau}, \quad i = 1, 2, \ldots, N-1,$$

where $\tau = \max_i \left|U_i^{(k)}\right|^{\frac{1}{2}}$. Set $\rho_0^{(k)} := \rho_1^{(k)}$ and $\rho_N^{(k)} := \rho_{N-1}^{(k)}$. Then $\mathcal{M}_i = \frac{\rho_{i-1}+\rho_i}{2}, \quad i = 1, 2, \ldots, N.$

Step 4. Terminating condition

Set $L_{1,0}^{(k)} = L_{2,0}^{(k)} = 0$.

For $1 \le i \le N/2$, set $L_{1,i}^{(k)} = \sum_{j=1}^{i} h_j^{(k)} \mathcal{M}_j^{(k)}$, $L_{2,i}^{(k)} = \sum_{j=N/2+1}^{N/2+i} h_j^{(k)} \mathcal{M}_j^{(k)}$ and define

$$C_*^{(k)} := \frac{N}{2L_{1,N/2}^{(k)}} \max_{1 \le i \le N/2} h_i^{(k)} \mathcal{M}_i^{(k)} \text{ and } C_{**}^{(k)} := \frac{N}{2L_{2,N/2}^{(k)}} \max_{N/2+1 \le i \le N} h_i^{(k)} \mathcal{M}_i^{(k)}.$$

If $C_*^{(k)}, C_{**}^{(k)} \le C_0$, then go to step 6; Otherwise, continue with the next step.

Step 5. Equidistribution

For $i = 0, 1, \ldots, N/2$, set $\omega_{1,i} := 2iL_{1,N}^{(k)}/N$ and $\omega_{2,i} := 2iL_{2,N}^{(k)}/N$. Then, interpolate to the points $(L_{1,i}^{(k)}, x_i^{(k)})$ and $(L_{2,i}^{(k)}, x_{N/2+i}^{(k)})$. Generate $\left\{x^{(k+1)}\right\}$ by computing the interpolants at $\{\omega_{1,i}\}_{i=0}^{N/2}$ and $\{\omega_{2,i}\}_{i=0}^{N/2}$. Increment the value of k by one and return to the second step.

Step 6. Set $\Omega_N^* := \left\{x_i^{(k)}\right\}_{i=0}^N$ and $\{U^*\} := \left\{U_i^{(k)}\right\}_{i=0}^N$, then stop.

5.4 Stability and uniform convergence

In this section, a detailed examination of the stability of the proposed scheme is provided, thereby enhancing understanding of its robustness. Furthermore, an error analysis is conducted to showcase the uniform convergence achieved by the scheme, establishing its reliability and accuracy.

5.4.1 A stability result

The forthcoming stability result will serve as a crucial stepping stone for the subsequent discourse, allowing for a seamless continuation of the investigation.

Lemma 5.4.1. *Suppose the conditions of Lemma 5.2.2 are satisfied and*

$$|\lambda| < \frac{\beta}{\max\limits_{1\le i\le N-1, i\ne N/2} \sum_{j=1}^{N} \frac{h_j}{2}\left(|K_{i,j-1}|+|K_{i,j}|\right)}. \tag{5.19}$$

Then, the solution of (5.12) satisfies the estimate

$$\max_{0\le i\le N}|U_i| \le \frac{|A|+|B|+\frac{1}{\beta}\max\limits_{1\le i\le N-1, i\ne N/2}|f_i|}{1-|\lambda|\frac{1}{\beta}\max\limits_{1\le i\le N-1, i\ne N/2}\sum_{j=1}^{N}\frac{h_j}{2}\left(|K_{i,j-1}|+|K_{i,j}|\right)}. \tag{5.20}$$

Proof. Let $\ell_\varepsilon^N = -\varepsilon\delta^2 + b_i$ be a finite difference operator in (5.12). Then, the maximum principle satisfied by ℓ_ε^N on $\bar{\Omega}_N$ gives

$$\max_{0\le i\le N}|U_i| \le |A|+|B|+\frac{1}{\beta}\max_{1\le i\le N-1, i\ne N/2}|F_i|,$$

where

$$F_i = f_i - \lambda\sum_{j=1}^{N}\frac{h_j}{2}\left(K_{i,j-1}U_{j-1}+K_{i,j}U_j\right).$$

This implies

$$\begin{aligned}\max_{0\le i\le N}|U_i| \le |A|+|B|+\frac{1}{\beta}\max_{1\le i\le N-1, i\ne N/2}|f_i| \\ +|\lambda|\frac{1}{\beta}\max_{1\le i\le N-1, i\ne N/2}\sum_{j=1}^{N}\frac{h_j}{2}\left(|K_{i,j-1}|+|K_{i,j}|\right)\max_{0\le i\le N}|U_i|,\end{aligned}$$

from which it follows that

$$\begin{aligned}\left(1-|\lambda|\frac{1}{\beta}\max_{1\le i\le N-1, i\ne N/2}\sum_{j=1}^{N}\frac{h_j}{2}\left(|K_{i,j-1}|+|K_{i,j}|\right)\right)\max_{0\le i\le N}|U_i| \le |A|+|B| \\ +\frac{1}{\beta}\max_{1\le i\le N-1, i\ne N/2}|f_i|.\end{aligned} \tag{5.21}$$

By using the condition (5.19), it is convenient to rewrite (5.21) as

$$\max_{0\le i\le N}|U_i|\le \frac{|A|+|B|+\frac{1}{\beta}\max\limits_{1\le i\le N-1,i\ne N/2}|f_i|}{1-|\lambda|\frac{1}{\beta}\max\limits_{1\le i\le N-1,i\ne N/2}\sum\limits_{j=1}^{N}\frac{h_j}{2}\left(|K_{i,j-1}|+|K_{i,j}|\right)},$$

which completes the proof. □

5.4.2 Error analysis

Denote the pointwise error $e_i=U_i-u_i$, along with (5.9) and (5.12), which leads to the error equation

$$\begin{cases}\mathcal{L}_\varepsilon^N e_i=\mathcal{R}_i, \quad 1\le i\le N-1, i\ne N/2,\\ e_0=e_N=0,\\ \mathcal{D}_2^- e_{N/2}=\mathcal{D}_2^+ e_{N/2},\end{cases} \tag{5.22}$$

where $\mathcal{R}_i$ is given by (5.10).

Lemma 5.4.2. *The truncation error $\mathcal{R}_i$ at the interior mesh points Ω_N satisfies the estimate*

$$\max_{1\le i\le N-1,i\ne N/2}|\mathcal{R}_i| \le C\left\{\max_i h_i^2+\max_i\max_{x\in[x_{i-1/2},x_i]}\sqrt{\varepsilon}h_i^2\left|u'''(x)\right|+\max_i\max_{x\in[x_{i-1/2},x_{i+1/2}]}\varepsilon\hbar_i^2\left|u^{(4)}(x)\right|\right\}. \tag{5.23}$$

Proof. For any point within the interior of the mesh, from (4.40) and (5.7),

$$\left|\mathcal{R}_i^{(1)}\right|\le C\left(\max_{x\in[x_{i-1/2},x_i]}\sqrt{\varepsilon}h_i^2\left|u'''(x)\right|+\max_{x\in[x_{i-1/2},x_{i+1/2}]}\varepsilon\hbar_i^2\left|u_i^{(4)}(x)\right|\right). \tag{5.24}$$

For $\mathcal{R}_i^{(2)}$, it follows from (5.8) that

$$\begin{aligned}\left|\mathcal{R}_i^{(2)}\right| &\le C\sum_{i=1}^{N}\int_{x_{i-1}}^{x_i}(\xi-x_{i-1})(x_i-\xi)(1+\left|u'(\xi)\right|+\left|u''(\xi)\right|)d\xi\\ &\le C\left\{\sum_{i=1}^{N}\frac{h_i^3}{6}+\sum_{i=1}^{N}h_i\int_{x_{i-1}}^{x_i}(\xi-x_{i-1})\left|u''(\xi)\right|d\xi\right\},\end{aligned}$$

which implies that

$$\left|\mathcal{R}_i^{(2)}\right| \leq C \left\{ \max_i h_i^2 + \sum_{i=1}^{N} h_i \left(\int_{x_{i-1}}^{x_i} \left|u''(\xi)\right|^{\frac{1}{2}} d\xi \right)^2 \right\}$$
$$\leq C \left\{ \max_i h_i^2 + \sum_{i=1}^{N} h_i \left(\int_{x_{i-1}}^{x_i} \rho(u(\xi),\xi) d\xi \right)^2 \right\}.$$

Using (5.14)-(5.15), it follows that

$$\left|\mathcal{R}_i^{(2)}\right| \leq C \left\{ \max_i h_i^2 + \left(\left(\frac{2}{N} \int_0^d \rho(u(\xi),\xi) d\xi \right)^2 + \left(\frac{2}{N} \int_d^1 \rho(u(\xi),\xi) d\xi \right)^2 \right) \sum_{i=1}^{N} h_i \right\}.$$

Since $\frac{2}{N} \leq \max_i h_i$, (5.16) and (5.17) can be used to conclude that

$$\left|\mathcal{R}_i^{(2)}\right| \leq C \left\{ \max_i h_i^2 \right\}. \tag{5.25}$$

At the point of discontinuity, it follows from (5.11) that

$$\left|\mathcal{R}_i^{(3)}\right| \leq \left| \left(\mathcal{D}_2^- - \frac{d}{dx} \right) u_{N/2} \right| + \left| \left(\mathcal{D}_2^+ - \frac{d}{dx} \right) u_{N/2} \right|. \tag{5.26}$$

The two terms on the right in (5.26) will be estimated separately. For the first term, using the definition of $\mathcal{D}_2^-$,

$$\left(\mathcal{D}_2^- - \frac{d}{dx} \right) u_{N/2} = \frac{h_{N/2}}{2h_{N/2-1}\hbar_{N/2-1}} u_{N/2-2} - \left(\frac{1}{h_{N/2-1}} + \frac{1}{h_{N/2}} \right) u_{N/2-1}$$
$$+ \left(\frac{1}{2\hbar_{N/2-1}} + \frac{1}{h_{N/2}} \right) u_{N/2} - u'_{N/2}. \tag{5.27}$$

Substituting the Taylor series expansions of $u_{N/2-1}$ and $u_{N/2-2}$ into (5.27) yields

$$\left| \left(\mathcal{D}_2^- - \frac{d}{dx} \right) u_{N/2} \right| = \frac{\hbar_{N/2-1} h_{N/2}}{3} \left| u'''(\xi_{N/2}^-) \right|, \tag{5.28}$$

where $\xi_{N/2}^- \in (x_{N/2-2}, x_{N/2})$. Similarly, for the last term in (5.26),

$$\left| \left(\mathcal{D}_2^+ - \frac{d}{dx} \right) u_{N/2} \right| = \frac{h_{N/2+1} \hbar_{N/2+1}}{3} \left| u'''(\xi_{N/2}^+) \right|, \tag{5.29}$$

where $\xi^{+}_{N/2} \in (x_{N/2}, x_{N/2+2})$. Substituting (5.28)-(5.29) into (5.26), it follows that

$$\left|\mathcal{R}_i^{(3)}\right| \leq C\left\{\max_{N/2-1\leq i\leq N/2+2}\ \max_{x\in[x_{N/2-2},x_{N/2+2}],x\neq x_{N/2}} h_i^2\left|u^{'''}(x)\right|\right\}.$$

Then, using the result in Lemma 5.2.2 and observing that the exponential terms tend to zero when $\varepsilon \to 0$ (for proof, see (Patidar, 2005)),

$$\left|\mathcal{R}_i^{(3)}\right| \leq C\left\{\max_{N/2-1\leq i\leq N/2+2} h_i^2\right\},$$

which, along with (5.24)-(5.25), leads to (5.23). □

Lemma 5.4.3. *For $x \in \Omega_N^- \cup \Omega_N^+$, the following estimates hold:*

$$\max_{x\in[x_{i-1/2},x_i]} \sqrt{\varepsilon} h_i^2\left|u'''(x)\right| \leq C\left\{\max_i h_i^2\right\} \tag{5.30}$$

and

$$\max_{x\in[x_{i-1/2},x_{i+1/2}]} \varepsilon \hbar_i^2\left|u_i^{(4)}(x)\right| \leq C\left\{\max_i h_i^2\right\}. \tag{5.31}$$

Proof. To prove (5.30), the estimate of $u'''(x)$ from (5.4) can be used. For each $x_i \in \Omega_N^-$,

$$\begin{aligned}
\max_{x\in[x_{i-1/2},x_i]} \sqrt{\varepsilon} h_i^2\left|u'''(x)\right| \leq& \sqrt{\varepsilon} h_i^2\left\{C\left[1+\varepsilon^{-\frac{3}{2}}\left(e^{-\sqrt{\frac{\beta}{\varepsilon}}x_{i-1/2}}+e^{-\sqrt{\frac{\beta}{\varepsilon}}(d-x_i)}\right)\right]\right\}\\
\leq& C\left\{h_i^2+\frac{h_i^2}{\varepsilon}\left(e^{-\sqrt{\frac{\beta}{\varepsilon}}x_{i-1/2}}+e^{-\sqrt{\frac{\beta}{\varepsilon}}(d-x_i)}\right)\right\}\\
\leq& C\left\{h_i^2+\frac{1}{\varepsilon}\left(\int_{x_{i-1}}^{x_i} e^{-\sqrt{\frac{\beta}{\varepsilon}}\frac{t}{2}}d\xi\right)^2+\frac{1}{\varepsilon}\left(\int_{x_i}^{x_i+1} e^{-\sqrt{\frac{\beta}{\varepsilon}}\frac{(d-\xi)}{2}}d\xi\right)^2\right\}.
\end{aligned}$$

From this, it follows that

$$\begin{aligned}
&\max_{x\in[x_{i-1/2},x_i]} \sqrt{\varepsilon} h_i^2\left|u'''(x)\right|\\
&\qquad\leq C\left\{h_i^2+\frac{1}{\varepsilon}\left(\sqrt{\varepsilon}\int_{x_{i-1}}^{x_i} \rho(u(\xi),\xi)d\xi\right)^2+\frac{1}{\varepsilon}\left(\sqrt{\varepsilon}\int_{x_i}^{x_i+1} \rho(u(\xi),\xi)d\xi\right)^2\right\}.
\end{aligned}$$

Using (5.14), it then gives

$$\max_{x\in[x_{i-1/2},x_i]} \sqrt{\varepsilon}h_i^2 \left|u'''(x)\right| \leq C\left\{h_i^2 + \left(\frac{2}{N}\int_0^d \rho(u(\xi),\xi)d\xi\right)^2 + \left(\frac{2}{N}\int_0^d \rho(u(\xi),\xi)d\xi\right)^2\right\}.$$

Noting that $\frac{2}{N} \leq \max_i h_i$ and using (5.16)-(5.17), it follows that

$$\max_{x\in[x_{i-1/2},x_i]} \sqrt{\varepsilon}h_i^2 \left|u'''(x)\right| \leq C\left\{\max_i h_i^2\right\}.$$

The same argument gives a similar result for $x_i \in \Omega_N^+$ and completes the proof for (5.30). The estimate in (5.31) can also be proven similarly. $\square$

Theorem 5.1. *Let u_i be the solution of (5.1) and U_i be the solution of (5.12) on the equidistributed grid $\bar{\Omega}_N$. Under the assumptions of Lemma 5.2.2,*

$$\max_{0\leq i\leq N} |U_i - u_i| \leq C\left\{\max_i h_i^2\right\}. \tag{5.32}$$

Proof. The proof follows from the error equation (5.22) and Lemma 5.4.1. First, apply Lemma 5.4.1 to (5.22), which gives

$$\max_{0\leq i\leq N} |U_i - u_i| = \max_{0\leq i\leq N} |e_i| \leq C \max_{1\leq i\leq N-1, i\neq N/2} |\mathcal{R}_i|. \tag{5.33}$$

From Lemma 5.4.2, the inequality

$$\max_{1\leq i\leq N-1, i\neq N/2} |\mathcal{R}_i| \leq C\left\{\max_i h_i^2\right\} \tag{5.34}$$

is also obtained because of Lemma 5.4.3. Finally, combining (5.33) with (5.34) gives (5.32). $\square$

5.5 Numerical results and discussion

This section offers a detailed overview of the effectiveness of the proposed numerical scheme by presenting two examples that validate the theoretical analysis. Additionally, the accuracy and efficiency of the scheme are compared to existing schemes discussed in the literature. In the numerical experiments, the user-chosen constant or stopping criterion C_0 mentioned in the algorithm is taken to be $C_0 = 1.05$ to generate the adaptive grid.

Example 5.1. *Consider the SPFIDE in ([Rathore et al., 2023]),*

$$-\varepsilon u''(x) + (2 - e^{-x})u(x) + \frac{1}{2}\int_0^1 e^{x\cos(\pi\xi)}u(\xi)d\xi = \begin{cases} \frac{-1}{1+x}, & 0 < x \leq 1/2, \\ \frac{1}{1+x}, & 1/2 < x < 1 \end{cases}$$

and boundary conditions

$$u(0) = 1, \quad u(1) = 0.$$

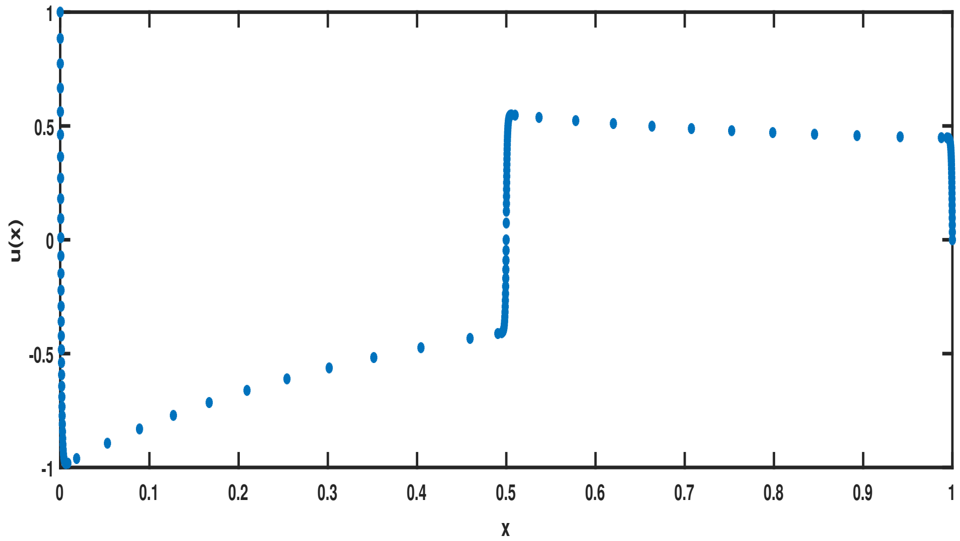

Figure 5.1: Numerical solution for $\varepsilon = 10^{-6}$ and $N = 128$ for Example 5.1.

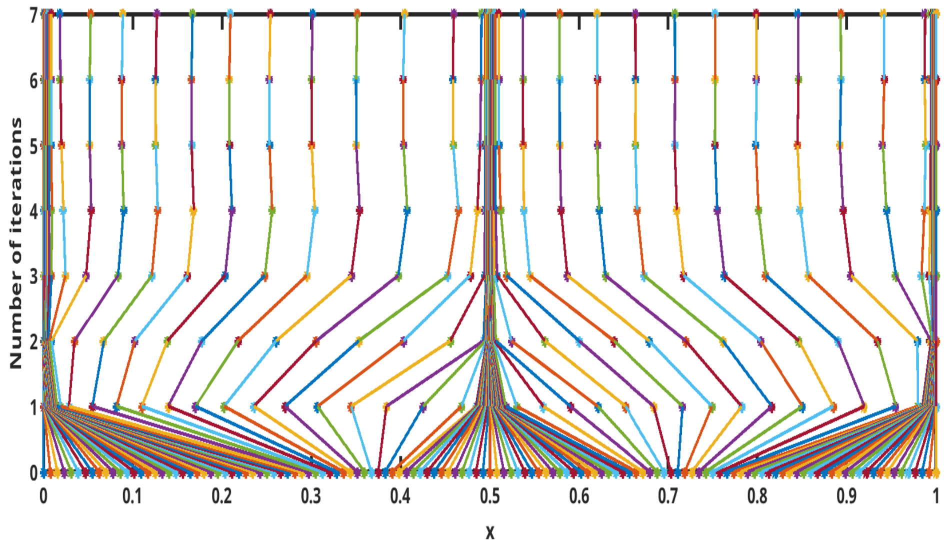

Figure 5.2: Mesh movement for $\varepsilon = 10^{-6}$ and $N = 128$ for Example 5.1.

Table 5.1: Rate of convergence and maximum absolute error of the proposed scheme for different values of ε and N for Example 5.1

ε	N=64	N=128	N=256	N=512	N=1024	N=2048
10^{-0}	2.0362e-05	5.0685e-06	1.2659e-06	3.1631e-07	7.9013e-08	1.9649e-08
	2.01	2.00	2.00	2.00	2.01	
10^{-1}	6.1832e-05	1.2755e-05	2.8268e-06	6.7608e-07	1.6582e-07	4.1070e-08
	2.28	2.17	2.06	2.03	2.01	
10^{-2}	1.2022e-03	2.9885e-04	7.4115e-05	1.8495e-05	4.6197e-06	1.1544e-06
	2.01	2.01	2.00	2.00	2.00	
10^{-3}	2.2008e-03	5.3740e-04	1.3209e-04	3.2988e-05	8.2248e-06	2.0525e-06
	2.03	2.02	2.00	2.00	2.00	
10^{-4}	3.0577e-03	7.1898e-04	1.7552e-04	4.3571e-05	1.0882e-05	2.7163e-06
	2.09	2.03	2.01	2.00	2.00	
10^{-5}	3.4415e-03	8.0966e-04	1.9663e-04	4.8706e-05	1.2127e-05	3.0268e-06
	2.09	2.04	2.01	2.01	2.00	
10^{-6}	3.7074e-03	8.5568e-04	2.0712e-04	5.0757e-05	1.2632e-05	3.1452e-06
	2.12	2.05	2.03	2.01	2.01	
10^{-7}	3.7936e-03	8.8612e-04	2.1003e-04	5.1829e-05	1.2836e-05	3.1978e-06
	2.10	2.08	2.02	2.01	2.01	
10^{-8}	3.8987e-03	9.0321e-04	2.1319e-04	5.2183e-05	1.2918e-05	3.2186e-06
	2.11	2.08	2.03	2.01	2.00	
10^{-9}	3.9746e-03	9.1422e-04	2.1584e-04	5.2596e-05	1.2985e-05	3.2257e-06
	2.12	2.08	2.04	2.02	2.01	
10^{-10}	4.0299e-03	9.2376e-04	2.1805e-04	5.2839e-05	1.3020e-05	3.2332e-06
	2.13	2.08	2.05	2.02	2.01	
10^{-11}	4.0746e-03	9.3306e-04	2.1870e-04	5.2992e-05	1.3034e-05	3.2374e-06
	2.13	2.09	2.05	2.02	2.01	
e^N	4.0746e-03	9.3306e-04	2.1870e-04	5.2992e-05	1.3034e-05	3.2374e-06
r^N	2.13	2.09	2.05	2.02	2.01	

Table 5.2: A comparison of the numerical results of Example 5.1 using the proposed scheme with the scheme in (Rathore et al., 2023)

Scheme	N=64	N=128	N=256	N=512	N=1024
Scheme in	3.0200e-02	1.5360e-02	7.7460e-03	3.8890e-03	1.9490e-03
(Rathore et al., 2023)	0.98	0.99	0.99	1.00	
Proposed scheme	4.0746e-03	9.3306e-04	2.1870e-04	5.2992e-05	1.3034e-05
	2.13	2.09	2.05	2.02	2.01

Example 5.2. *([Rathore et al.], [2023]) Consider the problem*

$$-\varepsilon u''(x)+(1+\sin(\pi x/2))u(x)+\frac{1}{2}\int_0^1 e^{1-x\xi}u(\xi)d\xi=\begin{cases}-8, & 0<x\leq 2/5,\\ 8, & 2/5<x<1\end{cases}$$

with boundary conditions

$$u(0)=1,\quad u(1)=1.$$

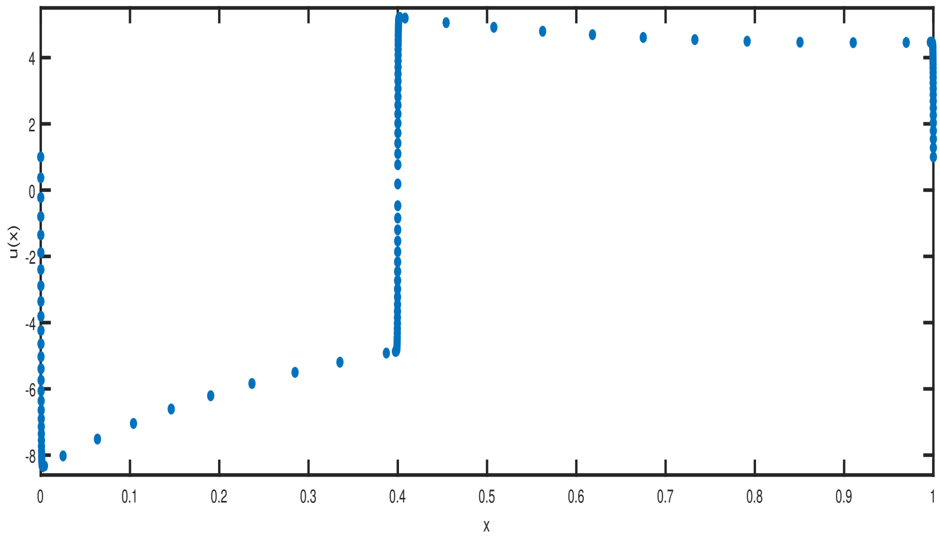

Figure 5.3: Numerical solution for $\varepsilon=10^{-7}$ and $N=128$ for Example 5.2.

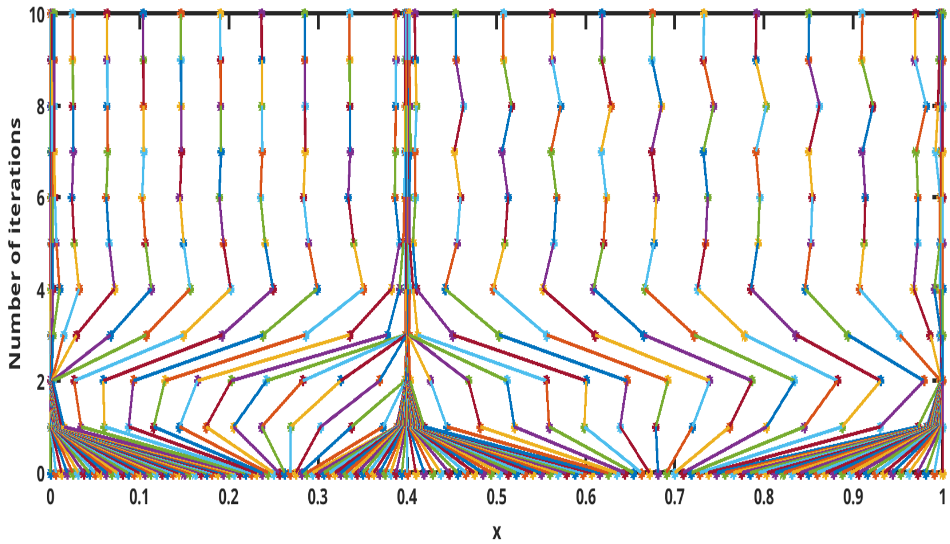

Figure 5.4: Mesh movement for $\varepsilon=10^{-7}$ and $N=128$ for Example 5.2.

Table 5.3: Rate of convergence and maximum absolute error of the proposed scheme for different values of ε and N of Example 5.2

ε	N=64	N=128	N=256	N=512	N=1024	N=2048
10^{-0}	7.3809e-05	1.8978e-05	4.8123e-06	1.2117e-06	3.0400e-07	7.5773e-08
	1.96	1.98	1.99	1.99	2.00	
10^{-1}	1.6311e-03	4.0982e-04	1.0274e-04	2.5721e-05	6.4348e-06	1.6091e-06
	1.99	2.00	2.00	2.00	2.00	
10^{-2}	3.5221e-03	7.6974e-04	1.7786e-04	4.2609e-05	1.0419e-05	2.5755e-06
	2.19	2.11	2.06	2.03	2.02	
10^{-3}	6.8027e-03	1.5309e-03	3.8306e-04	9.6572e-05	2.4206e-05	6.0600e-06
	2.15	2.00	1.99	2.00	2.00	
10^{-4}	1.0767e-02	2.4531e-03	5.9234e-04	1.2969e-04	3.1343e-05	7.7540e-06
	2.13	2.05	2.19	2.05	2.02	
10^{-5}	1.3539e-02	2.9981e-03	7.3896e-04	1.7972e-04	4.7550e-05	1.0141e-05
	2.18	2.02	2.04	1.92	2.23	
10^{-6}	1.4297e-02	3.2949e-03	7.8660e-04	1.9384e-04	4.8001e-05	1.1958e-05
	2.12	2.07	2.02	2.01	2.01	
10^{-7}	1.4960e-02	3.4507e-03	8.1893e-04	1.9965e-04	4.9447e-05	1.2305e-05
	2.12	2.08	2.04	2.01	2.01	
10^{-8}	1.5094e-02	3.5061e-03	8.3299e-04	2.0211e-04	5.0072e-05	1.2433e-05
	2.11	2.07	2.04	2.01	2.01	
10^{-9}	1.5429e-02	3.5443e-03	8.4304e-04	2.0373e-04	5.0143e-05	1.2494e-05
	2.12	2.07	2.05	2.02	2.00	
10^{-10}	1.5748e-02	3.5829e-03	8.4927e-04	2.0476e-04	5.0202e-05	1.2536e-05
	2.14	2.08	2.05	2.03	2.00	
10^{-11}	1.5926e-02	3.6146e-03	8.5588e-04	2.0511e-04	5.0201e-05	1.2564e-05
	2.12	2.07	2.05	2.02	2.00	
10^{-12}	1.6193e-02	3.6384e-03	8.5704e-04	2.0587e-04	5.0339e-05	1.2580e-05
	2.15	2.09	2.06	2.03	2.00	
e^N	1.6193e-02	3.6384e-03	8.5704e-04	2.0587e-04	5.0339e-05	1.2580e-05
r^N	2.15	2.09	2.06	2.03	2.00	

Table 5.4: A comparison of the numerical results of Example 5.2 using the proposed scheme with the scheme in (Rathore et al., 2023)

Scheme	N=64	N=128	N=256	N=512	N=1024
Scheme in	1.5120e-01	7.6480e-02	3.9100e-02	1.9890e-02	1.0030e-02
(Rathore et al., 2023)	0.98	0.97	0.98	0.99	
Proposed scheme	1.6193e-02	3.6384e-03	8.5704e-04	2.0587e-04	5.0339e-05
	2.15	2.09	2.06	2.03	2.00

Figures 5.1 and 5.3 display the well-resolved mesh distributions of the numerical

solution using the equidistribution of the mesh density function in (5.13). Figures 5.2 and 5.4 correspondingly depict the resulting mesh movement. These plots conclusively demonstrate the presence of boundary layers at $x = 0$ and $x = 1$, along with an interior layer at the point of discontinuity.

After analyzing Tables 5.1 and 5.3, it can be concluded that the errors in the results remain uniform and are not affected by the perturbation parameter ε. Moreover, the calculated solution achieved second-order accuracy, which perfectly aligns with the estimation in Theorem 5.1. Based on the data presented in Tables 5.2 and 5.4, it can also be concluded that the proposed scheme exhibits superior accuracy compared to that of (Rathore et al., 2023). These tables provide strong evidence of the superiority of the scheme in terms of accuracy and convergence.

5.6 Summary

A novel numerical approach for solving a second-order singularly perturbed Fredholm integro-differential equation with a discontiguous source term is proposed. The equation exhibits two boundary layers resulting from the perturbation parameter and an interior layer caused by a single discontinuity in the source function. To solve the problem, a centered finite difference scheme and a composite trapezoidal rule are employed. The impact of the perturbation parameter is effectively addressed by implementing an adaptive mesh, which is generated using the grid equidistribution method. The proposed scheme demonstrated better numerical outcomes compared to other existing numerical schemes. Furthermore, the theoretical error calculations are confirmed through numerical experiments, which showed a second-order uniform convergence independent of the perturbation parameter.

CHAPTER SIX

CONVECTION DIFFUSION TYPE SINGULARLY PERTURBED FREDHOLM INTEGRO-DIFFERENTIAL EQUATION WITH A DISCONTINUOUS SOURCE

Transitioning from Chapter 5's reaction-diffusion focus, this chapter explores a new frontier: convection-diffusion SPFIDEs. Similar to Chapter 5, a discontinuity is introduced in the source term to add complexity and challenge the numerical scheme. While the core numerical method remains the same as in Chapter 5, a key distinction lies in the utilization of a different mesh density function.

6.1 Description of the problem

The problem considered is the following second-order SPFIDE of convection-diffusion type:

$$\begin{cases} \mathcal{L}_\varepsilon u := \varepsilon^2 u''(x) + \varepsilon a(x)u'(x) - b(x)u(x) + \lambda \int\limits_0^1 K(x,\xi)u(\xi)d\xi = f(x), \, x \in \Omega^- \cup \Omega^+, \\ f(d-) \neq f(d+), \\ u(0) = A, \quad u(1) = B, \end{cases} \tag{6.1}$$

where d is a point within the domain $\Omega = (0,1)$ where the discontinuity in the source term f emerges, $\Omega^- = (0,d)$ and $\Omega^+ = (d,1)$. Moreover, $0 < \varepsilon \ll 1$ is a perturbation parameter and λ is a real parameter. The function a and b belong to the class $C^2(\bar{\Omega})$ and satisfy the conditions $a(x) > \alpha > 0$ and $b(x) \geq \beta > 0$, respectively. Similarly, the function K is also in $C^2(\bar{\Omega} \times \bar{\Omega})$. Boundary layers appear at $x = 0$ and $x = 1$, while an interior layer arises at $x = d$.

6.2 A priori bounds on the solution and its derivatives

This section begins by establishing a foundational analytical result. This result serves as a cornerstone for the subsequent error analysis of the proposed numerical scheme. The differential operator ℓ_ε in (6.1) for all $\Psi \in C^0(\bar{\Omega}) \cap C^2(\Omega^- \cup \Omega^+)$ satisfies the following minimum principle on $\bar{\Omega}$.

Lemma 6.2.1. *(**Minimum principle**) Assume that a function $\Psi \in C^0(\bar{\Omega}) \cap C^2(\Omega^- \cup \Omega^+)$ satisfies*

$$\begin{aligned} \Psi(0) &\geq 0, \quad \Psi(1) \geq 0 \\ \ell_\varepsilon \Psi(x) &\leq 0, \quad \textit{for all}\, x \in \Omega^- \cup \Omega^+ \\ [\Psi](d) &= 0, \quad [\Psi'](d) \leq 0. \\ \textit{Then} \quad \Psi(x) &\geq 0, \quad \textit{for all}\, x \in \bar{\Omega}. \end{aligned}$$

Proof. The proof is similar to that of Lemma 2 in (Farrell et al., 2000). ☐

Lemma 6.2.2. *Assume that $a, b \in C^2(\bar{\Omega})$, $f \in C^2(\Omega^- \cup \Omega^+)$ and $\frac{\partial^s K}{\partial x^s}, \frac{\partial^s K}{\partial \xi^s} \in C(\bar{\Omega} \times \bar{\Omega})$, $s = 0, 1, 2$. Let*

$$|\lambda| < \frac{\beta}{\max\limits_{0 \leq x \leq 1} \int_0^1 |K(x,\xi)|\, d\xi} \tag{6.2}$$

and u be the solution of (6.1). Then for all $x \in \bar{\Omega}$,

$$\|u\|_\infty \leq C, \tag{6.3}$$

and, $\forall k$, $1 \leq k \leq 3$,

$$\left|u^{(k)}(x)\right| \leq C \begin{cases} 1 + \varepsilon^{-k}\left(e^{-\frac{c_0}{\varepsilon}x} + e^{-\frac{c_1}{\varepsilon}(d-x)}\right), & x \in \Omega^-, \\ 1 + \varepsilon^{-k}\left(e^{-\frac{c_1}{\varepsilon}(x-d)} + e^{-\frac{c_2}{\varepsilon}(1-x)}\right), & x \in \Omega^+, \end{cases} \tag{6.4}$$

where

$$c_0 = \frac{1}{2}\left(\sqrt{a^2(0)+4b(0)}+a(0)\right), c_1 = \frac{1}{2}\left(\sqrt{a^2(d)+4b(d)}+a(d)\right) \text{ and}$$
$$c_2 = \frac{1}{2}\left(\sqrt{a^2(1)+4b(1)}-a(1)\right).$$

Proof. The result for (6.3) follows from the minimum principle satisfied by the difference operator $\ell_\varepsilon u(x) := \varepsilon^2 u''(x) + \varepsilon a(x)u' - b(x)u$. Likewise, for (6.4), the result can be derived by employing the method utilized for the corresponding first-type boundary value problem in Lemma 2.2 (Amiraliyev & Cakir, 2000), along with the analogous approach used for cases involving discontinuous source and convection terms in (Farrell et al., 2000). □

6.3 The numerical scheme

This section explores the discretization of problem (6.1) to develop the numerical scheme, followed by implementing it on an adaptive mesh.

6.3.1 The discrete scheme

To generate the adaptive grid $\bar{\Omega}$, the same technique as detailed in section 5.3.1 is utilized. A smooth transition at the point of discontinuity is ensured by imposing the condition

$$\mathcal{D}^- u_{N/2} = \mathcal{D}^+ u_{N/2},$$

where

$$D^- u_{N/2} = \frac{u_{N/2} - u_{N/2-1}}{h_{N/2}}$$

and

$$D^+ u_{N/2} = \frac{u_{N/2+1} - u_{N/2}}{h_{N/2+1}}.$$

To derive the discretization scheme for (6.1), a finite difference approximation is employed to calculate the derivative component. Simultaneously, the composite trapezoidal rule is employed for the numerical approximation of the integral, resulting in

$$\begin{cases} \mathcal{L}_\varepsilon u_i := \left(\varepsilon^2\delta^2 + \varepsilon a_i D^+ - b_i\right) u_i + \frac{\lambda}{2} \sum\limits_{j=1}^{N} h_j \left(K_{i,j-1}u_{j-1} + K_{i,j}u_j\right) + \mathcal{R}_i = f_i \\ u_0 = A, \quad u_N = B, \\ \mathcal{D}^- u_{N/2} = \mathcal{D}^+ u_{N/2}. \end{cases} \tag{6.5}$$

$\mathcal{R}_i$ in (6.5) is the truncation error

$$\mathcal{R}_i = \mathcal{R}_i^{(1)} + \mathcal{R}_i^{(2)} + \mathcal{R}^{(3)}, \tag{6.6}$$

where

$$\mathcal{R}_i^{(1)} = \varepsilon^2 \left(u_i'' - \delta^2 u_i\right) + \varepsilon a_i \left(u_i' - D^+ u_i\right), \tag{6.7}$$

$$\mathcal{R}_i^{(2)} = \frac{\lambda}{2} \sum_{j=1}^{N} \int_{x_{j-1}}^{x_j} (x_{j-1} - \xi)(x_j - \xi) \frac{\partial^2}{\partial \xi^2} \left(K(x_i, \xi) u(\xi)\right) d\xi, \tag{6.8}$$

$$\mathcal{R}^{(3)} = \left(D^- - \frac{d}{dx}\right) u(x_{N/2}) - \left(D^+ - \frac{d}{dx}\right) u(x_{N/2}). \tag{6.9}$$

After neglecting the remainder term in (6.5), the following scheme is obtained to approximate (6.1):

$$\begin{cases} \mathcal{L}_\varepsilon^N U_i := \left(\varepsilon^2\delta^2 + \varepsilon a_i D^+ - b_i\right) U_i + \frac{\lambda}{2} \sum\limits_{j=1}^{N} h_j \left(K_{i,j-1}U_{j-1} + K_{i,j}U_j\right) = f_i, \\ U_0 = A, \quad U_N = B, \\ D^- U_{N/2} = D^+ U_{N/2}. \end{cases} \tag{6.10}$$

6.3.2 Adaptive grid generation via equidistribution

The implementation of equidistribution begins with defining a mesh density function,

$$\rho(u(\xi), \xi) = 1 + \left|u''(\xi)\right|^{\frac{1}{2}}, \tag{6.11}$$

which quantifies the expected error at each point in the domain $\bar{\Omega}_N$. Independently employing equidistribution to the two sides of the domain $\bar{\Omega}_N$, which has been divided using d, one obtains the following equalities:

$$\int_{x_{i-1}}^{x_i} \rho(u(\xi), \xi) d\xi = \frac{2}{N} \int_0^d \rho(u(\xi), \xi) d\xi, \quad i = 1, 2, \ldots, N/2 \tag{6.12}$$

and

$$\int_{x_{i-1}}^{x_i} \rho(u(\xi),\xi)d\xi = \frac{2}{N}\int_d^1 \rho(u(\xi),\xi)d\xi, \quad i = N/2+1, N/2+2, \ldots, N. \tag{6.13}$$

Lemma 6.3.1. *The mesh density function $\rho(u(\xi),\xi)$ defined in (6.11) satisfies the estimates*

$$\int_0^d \rho(u(\xi),\xi)d\xi \le C \text{ and } \int_d^1 \rho(u(\xi),\xi)d\xi \le C. \tag{6.14}$$

Proof. By integrating (6.11) over $[0,d]$ and using (6.4) gives

$$\begin{aligned}
\int_0^d \rho(u(\xi),\xi)d\xi &= \int_0^d \left(1+\left|u''(\xi)\right|^{\frac{1}{2}}\right)d\xi \\
&\le d + C\int_0^d \left(1+\varepsilon^{-2}\left(e^{-\frac{c_0}{\varepsilon}\xi}+e^{-\frac{c_1}{\varepsilon}(d-\xi)}\right)\right)^{\frac{1}{2}}d\xi \\
&\le d + C\int_0^d \left(1+\varepsilon^{-1}\left(e^{-\frac{c_0}{2\varepsilon}\xi}+e^{-\frac{c_1}{2\varepsilon}(d-\xi)}\right)\right)d\xi \\
&= d + C\left(d+\frac{2}{c_0}\left(1-e^{-\frac{c_0}{2\varepsilon}d}\right)+\frac{2}{c_1}\left(1-e^{-\frac{c_1}{2\varepsilon}d}\right)\right) \\
&\le C.
\end{aligned}$$

Similarly, for the second result in (6.14), it follows that

$$\begin{aligned}
\int_d^1 \rho(u(\xi),\xi)d\xi &= \int_d^1 \left(1+\left|u''(\xi)\right|^{\frac{1}{2}}\right)d\xi \\
&\le 1-d + C\int_d^1 \left(1+\varepsilon^{-2}\left(e^{-\frac{c_1}{\varepsilon}(\xi-d)}+e^{-\frac{c_2}{\varepsilon}(1-\xi)}\right)\right)^{\frac{1}{2}}d\xi \\
&\le 1-d + C\int_d^1 \left(1+\varepsilon^{-1}\left(e^{-\frac{c_1}{2\varepsilon}(\xi-d)}+e^{-\frac{c_2}{2\varepsilon}(1-\xi)}\right)\right)d\xi \\
&= 1-d + C\left(1-d+\frac{2}{c_1}\left(1-e^{-\frac{c_1}{2\varepsilon}(1-d)}\right)+\frac{2}{c_2}\left(1-e^{-\frac{c_2}{2\varepsilon}(1-d)}\right)\right) \\
&\le C,
\end{aligned}$$

and the proof is complete. □

Lemma 6.3.2. *The grid spacing h_i satisfies the estimate*

$$h_i \le CN^{-1}, \quad i = 1,2,\ldots,N. \tag{6.15}$$

Proof. For $i = 1,2,\ldots,N/2$, using Lemma 6.3.1 and (6.12),

$$h_i = x_i - x_{i-1} \leq \int_{x_{i-1}}^{x_i} \rho(u(\xi),\xi)d\xi = \frac{2}{N}\int_0^d \rho(u(\xi),\xi)d\xi \leq CN^{-1}.$$

The proof for $i = N/2+1, N/2+2, \ldots, N$ can be achieved using similar steps. □

The problem (6.1) is addressed by employing a modified variant of the algorithm introduced in Chapter 5. This approach utilizes (6.10) and achieves equidistribution through the mesh density function

$$\rho_i = 1 + \left|\delta^2 U_i^{(k)}\right|^{\frac{1}{2}},$$

which serves as the discrete counterpart of equation (6.11). Given the unknown values of the grid $\{x_i\}_{i=0}^N$ and the solution $\{U_i\}_{i=0}^N$, resolving the equidistribution problem necessitates simultaneously solving (6.10) and the relations

$$h_j\rho_j = \frac{2}{N}\sum_{i=1}^{N/2} h_i\rho_i,\ 1 \leq j \leq N/2 \ \text{ and } \ h_j\rho_j = \frac{2}{N}\sum_{i=N/2+1}^{N} h_i\rho_i,\ N/2 \leq j \leq N$$

to determine the values of $\{x_i, U_i\}$.

Algorithm 3 Adaptive mesh generation

1. Initialize the piecewise uniform mesh $\Omega_N^{(0)}$ and the user-specified constant $C_0 > 1$.
2. Obtain $\left\{U_i^{(k)}\right\}_{i=0}^N$ by solving (6.10) on $\Omega_N^{(k)}$ and compute $\rho_i^{(k)} = 1 + \left|\delta^2 U_i^{(k)}\right|^{\frac{1}{2}}$. Set $\rho_0^{(k)} = \rho_1^{(k)}$, $\rho_N^{(k)} = \rho_{N-1}^{(k)}$; define $w_i^{(k)} = \frac{\rho_{i-1}^{(k)}+\rho_i^{(k)}}{2}$, $i = 1,2,\ldots,N$.
3. Let $L_{1,0}^{(k)} = 0$ and $L_{2,0}^{(k)} = 0$. For $1 \leq i \leq N/2$, set $L_{1,i}^{(k)} = \sum_{j=1}^{i} h_j^{(k)} w_j^{(k)}$ and $L_{2,i}^{(k)} = \sum_{j=N/2+1}^{N/2+i} h_j^{(k)} w_j^{(k)}$, where $h_i^{(k)} = x_i^{(k)} - x_{i-1}^{(k)}$. Then, define $C_*^{(k)} = \frac{N}{2L_{1,N/2}^{(k)}} \max_{1\leq i\leq N/2} h_i^{(k)} w_i^{(k)}$ and $C_{**}^{(k)} = \frac{N}{2L_{2,N/2}^{(k)}} \max_{N/2+1\leq i\leq N} h_i^{(k)} w_i^{(k)}$. If $C_*^{(k)}, C_{**}^{(k)} \leq C_0$, go to 5; Otherwise, proceed to the next step.
4. Set $\omega_{1,i}^{(k)} := 2iL_{1,N}^{(k)}/N$ and $\omega_{2,i}^{(k)} := 2iL_{2,N}^{(k)}/N$, $i = 0,1,\ldots,N/2$. Then, interpolate to the points $(L_{1,i}^{(k)}, x_i^{(k)})$ and $(L_{2,i}^{(k)}, x_{N/2+i}^{(k)})$. Generate $\left\{x^{(k+1)}\right\}$ by computing the interpolants at $\left\{\omega_{1,i}^{(k)}\right\}_{i=0}^{N/2}$ and $\left\{\omega_{2,i}^{(k)}\right\}_{i=0}^{N/2}$. Increment k and go to step 2.
5. Set $\Omega_N^* = \left\{x_i^{(k)}\right\}_{i=0}^N$ and $U^* = \left\{U_i^{(k)}\right\}_{i=0}^N$ as the final mesh and solution; stop.

6.4 Stability and uniform convergence

This section presents the outcome of a stability assessment alongside an analysis of truncation errors. This combined analysis leads to an estimation of errors aligned with specified requirements.

6.4.1 A stability result

The following stability result is presented to establish the convergence of the numerical solution.

Lemma 6.4.1. *Under the assumptions of Lemma 6.2.2 and*

$$|\lambda| < \frac{\beta}{\max\limits_{1\leq i\leq N-1, i\neq N/2} \sum\limits_{j=1}^{N} \frac{h_j}{2}\left(|K_{i,j-1}|+|K_{i,j}|\right)},$$

the solution of (6.10) satisfies

$$\max_{0\leq i\leq N} |U_i| \leq \frac{|A|+|B|+\frac{1}{\beta}\max\limits_{1\leq i\leq N-1, i\neq N/2} |f_i|}{1-|\lambda|\frac{1}{\beta}\max\limits_{i\neq N/2, 1\leq i\leq N-1} \sum\limits_{j=1}^{N} \frac{h_j}{2}\left(|K_{i,j-1}|+|K_{i,j}|\right)}.$$

Proof. The proof is similar to that of Lemma 5.4.1, but utilizes the minimum principle satisfied by the difference operator $\ell_\varepsilon^N = \varepsilon^2\delta^2 + \varepsilon a_i D^+ - b_i$. □

6.4.2 Error analysis

The error in the solution defined by (6.10) is now analyzed. The pointwise error can be denoted as $e_i = U_i - u_i$. Deducting (6.5) from (6.10) yields a simplified expression for the error:

$$\begin{cases} \mathcal{L}_\varepsilon^N e_i = \mathcal{R}_i, \quad 1\leq i\leq N-1, i\neq N/2, \\ e_0 = e_N = 0, \\ \mathcal{D}^- e_{N/2} = \mathcal{D}^+ e_{N/2}, \end{cases} \tag{6.16}$$

where $\mathcal{R}_i$ is given by (6.6).

Lemma 6.4.2. *For all interior mesh points Ω_N, the truncation error $\mathcal{R}_i$ satisfies the estimate*

$$\max_{1\le i\le N-1, i\ne N/2} |\mathcal{R}_i| \le CN^{-1}. \tag{6.17}$$

Proof. To establish the validity of the lemma, separate estimations of the truncation errors found within (6.6) are conducted. For $\mathcal{R}_i^{(1)}$, it follows from (6.7) that

$$\begin{aligned}\mathcal{R}_i^{(1)} =& \frac{\varepsilon^2}{2\hbar_i}\left(\frac{1}{h_i}\int_{x_{i-1}}^{x_i}(\xi - x_{i-1})^2 u'''(\xi)d\xi - \frac{1}{h_{i+1}}\int_{x_i}^{x_{i+1}}(x_{i+1}-\xi)^2 u'''(\xi)d\xi\right)\\ &+ \frac{\varepsilon a_i}{h_{i+1}}\int_{x_i}^{x_{i+1}}(x_{i+1}-\xi)u''(\xi)d\xi.\end{aligned}$$

From this, it follows that

$$\begin{aligned}\left|\mathcal{R}_i^{(1)}\right| \le& \frac{\varepsilon^2}{2\hbar_i}\left(h_i\int_{x_{i-1}}^{x_i}\left|u'''(\xi)\right|d\xi + h_{i+1}\int_{x_i}^{x_{i+1}}\left|u'''(\xi)\right|d\xi\right) + \varepsilon a_i\int_{x_i}^{x_{i+1}}\left|u''(\xi)\right|d\xi\\ \le& \int_{x_{i-1}}^{x_{i+1}}\varepsilon^2\left|u'''(\xi)\right|d\xi + a_i\int_{x_i}^{x_{i+1}}\varepsilon\left|u''(\xi)\right|d\xi.\end{aligned}$$

From Lemma 6.2.2, note that $\varepsilon^2|u'''|$, $\varepsilon|u''|$ and $\sqrt{|u''|}$ are $O(1/\varepsilon)$. On this basis, it is reasonable to infer that

$$\begin{aligned}\left|\mathcal{R}_i^{(1)}\right| \le& C\int_{x_{i-1}}^{x_{i+1}}\left|u''(\xi)\right|^{\frac{1}{2}}d\xi\\ \le& C\int_{x_{i-1}}^{x_{i+1}}\rho(u(\xi),\xi)d\xi\\ \le& C\left\{\frac{2}{N}\int_0^d\rho(u(\xi),\xi)d\xi + \frac{2}{N}\int_d^1\rho(u(\xi),\xi)d\xi\right\}.\end{aligned}$$

By applying (6.14),

$$\left|\mathcal{R}_i^{(1)}\right| \le CN^{-1}. \tag{6.18}$$

For $\mathcal{R}_i^{(2)}$, it follows from (6.8) that

$$\left|\mathcal{R}_i^{(2)}\right| \leq C \left\{ \sum_{i=1}^{N} h_i^3 + \sum_{i=1}^{N} h_i \int_{x_{i-1}}^{x_i} (\xi - x_{i-1}) \left|u''(\xi)\right| d\xi \right\},$$

and using Lemma 6.3.2, it can be deduced that

$$\left|\mathcal{R}_i^{(2)}\right| \leq C \left\{ N^{-2} + \left(\int_{x_{i-1}}^{x_i} \left|u''(\xi)\right|^{\frac{1}{2}} d\xi \right)^2 \right\}.$$

Using (6.12)-(6.13),

$$\left|\mathcal{R}_i^{(2)}\right| \leq C \left\{ N^{-2} + \left(\frac{2}{N} \int_0^d \rho(u(\xi), \xi) d\xi \right)^2 + \left(\frac{2}{N} \int_d^1 \rho(u(\xi), \xi) d\xi \right)^2 \right\}.$$

By (6.14), it can be concluded that

$$\left|\mathcal{R}_i^{(2)}\right| \leq C N^{-2}. \tag{6.19}$$

From (6.9), it can be deduced that the following holds at the point of discontinuity:

$$\left|\mathcal{R}^{(3)}\right| \leq \frac{h_{N/2}}{2} \left|u''(\eta_{N/2}^-)\right| + \frac{h_{N/2+1}}{2} \left|u''(\eta_{N/2}^+)\right|,$$

where $\eta_{N/2}^- \in (x_{N/2-1}, x_{N/2})$ and $\eta_{N/2}^+ \in (x_{N/2}, x_{N/2+1})$. It follows that

$$\left|\mathcal{R}^{(3)}\right| \leq C N^{-1} \left\{ \max_{x \in [x_{N/2-1}, x_{N/2+1}]} \left|u''(x)\right| \right\}.$$

As shown in (Patidar, 2005), the exponential terms in Lemma 6.2.2 vanish as $\varepsilon \to 0$, which implies that

$$\left|\mathcal{R}^{(3)}\right| \leq C N^{-1}.$$

Combining this result with (6.18) and (6.19) then yields

$$\max_{1 \leq i \leq N-1, i \neq N/2} |\mathcal{R}_i| \leq C N^{-1},$$

which completes the proof of the lemma. $\square$

Theorem 6.1. *Let u_i and U_i be the exact and discrete solutions on the equidistributed grid $\bar{\Omega}_N$, respectively. Suppose that the assumptions of Lemma 6.2.2 are satisfied. Then, there exists a constant C such that:*

$$\max_{0\le i\le N}|U_i-u_i|\le CN^{-1}. \tag{6.20}$$

Proof. Applying Lemma 6.4.1 to the error equation (6.16) gives

$$\max_{0\le i\le N}|e_i|=\max_{0\le i\le N}|U_i-u_i|\le C\max_{1\le i\le N-1, i\ne N/2}|\mathcal{R}_i|. \tag{6.21}$$

Then, using (6.17) in (6.21) leads to

$$\max_{0\le i\le N}|U_i-u_i|\le CN^{-1}.$$

This completes the proof of the theorem. □

6.5 Numerical results and discussion

This section offers compelling evidence of the proposed scheme's efficiency by illustrating its effectiveness through two examples, thus solidifying the theoretical analysis. Due to the absence of a closed-form solution for the problems, the double mesh method is employed to compute the maximum absolute error and rate of convergence. In the numerical experiments, the user-specified parameter C_0, mentioned in the algorithm, is set to 1.05 to generate the adaptive grid.

Example 6.1. *Consider the problem*

$$\varepsilon^2u''(x)+\varepsilon(2-e^{1-x^2})u'(x)-\frac{1}{3}u(x)-\frac{1}{3}\int_0^1 e^{(x-\xi)}u(\xi)d\xi=\begin{cases}0.7, \ 0<x<1/2,\\ -0.6, \ 1/2<x<1\end{cases}$$

and boundary conditions

$$u(0)=1, \quad u(1)=0.$$

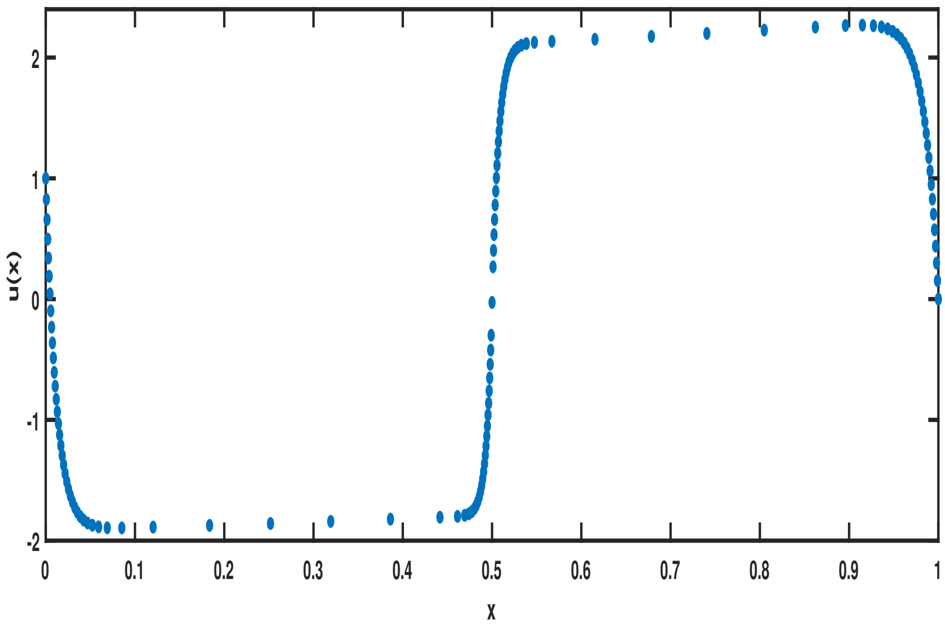

Figure 6.1: Numerical solution for $N = 128$ and $\varepsilon = 2^{-8}$ for Example 6.1.

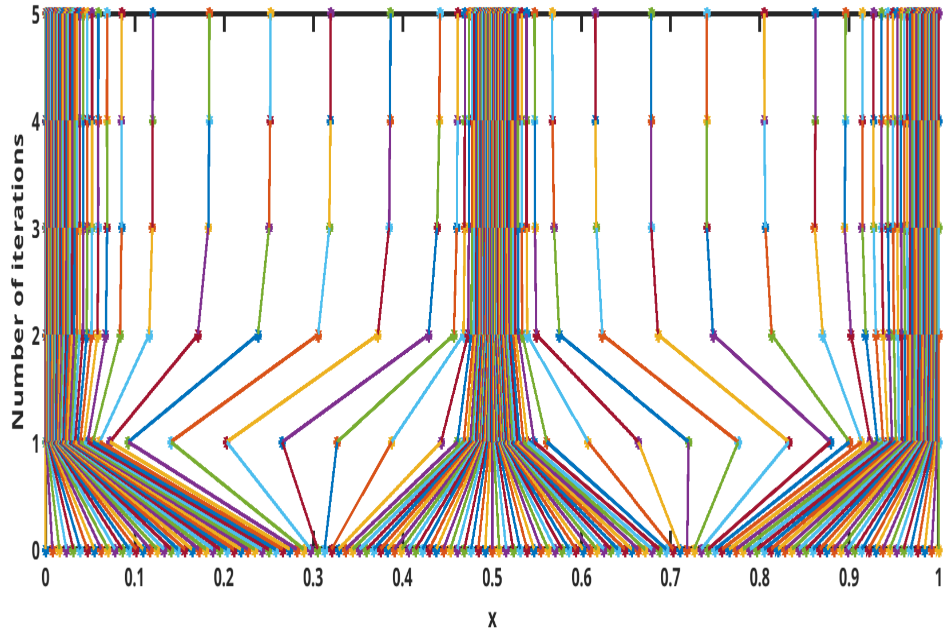

Figure 6.2: Mesh movement for $N = 128$ and $\varepsilon = 2^{-8}$ for Example 6.1.

Table 6.1: Maximum absolute error and convergence rate of the present scheme for Example 6.1 for various values of N and ε.

ε	N=64	N=128	N=256	N=512	N=1024	N=2048
2^{-0}	4.6444e-04	2.3188e-04	1.1586e-04	5.7913e-05	2.8952e-05	1.4475e-05
	1.00	1.00	1.00	1.00	1.00	
2^{-2}	1.6525e-03	8.3851e-04	4.2249e-04	2.1207e-04	1.0625e-04	5.3175e-05
	0.98	0.99	0.99	1.00	1.00	
2^{-4}	1.2122e-02	6.0671e-03	3.0329e-03	1.5161e-03	7.5789e-04	3.7891e-04
	1.00	1.00	1.00	1.00	1.00	
2^{-6}	2.2189e-02	1.1076e-02	5.5278e-03	2.7613e-03	1.3799e-03	6.8978e-04
	1.00	1.00	1.00	1.00	1.00	
2^{-8}	2.5723e-02	1.2808e-02	6.4181e-03	3.2112e-03	1.6063e-03	8.0338e-04
	1.01	1.00	1.00	1.00	1.00	
2^{-10}	2.7043e-02	1.3585e-02	6.8898e-03	3.4753e-03	1.7442e-03	8.7501e-04
	0.99	0.98	0.99	0.99	1.00	
2^{-12}	2.8085e-02	1.4027e-02	7.1281e-03	3.5843e-03	1.7968e-03	9.0025e-04
	1.00	0.98	0.99	1.00	1.00	
2^{-14}	2.8266e-02	1.4420e-02	7.2038e-03	3.6167e-03	1.8133e-03	9.0747e-04
	0.97	1.00	0.99	1.00	1.00	
2^{-16}	2.9220e-02	1.4538e-02	7.2476e-03	3.6297e-03	1.8205e-03	9.1016e-04
	1.01	1.00	1.00	1.00	1.00	
2^{-18}	3.0767e-02	1.4580e-02	7.2599e-03	3.6456e-03	1.8207e-03	9.1103e-04
	1.08	1.01	0.99	1.00	1.00	
2^{-20}	3.1409e-02	1.4795e-02	7.3042e-03	3.6477e-03	1.8208e-03	9.1134e-04
	1.09	1.02	1.00	1.00	1.00	
e^N	3.1409e-02	1.4795e-02	7.3042e-03	3.6477e-03	1.8208e-03	9.1134e-04
r^N	1.09	1.02	1.00	1.00	1.00	

Example 6.2. *Consider the following:*

$$\varepsilon^2 u''(x) + \varepsilon(3x)u'(x) - u(x) + \frac{1}{2}\int_0^1 x u(\xi)d\xi = \begin{cases} -e^x, & 0 < x < 1/3, \\ 5x, & 1/3 < x < 1 \end{cases}$$

with boundary conditions

$$u(0) = 2, \quad u(1) = 3.$$

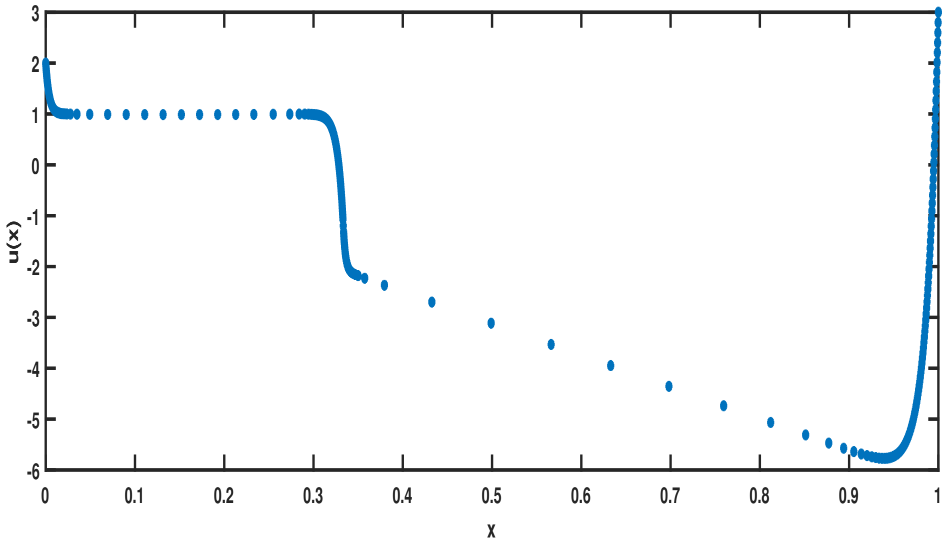

Figure 6.3: Numerical solution for $N = 256$ and $\varepsilon = 2^{-8}$ for Example 6.2.

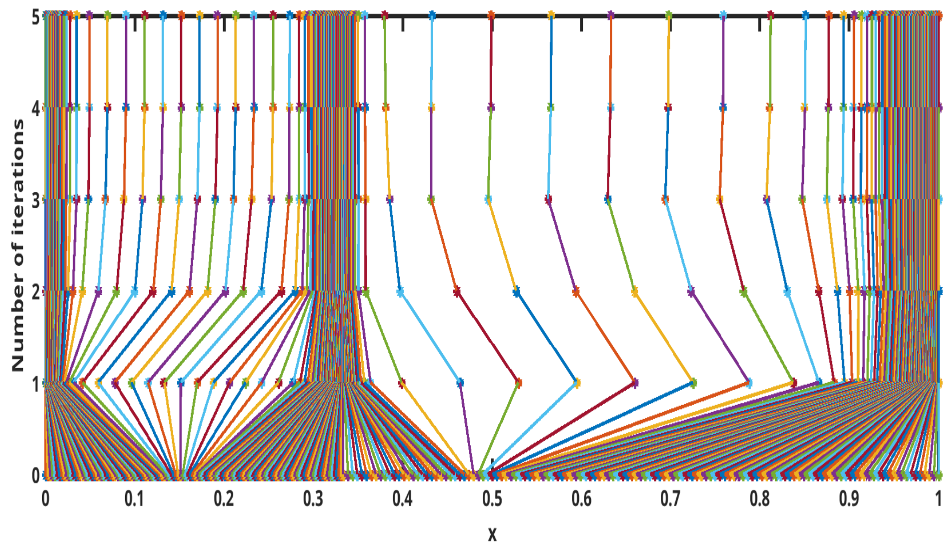

Figure 6.4: Mesh movement for $N = 256$ and $\varepsilon = 2^{-8}$ for Example 6.2.

Figures 6.1 and 6.3 illustrate the numerical solution for Examples 6.1 and 6.2, respectively. The corresponding mesh movements are depicted in Figures 6.2 and 6.4. These figures present the progression of the mesh achieved through the grid generation algorithm and the numerical solution graph for $\varepsilon = 2^{-8}$ at $N = 128$ and $N = 256$. The plots reveal the emergence of a boundary layer at $x = 0$ and $x = 1$, as well as an interior layer at the point of discontinuity. Moreover, the figures show the progression of mesh points towards these layers, resulting in a denser mesh near these regions.

Table 6.2: Maximum absolute error and convergence rate of the present scheme for Example 6.2 for various values of N and ε.

ε	N=64	N=128	N=256	N=512	N=1024	N=2048
2^{-0}	4.6809e-03	2.3681e-03	1.1912e-03	5.9739e-04	2.9915e-04	1.4968e-04
	0.98	0.99	1.00	1.00	1.00	
2^{-2}	4.7663e-02	2.3890e-02	1.1959e-02	5.9827e-03	2.9922e-03	1.4963e-03
	1.00	1.00	1.00	1.00	1.00	
2^{-4}	8.2790e-02	4.0549e-02	2.0019e-02	9.9304e-03	4.9478e-03	2.4689e-03
	1.03	1.02	1.01	1.01	1.00	
2^{-6}	8.9381e-02	4.5048e-02	2.2577e-02	1.1298e-02	5.6518e-03	2.8264e-03
	0.99	1.00	1.00	1.00	1.00	
2^{-8}	9.2838e-02	4.4957e-02	2.2414e-02	1.1179e-02	5.5830e-03	2.7902e-03
	1.05	1.00	1.00	1.00	1.00	
2^{-10}	9.1193e-02	4.4998e-02	2.2319e-02	1.1117e-02	5.5484e-03	2.7717e-03
	1.02	1.01	1.01	1.00	1.00	
2^{-12}	9.2668e-02	4.5264e-02	2.2387e-02	1.1119e-02	5.5417e-03	2.7674e-03
	1.03	1.02	1.01	1.00	1.00	
2^{-14}	9.3690e-02	4.5532e-02	2.2435e-02	1.1136e-02	5.5460e-03	2.7675e-03
	1.04	1.02	1.01	1.01	1.00	
2^{-16}	9.4667e-02	4.5831e-02	2.2535e-02	1.1155e-02	5.5501e-03	2.7684e-03
	1.05	1.02	1.01	1.01	1.00	
2^{-18}	9.5370e-02	4.5962e-02	2.2572e-02	1.1166e-02	5.5547e-03	2.7697e-03
	1.05	1.03	1.02	1.01	1.00	
e^N	9.5370e-02	4.5962e-02	2.2577e-02	1.1298e-02	5.6518e-03	2.8264e-03
r^N	1.05	1.03	1.00	1.00	1.00	

By thoroughly examining the two tables, it is evident that the accuracy of the scheme remains consistent regardless of changes in the perturbation parameter ε, which ensures that the proposed scheme is parameter uniform. Additionally, it can be observed that the computed solution is accurate to the first order, which perfectly matches the prediction in Theorem 6.1.

6.6 Summary

In this chapter, a highly complex convection-diffusion type Fredholm integro-differential equation of the second order has been successfully solved. The equation possesses unique challenges due to the presence of a discontinuous source term and the effects of both a perturbation parameter and a discontinuity. No prior literature has presented a numerical scheme that adequately addresses these obstacles. To bridge this gap, an innovative and effective $\varepsilon-$uniform convergent scheme is introduced. To overcome the limitations of traditional numerical methods when handling perturbation parameters, the finite difference method is utilized on a specially generated grid, created using the grid equidistribution method. This meticulously designed scheme has consistently yielded accurate and efficient results, as verified by numerous numerical experiments. Furthermore, a linear order of convergence has been achieved, and the scheme adheres to $\varepsilon-$uniform convergence rates.

CHAPTER SEVEN

SINGULARLY PERTURBED REACTION DIFFUSION TYPE VOLTERRA-FREDHOLM INTEGRO-DIFFERENTIAL EQUATION

This chapter furthers the exploration of the numerical scheme introduced in Chapter 4. The concentration is primarily on solving SPVFIDEs of the reaction-diffusion type.

7.1 Description of the problem

The problem considered is the following linear reaction-diffusion SPVFIDE:

$$\begin{cases} \mathcal{L}_\varepsilon u := \ell_\varepsilon u + \lambda_1 \int\limits_0^x K_1(x,\xi)u(\xi)d\xi + \lambda_2 \int\limits_0^1 K_2(x,\xi)u(\xi)d\xi = f(x), x \in (0,1), \\ u(0) = A, \quad u(1) = B, \end{cases} \tag{7.1}$$

where $\ell_\varepsilon u = -\varepsilon u'' + b(x)u$ and $0 < \varepsilon \ll 1$. λ_1 and λ_2 are real parameters. The function b, which belongs to the class $C^2([0,1])$, satisfies the condition

$$b(x) \geq \beta > 0.$$

Moreover, the functions K_1 and K_2, also in $C^2([0,1] \times [0,1])$.

The introduction of the small parameter ε significantly impacts the solution's behavior. As ε approaches zero, specific regions of the solution exhibit heightened sensitivity to variations in the independent variable. This is evident from the estimates established in the forthcoming lemma for the solution and its derivative.

When solving (7.1), a boundary layer typically emerges at both extremities of the interval $\bar{\Omega}$. This singular perturbation presents a challenge for conventional numerical methods, as they might struggle to capture the rapid fluctuations within the narrow boundary layer. To effectively handle these equations, specialized techniques are necessary.

7.2 Preliminary results

First, a key analytical result is derived. This result will provide valuable insights and underpin the error analysis of the forthcoming numerical scheme. The maximum principle provides bounds for a priori bound on the solution. As shown in Chapter 4, Lemma 4.2.1, the differential operator ℓ_ε in (7.1) for all $\Psi \in C^2(\bar{\Omega})$ satisfies the maximum principle.

Lemma 7.2.1. *(Durmaz, 2023) Assume that* $b, f \in C^2[0,1]$, *and for* $m = 1,2$ $\frac{\partial^n K_m}{\partial x^n}, \frac{\partial^n K_m}{\partial \xi^n} \in C([0,1]\times[0,1])$, $n = 0,1,2$. *Let*

$$\beta^{-1}\left(|\lambda_1| \max_{0\le x\le 1}\int_0^x |K_1(x,\xi)|\,d\xi + |\lambda_2| \max_{0\le x\le 1}\int_0^1 |K_2(x,\xi)|\,d\xi\right) < 1 \tag{7.2}$$

and u *be the solution of (7.1). Then for all* $x \in [0,1]$,

$$\|u\|_\infty \le C \tag{7.3}$$

and

$$\left|u^{(k)}(x)\right| \le C\left\{1 + \varepsilon^{-\frac{k}{2}}\left(e^{-\sqrt{\frac{\beta}{\varepsilon}}x} + e^{-\sqrt{\frac{\beta}{\varepsilon}}(1-x)}\right)\right\}, \quad 1 \le k \le 4. \tag{7.4}$$

Proof. The bound in (7.3) is an immediate consequence of the maximum principle, and is derived by applying the maximum principle to the functions

$$\Psi^{\pm}(x) = \frac{1}{\beta}\|F\| + max\{|A|,|B|\} \pm u(x), \tag{7.5}$$

where

$$F(x) = f(x) - \lambda_1 \int\limits_0^x K_1(x,\xi)u(\xi)d\xi + \lambda_2 \int\limits_0^1 K_2(x,\xi)u(\xi)d\xi. \tag{7.6}$$

Clearly $\Psi^{\pm}(0) \ge 0$, $\Psi^{\pm}(1) \ge 0$ and that $\ell_\varepsilon \Psi^{\pm}(x) \ge 0$. Applying the maximum principle then gives $\Psi^{\pm}(x) \geq 0$, and so

$$\|u\|_{\infty} \leq \frac{1}{\beta}\|F\| + max\{|A|,|B|\}. \tag{7.7}$$

Using (7.6) in the expression (7.7) gives

$$\begin{aligned}\|u\|_{\infty} &\leq |A|+|B| \\ &+ \beta^{-1}\left(\|f\|_{\infty} + |\lambda_1| \max_{0\leq x\leq 1}\int_0^x |K_1(x,\xi)||u(\xi)|d\xi + |\lambda_2| \max_{0\leq x\leq 1}\int_0^1 |K_2(x,\xi)||u(\xi)|d\xi\right).\end{aligned}$$

It follows from this inequality that

$$\begin{aligned}\|u\|_{\infty}\left(1-\frac{|\lambda_1|}{\beta}\max_{0\leq x\leq 1}\int_0^x |K_1(x,\xi)|d\xi - \frac{|\lambda_2|}{\beta}\max_{0\leq x\leq 1}\int_0^1 |K_2(x,\xi)|d\xi\right) \\ \leq |A|+|B|+\beta^{-1}\|f\|_{\infty}.\end{aligned}$$

Under the condition of (7.2), this simplifies to

$$\|u\|_{\infty} \leq \frac{|A|+|B|+\beta^{-1}\|f\|_{\infty}}{1-\left(\frac{|\lambda_1|}{\beta}\max_{0\leq x\leq 1}\int_0^x |K_1(x,\xi)|d\xi + \frac{|\lambda_2|}{\beta}\max_{0\leq x\leq 1}\int_0^1 |K_2(x,\xi)|d\xi\right)}$$

and so it is obvious that, on $\bar{\Omega}$,

$$\|u\|_{\infty} \leq C,$$

which completes the proof of (7.3). The bound in (7.4) can be proved using the same techniques as for the analogous result in Chapter 4, with appropriate modifications on the integral part. □

7.3 The numerical scheme

This section embarks on a detailed exploration of the two pillars of the numerical scheme: discretization and adaptive mesh generation.

7.3.1 The discrete scheme

To develop the discrete scheme for equation (7.1), finite difference approximation is utilized to estimate the derivative portion. Simultaneously, the composite trapezoidal rule is employed for the numerical approximation of the integral, resulting in

$$\begin{cases} \mathcal{L}_\varepsilon u_i := \left(-\varepsilon\delta^2 + b_i\right) u_i + \dfrac{\lambda_1}{2} \displaystyle\sum_{j=1}^{i} h_j \left(K_{1_{i,j-1}} u_{j-1} + K_{1_{i,j}} u_j\right) \\ \qquad\qquad + \dfrac{\lambda_2}{2} \displaystyle\sum_{j=1}^{N} h_j \left(K_{2_{i,j-1}} u_{j-1} + K_{2_{i,j}} u_j\right) + \mathcal{R}_i = f_i \\ u_0 = A, \quad u_N = B. \end{cases} \tag{7.8}$$

The term $\mathcal{R}_i$ in (7.8) is the truncation error

$$\mathcal{R}_i = \mathcal{R}_i^{(1)} + \mathcal{R}_i^{(2)} + \mathcal{R}_i^{(3)}, \tag{7.9}$$

where

$$\mathcal{R}_i^{(1)} = -\varepsilon\left(u_i'' - \delta^2 u_i\right), \tag{7.10}$$

$$\mathcal{R}_i^{(2)} = \frac{\lambda_1}{2} \sum_{j=1}^{i} \int_{x_{j-1}}^{x_j} (x_{j-1}-\xi)(x_j-\xi) \frac{\partial^2}{\partial \xi^2} \left(K_1(x_i,\xi) u(\xi)\right) d\xi, \tag{7.11}$$

$$\mathcal{R}_i^{(3)} = \frac{\lambda_2}{2} \sum_{j=1}^{N} \int_{x_{j-1}}^{x_j} (x_{j-1}-\xi)(x_j-\xi) \frac{\partial^2}{\partial \xi^2} \left(K_2(x_i,\xi) u(\xi)\right) d\xi. \tag{7.12}$$

After neglecting the truncation error in (7.8), the following scheme is obtained to approximate (7.1):

$$\begin{cases} \mathcal{L}_\varepsilon U_i := \left(-\varepsilon\delta^2 + b_i\right) U_i + \dfrac{\lambda_1}{2} \displaystyle\sum_{j=1}^{i} h_j \left(K_{1_{i,j-1}} U_{j-1} + K_{1_{i,j}} U_j\right) \\ \qquad\qquad + \dfrac{\lambda_2}{2} \displaystyle\sum_{j=1}^{N} h_j \left(K_{2_{i,j-1}} U_{j-1} + K_{2_{i,j}} U_j\right) = f_i, \\ U_0 = A, \quad U_N = B. \end{cases} \tag{7.13}$$

7.3.2 Adaptive grid generation via equidistribution

Here, the equidistribution method is utilized as a fundamental tool for creating adaptive grids. To implement equidistribution, a positive mesh density function is used, which is provided in Chapter 5 as

$$\rho(u(\xi),\xi) = 1 + \frac{|u''(\xi)|^{\frac{1}{2}} + |(bu)''(\xi)|^{\frac{1}{2}}}{\|u\|_\infty^{\frac{1}{2}}}. \tag{7.14}$$

$\rho(u(\xi),\xi)$ quantifies the expected error at each point in the domain $\bar{\Omega}_N$ and satisfies

$$\int_{x_{i-1}}^{x_i} \rho(u(\xi),\xi)d\xi = \frac{1}{N}\int_0^1 \rho(u(\xi),\xi)d\xi, \quad i = 1,2,\ldots,N. \tag{7.15}$$

Lemma 7.3.1. *Let $\rho(u(\xi),\xi)$ be the mesh density function defined in (7.14) and $\bar{\Omega}_N = \{x_i\}_0^N$ be a grid satisfying (7.15). Then,*

$$\int_0^1 \rho(u(\xi),\xi)d\xi \le C \tag{7.16}$$

$$h_i \le CN^{-1}, \quad i = 1,2,\ldots,N. \tag{7.17}$$

Proof. The proof is analogous to that of Lemma 4.3.1. □

To solve (7.1), (7.13) is utilized and equidistribution is achieved using the mesh density function (7.14). Given the unknown values of the grid $\{x_i\}_{i=0}^N$ and the solution $\{U_i\}_{i=0}^N$, resolving the equidistribution problem necessitates simultaneously solving (7.13) and the relations $h_j\rho_j = \frac{1}{N}\sum_{i=1}^N h_i\rho_i$, $1 \le j \le N$ to determine the values of $\{x_i, U_i\}$. the modified version of the algorithm presented in Chapter 4 is used, as detailed in Algorithm 4.

Algorithm 4 Adaptive mesh generation

Input $N \in \mathbb{Z}^+$, $0 < \varepsilon \le 1$ and a user-chosen constant $C_0 > 1$.
Output Adaptive mesh Ω_N^* and corresponding solution $\{U_i^*\}_{i=0}^N$
Step 1. Begin with an initial uniform mesh $\Omega_N^{(0)} = \{x_i^{(0)}\}_{i=0}^N$ with N intervals.
Step 2. Compute $\{U_i^{(k)}\}_{i=0}^N$ by solving (7.13) on the mesh $\Omega_N^{(k)} = \{x_i^{(k)}\}_{i=0}^N$.
Let $h_i^{(k)} = x_i^{(k)} - x_{i-1}^{(k)}$ for $i = 1,2,\ldots,N$ and compute
$\rho_i^{(k)} = 1 + \frac{|\delta^2 U_i^{(k)}|^{\frac{1}{2}} + |\delta^2 b_i U_i^{(k)}|^{\frac{1}{2}}}{\max\limits_i \left|U_i^{(k)}\right|^{\frac{1}{2}}}, \quad i = 1,2,\ldots,N-1.$
Set $\rho_0^{(k)} := \rho_1^{(k)}$ and $\rho_N^{(k)} := \rho_{N-1}^{(k)}$. Then $\varrho_i = \frac{\rho_{i-1}+\rho_i}{2}, \quad i = 1,2,\ldots,N.$
Step 3. Termination criterion
Set $L_0^{(k)} := 0$. For $1 \le i \le N$, let $l_i^{(k)} = h_i^{(k)}\varrho_i^{(k)}$, $L_i^{(k)} = \sum_{j=1}^i l_j^{(k)}$ and $C_*^{(k)} = \frac{N}{L_N^{(k)}}\max\limits_i l_i^{(k)}$.
If $C_*^{(k)} \le C_0$, then go to step 5, otherwise continue with next step.
Step 4. Set $\omega_i := iL_N^{(k)}/N$ for $i = 0,1,\ldots,N$. Interpolate to the points $(L_i^{(k)}, x_i^{(k)})$. Generate $\{x^{(k+1)}\}$ by evaluating the interpolant at $\{\omega_i\}_{i=0}^N$. Increment k and go back to step 2.
Step 5. Set $\Omega_N^* := \{x_i^{(k)}\}_{i=0}^N$ and $\{U^*\} := \{U_i^{(k)}\}_{i=0}^N$, then stop.

7.4 Stability and uniform convergence

To guarantee the numerical solution reflects the actual problem and doesn't diverge due to errors, two fundamental factors that are crucial for the development and implementation of numerical schemes are introduced: stability and uniform convergence.

7.4.1 A stability result

The following stability result is presented to establish the convergence of the numerical solution.

Lemma 7.4.1. *Let*

$$\frac{|\lambda_1|}{\beta}\max_{1\le i<N}\sum_{j=1}^{i}\frac{h_j}{2}\left(\left|K_{1_{i,j-1}}\right|+\left|K_{1_{i,j}}\right|\right)+\frac{|\lambda_2|}{\beta}\max_{1\le i<N}\sum_{j=1}^{N}\frac{h_j}{2}\left(\left|K_{2_{i,j-1}}\right|+\left|K_{2_{i,j}}\right|\right)<1.$$

Under the assumptions of Lemma 7.2.1 the solution of (7.13) satisfies

$$\max_{0\le i\le N}|U_i|\le\frac{|A|+|B|+\beta^{-1}\|f\|_\infty}{1-\left(\frac{|\lambda_1|}{\beta}\max\limits_{1\le i<N}\sum\limits_{j=1}^{i}\frac{h_j}{2}\left(\left|K_{1_{i,j-1}}\right|+\left|K_{1_{i,j}}\right|\right)+\frac{|\lambda_2|}{\beta}\max\limits_{1\le i<N}\sum\limits_{j=1}^{N}\frac{h_j}{2}\left(\left|K_{2_{i,j-1}}\right|+\left|K_{2_{i,j}}\right|\right)\right)}. \tag{7.18}$$

Proof. The discrete scheme (7.13) can be expressed as

$$\begin{cases}\ell_\varepsilon^N U_i:=-\varepsilon\delta^2U_i+b_iU_i=F_i,\\ U_0=A,\quad U_N=B,\end{cases} \tag{7.19}$$

where

$$F_i=f_i-\frac{\lambda_1}{2}\sum_{j=1}^{i}h_j\left(K_{1_{i,j-1}}U_{j-1}+K_{1_{i,j}}U_j\right)-\frac{\lambda_2}{2}\sum_{j=1}^{N}h_j\left(K_{2_{i,j-1}}U_{j-1}+K_{2_{i,j}}U_j\right). \tag{7.20}$$

The maximum principle on Ω_N for the finite difference operator $\ell_\varepsilon^N U$ in (7.19) gives,

$$\max_{0\le i\le N}|U_i|\le|A|+|B|+\beta^{-1}|F_i|. \tag{7.21}$$

Estimating the value of F_i from (7.20) and plugging in (7.21) yields

$$\max_{0\le i\le N}|U_i| \le |A|+|B|+\frac{\|f\|_\infty}{\beta}+\frac{|\lambda_1|}{\beta}\max_{1\le i<N}\sum_{j=1}^{i}\frac{h_j}{2}\left(\left|K_{1_{i,j-1}}\right|+\left|K_{1_{i,j}}\right|\right)\max_{0\le i\le N}|U_i|$$
$$+\frac{|\lambda_2|}{\beta}\max_{1\le i<N}\sum_{j=1}^{N}\frac{h_j}{2}\left(\left|K_{2_{i,j-1}}\right|+\left|K_{2_{i,j}}\right|\right)\max_{0\le i\le N}|U_i|.$$

It follows that

$$\max_i|U_i|\left(1-\frac{|\lambda_1|}{\beta}\max_i\sum_{j=1}^{i}\frac{h_j}{2}\left(\left|K_{1_{i,j-1}}\right|+\left|K_{1_{i,j}}\right|\right)-\frac{|\lambda_2|}{\beta}\max_i\sum_{j=1}^{N}\frac{h_j}{2}\left(\left|K_{2_{i,j-1}}\right|+\left|K_{2_{i,j}}\right|\right)\right)$$
$$\le |A|+|B|+\frac{\|f\|_\infty}{\beta}.$$

This, in turn, yields (7.18). □

7.4.2 Error analysis

The error associated with the discrete scheme (7.13) is now examined. Considering the pointwise error, $e_i=U_i-u_i$, which, when combined with (7.8) and (7.13), results in

$$\begin{cases}\mathcal{L}_\varepsilon^N e_i=\mathcal{R}_i, & 1\le i\le N-1,\\ e_0=e_N=0,\end{cases} \tag{7.22}$$

where $\mathcal{R}_i$ is given by (7.9).

Lemma 7.4.2. *Under the assumptions of Lemma 7.2.1 the truncation error $\mathcal{R}_i$ in (7.9) satisfies the estimate*

$$\max_{1\le i\le N-1}|\mathcal{R}_i|\le CN^{-2}. \tag{7.23}$$

Proof. For the error term $\mathcal{R}_i^{(1)}$, from (7.10) and (4.40), it follows that

$$\left|\mathcal{R}_i^{(1)}\right|\le C\left(\max_{x\in[x_{i-1/2},x_i]}\sqrt{\varepsilon}h_i^2\left|u'''(x)\right|+\max_{x\in[x_{i-1/2},x_{i+1/2}]}\varepsilon\hbar_i^2\left|u_i^{(4)}(x)\right|\right).$$

Using the result in Lemma 4.4.4 and applying (7.17),

$$\left|\mathcal{R}_i^{(1)}\right|\le CN^{-2}. \tag{7.24}$$

For $\mathcal{R}_i^{(2)}$ and $\mathcal{R}_i^{(3)}$, it follows from (7.11)-(7.12) that

$$\left|\mathcal{R}_i^{(2)}\right|+\left|\mathcal{R}_i^{(3)}\right| \leq C\left\{\sum_{i=1}^{N} h_i^3+\sum_{i=1}^{N} h_i \int\limits_{x_{i-1}}^{x_i}(\xi-x_{i-1})\left|u''(\xi)\right| d\xi\right\},$$

and by applying Lemma 7.3.1,

$$\left|\mathcal{R}_i^{(2)}\right|+\left|\mathcal{R}_i^{(3)}\right| \leq C\left\{N^{-2}+\left(\int\limits_{x_{i-1}}^{x_i}\left|u''(\xi)\right|^{\frac{1}{2}} d\xi\right)^2\right\}.$$

Using (7.15), it follows that

$$\left|\mathcal{R}_i^{(2)}\right|+\left|\mathcal{R}_i^{(3)}\right| \leq C\left\{N^{-2}+\left(\frac{1}{N}\int\limits_0^1 \rho(u(\xi),\xi) d\xi\right)^2\right\}.$$

By (7.16), it can be concluded that

$$\left|\mathcal{R}_i^{(2)}\right|+\left|\mathcal{R}_i^{(3)}\right| \leq C N^{-2}. \tag{7.25}$$

Combining (7.24) and (7.25) results in (7.23). □

Theorem 7.1. *Let u_i and U_i be the exact and discrete solutions on the equidistributed grid $\bar{\Omega}_N$, respectively. Then, there exists a constant C such that:*

$$\max_{0\leq i\leq N}|U_i-u_i| \leq C N^{-2}. \tag{7.26}$$

Proof. Based on Lemma 7.4.1, the following result can be derived from error equation (7.22):

$$\max_{0\leq i\leq N}|U_i-u_i| = \max_{0\leq i\leq N}|e_i| \leq C \max_{1\leq i\leq N-1}|\mathcal{R}_i|. \tag{7.27}$$

Subsequently, applying (7.23) to (7.27) yields (7.26). □

7.5 Numerical results and discussion

To validate the theoretical outcome and provide further insights on the efficiency of the suggested scheme, three examples are presented.

Example 7.1. *(Durmaz, 2023) Consider the Volterra-Fredholm integro-differential equation,*

$$-\varepsilon u'' + u + \int_0^x u(\xi)d\xi + \int_0^1 u(\xi)d\xi = x\sin x, \quad x \in (0,1),$$

$$u(0) = 0, \quad u(1) = 0.$$

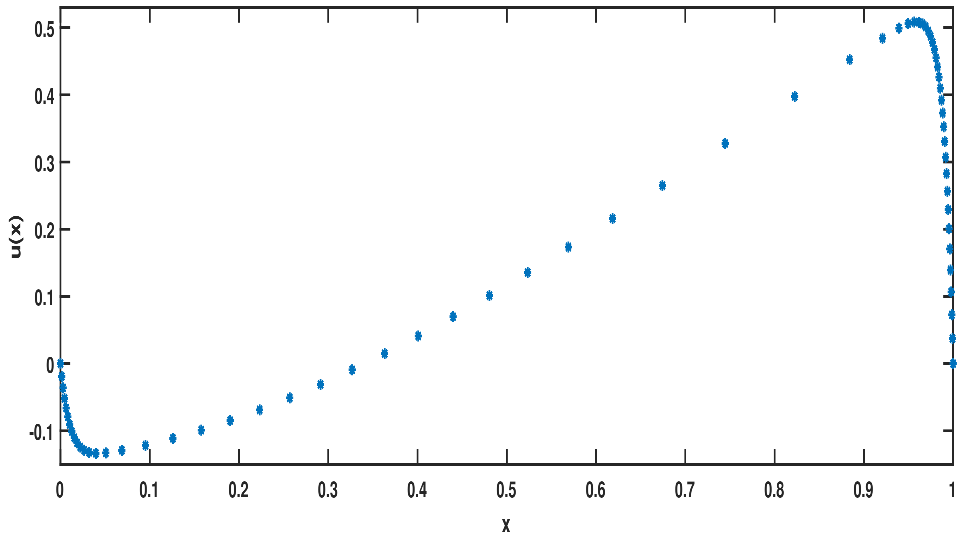

Figure 7.1: Numerical solution for $N = 64$ and $\varepsilon = 10^{-4}$ for Example 7.1.

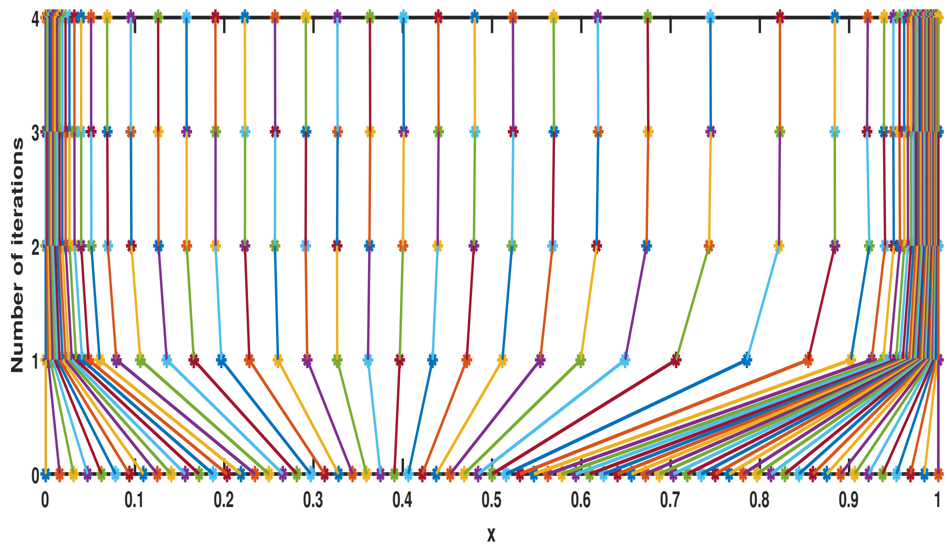

Figure 7.2: Mesh movement for $N = 64$ and $\varepsilon = 10^{-4}$ for Example 7.1.

Table 7.1: Maximum absolute error and convergence rate of the present scheme of Example 7.1 for various values of N and ε.

ε	N=32	N=64	N=128	N=256	N=512	N=1024
10^{-0}	4.0951e-05	1.0682e-05	2.8605e-06	7.5598e-07	1.9132e-07	4.8875e-08
	1.94	1.90	1.92	1.98	1.97	
10^{-1}	2.0472e-04	5.3143e-05	1.3325e-05	3.4742e-06	9.4100e-07	2.3725e-07
	1.95	2.00	1.94	1.88	1.99	
10^{-2}	2.2699e-04	9.5537e-05	2.3910e-05	6.0528e-06	1.5523e-06	4.0868e-07
	1.25	2.00	1.98	1.96	1.93	
10^{-3}	3.0439e-04	7.5325e-05	1.8845e-05	4.6787e-06	1.1702e-06	2.9227e-07
	2.01	2.00	2.01	2.00	2.00	
10^{-4}	4.9996e-04	1.2956e-04	3.2472e-05	8.1273e-06	2.0313e-06	5.0787e-07
	1.95	2.00	2.00	2.00	2.00	
10^{-5}	6.4352e-04	1.6703e-04	4.1483e-05	1.0348e-05	2.5850e-06	6.4538e-07
	1.95	2.01	2.00	2.00	2.00	
10^{-6}	7.0857e-04	1.8725e-04	4.6604e-05	1.1513e-05	2.8622e-06	7.1404e-07
	1.92	2.01	2.02	2.01	2.00	
10^{-7}	7.4379e-04	1.9649e-04	4.9092e-05	1.2145e-05	3.0005e-06	7.4631e-07
	1.92	2.00	2.02	2.02	2.01	
10^{-8}	7.6280e-04	2.0258e-04	5.0405e-05	1.2489e-05	3.0847e-06	7.6280e-07
	1.91	2.01	2.01	2.02	2.02	
10^{-9}	7.7861e-04	2.0682e-04	5.0937e-05	1.2623e-05	3.1407e-06	7.7871e-07
	1.91	2.02	2.01	2.01	2.01	
10^{-10}	8.0250e-04	2.0975e-04	5.1360e-05	1.2678e-05	3.1660e-06	7.8695e-07
	1.94	2.03	2.02	2.00	2.01	
10^{-11}	8.2190e-04	2.1198e-04	5.1629e-05	1.2703e-05	3.1761e-06	7.8952e-07
	1.96	2.04	2.02	2.00	2.01	
10^{-12}	8.3727e-04	2.1346e-04	5.1791e-05	1.2725e-05	3.1796e-06	7.9000e-07
	1.97	2.04	2.03	2.00	2.01	
10^{-13}	8.4832e-04	2.1480e-04	5.1903e-05	1.2748e-05	3.1811e-06	7.8980e-07
	1.98	2.05	2.03	2.00	2.01	
e^N	8.4832e-04	2.1480e-04	5.1903e-05	1.2748e-05	3.1811e-06	7.9000e-07
r^N	1.98	2.05	2.03	2.00	2.01	

Example 7.2. *(Durmaz, 2023) Consider the Volterra-Fredholm integro-differential equation,*

$$-\varepsilon u'' + u + \int_0^x \sin(x\xi)\, u(\xi) d\xi + \int_0^1 e^{xs} u(\xi) d\xi = \frac{1}{1+x}, \quad x \in (0,1),$$

$$u(0) = 1, \quad u(1) = 1.$$

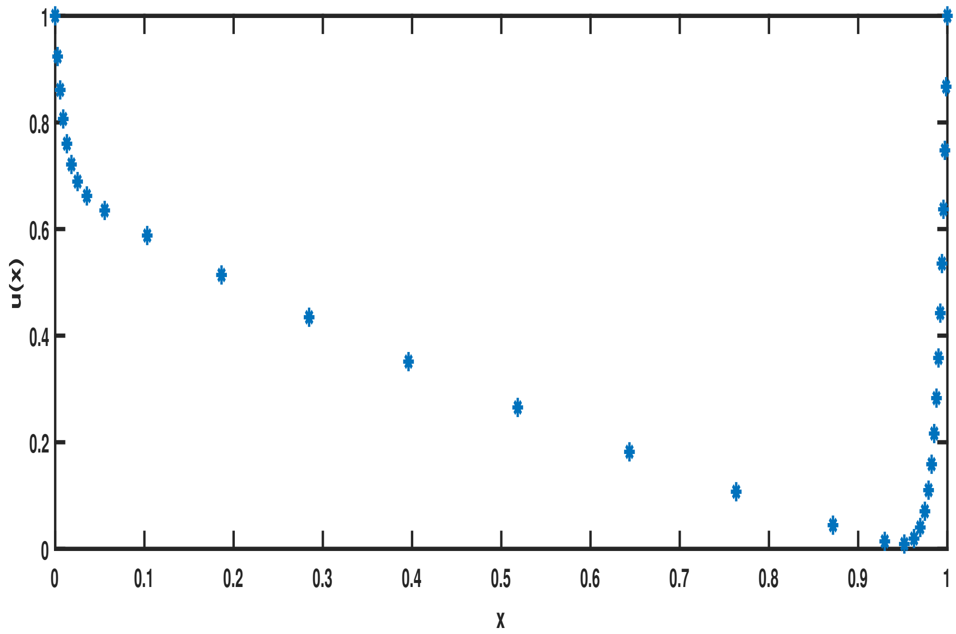

Figure 7.3: Numerical solution for $N = 32$ and $\varepsilon = 10^{-4}$ for Example 7.2.

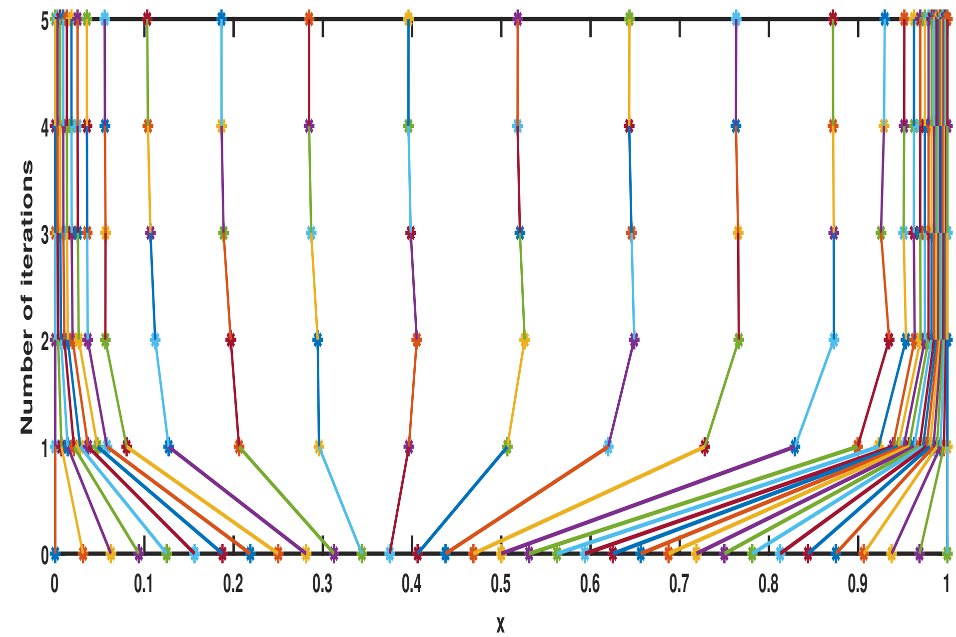

Figure 7.4: Mesh movement for $N = 32$ and $\varepsilon = 10^{-4}$ for Example 7.2.

Table 7.2: Maximum absolute error and convergence rate of the present scheme of Example 7.2 for various values of N and ε.

ε	N=32	N=64	N=128	N=256	N=512	N=1024
10^{-0}	1.1458e-05	2.8794e-06	7.2070e-07	1.8024e-07	4.5063e-08	1.1126e-08
	1.99	2.00	2.00	2.00	2.02	
10^{-1}	1.5600e-04	3.9100e-05	9.7890e-06	2.4483e-06	6.1214e-07	1.5303e-07
	2.00	2.00	2.00	2.00	2.00	
10^{-2}	5.1287e-04	1.2866e-04	3.2169e-05	8.0423e-06	2.0104e-06	5.0264e-07
	2.00	2.00	2.00	2.00	2.00	
10^{-3}	7.9628e-04	2.0451e-04	5.1608e-05	1.2928e-05	3.2340e-06	8.0858e-07
	1.96	1.99	2.00	2.00	2.00	
10^{-4}	1.1959e-03	3.0596e-04	7.7042e-05	1.9288e-05	4.8213e-06	1.2054e-06
	1.97	1.99	2.00	2.00	2.00	
10^{-5}	1.4506e-03	3.7405e-04	9.3419e-05	2.3282e-05	5.8176e-06	1.4543e-06
	1.96	2.00	2.00	2.00	2.00	
10^{-6}	1.6001e-03	4.1169e-04	1.0249e-04	2.5411e-05	6.3273e-06	1.5799e-06
	1.96	2.01	2.01	2.01	2.00	
10^{-7}	1.6618e-03	4.3051e-04	1.0715e-04	2.6572e-05	6.5841e-06	1.6392e-06
	1.95	2.01	2.01	2.01	2.01	
10^{-8}	1.7089e-03	4.4069e-04	1.0938e-04	2.7189e-05	6.7295e-06	1.6698e-06
	1.96	2.01	2.01	2.01	2.01	
10^{-9}	1.7664e-03	4.4917e-04	1.1087e-04	2.7475e-05	6.8335e-06	1.6942e-06
	1.98	2.02	2.01	2.01	2.01	
10^{-10}	1.8157e-03	4.5485e-04	1.1189e-04	2.7598e-05	6.8752e-06	1.7113e-06
	2.00	2.02	2.02	2.01	2.01	
10^{-11}	1.8589e-03	4.5941e-04	1.1528e-04	2.7663e-05	6.8994e-06	1.7214e-06
	2.02	1.99	2.06	2.00	2.00	
10^{-12}	1.8967e-03	4.6274e-04	1.1303e-04	2.7704e-05	6.9108e-06	1.7205e-06
	2.04	2.03	2.03	2.00	2.01	
e^N	1.8967e-03	4.6274e-04	1.1528e-04	2.7704e-05	6.9108e-06	1.7214e-06
r^N	2.04	2.01	2.06	2.00	2.01	

Example 7.3. *(Cakir & Gunes, 2022) Consider the Volterra-Fredholm integro-differential equation,*

$$-\varepsilon^2 u'' + (1+e^x)\,u + \int_0^x \sinh(x)\,u(\xi)d\xi + \int_0^1 \cosh(x)\,u(\xi)d\xi = \sin(x) - \cos(x)\,, x \in (0,1),$$

$$u(0) = 0, \quad u(1) = 1 + e^{-1/\varepsilon}.$$

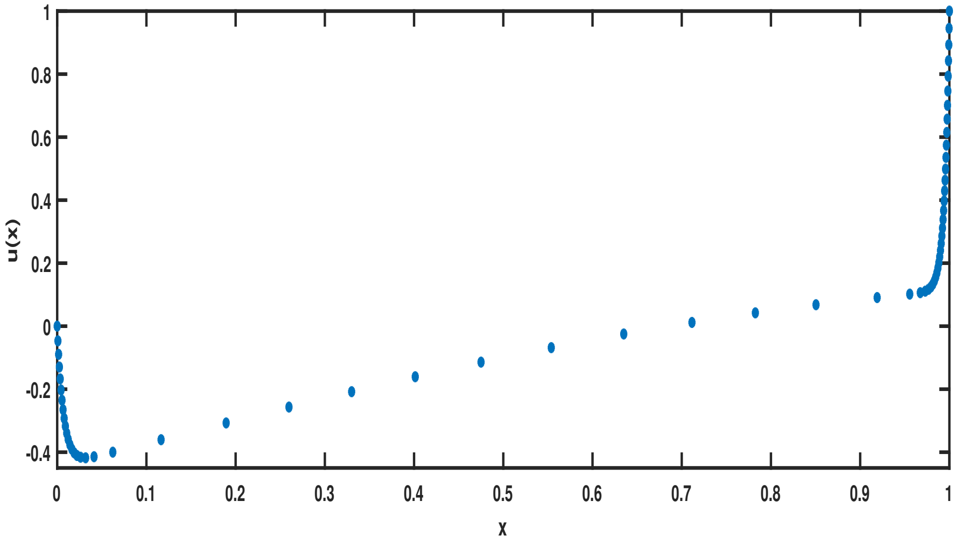

Figure 7.5: Numerical solution for $N = 64$ and $\varepsilon = 10^{-2}$ for Example 7.3.

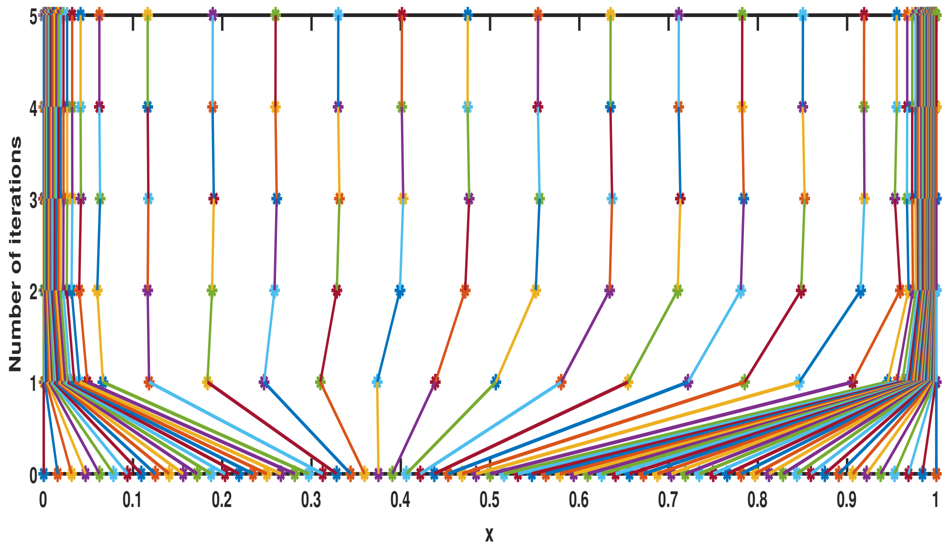

Figure 7.6: Mesh movement for $N = 64$ and $\varepsilon = 10^{-2}$ for Example 7.3.

The effectiveness of the mesh adjustment to the unique features of the solutions for the three problems can be observed in Figures 7.1, 7.3, and 7.5. These figures demonstrate the evolution of the mesh using the grid generation algorithm and the graphical representation of the numerical solution. The graphs illustrate the emergence of a boundary layer at $x = 0$ and $x = 1$. Additionally, Figures 7.2, 7.4, and 7.6 depict the movement of mesh points towards these layers, leading to a higher concentration of mesh points in these areas.

Table 7.3: Maximum absolute error and convergence rate of the present scheme of Example 7.2 for various values of N and ε.

ε^2	N=64	N=128	N=256	N=512	N=1024	N=2048
10^{-0}	9.0430e-06	2.2665e-06	5.6702e-07	1.4177e-07	3.5439e-08	8.5904e-09
	2.00	2.00	2.00	2.00	2.04	
10^{-2}	1.7299e-04	4.3586e-05	1.0895e-05	2.7243e-06	6.8121e-07	1.7032e-07
	1.99	2.00	2.00	2.00	2.00	
10^{-4}	2.4647e-04	6.1229e-05	1.5240e-05	3.8078e-06	9.5178e-07	2.3794e-07
	2.01	2.01	2.00	2.00	2.00	
10^{-6}	2.7661e-04	6.7844e-05	1.6724e-05	4.1389e-06	1.0323e-06	2.5792e-07
	2.03	2.02	2.01	2.00	2.00	
10^{-8}	2.9081e-04	7.1462e-05	1.7540e-05	4.3286e-06	1.0693e-06	2.6393e-07
	2.02	2.03	2.02	2.02	2.02	
10^{-10}	2.9888e-04	7.2378e-05	1.7863e-05	4.4137e-06	1.0983e-06	2.7311e-07
	2.05	2.02	2.02	2.01	2.01	
10^{-12}	3.0384e-04	7.3485e-05	1.7883e-05	4.4325e-06	1.1032e-06	2.7544e-07
	2.05	2.04	2.01	2.01	2.00	
e^N	3.0384e-04	7.3485e-05	1.7883e-05	4.4325e-06	1.1032e-06	2.7544e-07
r^N	2.05	2.04	2.01	2.01	2.00	

Table 7.4: Comparison of numerical results for Example 7.3 between the proposed scheme and the scheme in (Cakir & Gunes, 2022)

Scheme	N=64	N=128	N=256	N=512	N=1024
Scheme in	1.5165e-02	7.6949e-03	4.0376e-03	1.9357e-03	9.6936e-04
(Cakir & Gunes, 2022)	0.97	0.93	0.99	0.99	
Proposed scheme	3.0384e-04	7.3485e-05	1.7883e-05	4.4325e-06	1.1032e-06
	2.05	2.04	2.01	2.01	2.00

Upon a comprehensive analysis of tables 7.1, 7.2 and 7.3, it is apparent that the scheme's accuracy remains steady despite variations in the perturbation parameter ε, thus establishing its parameter uniformity. From table 7.4, it is evident that the proposed scheme outperforms the scheme discussed in source (Cakir & Gunes, 2022). The table strongly supports the claim that the approach excels in both accuracy and convergence. Moreover, it can be observed that the calculated solution aligns perfectly with the prediction in Theorem 7.1, demonstrating its second-order accuracy.

7.6 Summary

A novel approach to solving the second-order singularly perturbed Volterra-Fredholm integro-differential equation has been introduced in this chapter. The scheme utilizes the equidistribution technique to overcome difficulties associated with perturbation parameters that plague conventional numerical methods. The proposed scheme combines FDM and the trapezoidal rule for an efficient solution. Numerical experiments demonstrate the superior performance of the approach, yielding improved numerical results and achieving $\varepsilon-$uniform convergence rates. This successful application paves the way for further exploration of the equidistribution method for tackling various challenging numerical problems.

CHAPTER EIGHT

SINGULARLY PERTURBED VOLTERRA DELAY-INTEGRO-DIFFERENTIAL EQUATION WITH INITIAL LAYER

While the grid equidistribution method has served as a foundational approach in the previous chapters, it is generally not the most efficient method when dealing with problems that involve delay and is not considered here; instead, this chapter presents a simple and efficient nonstandard finite difference scheme combined with a quadrature rule for solving SPVDIDE, which works well on both uniform and Shishkin-type meshes and achieves linear convergence.

8.1 Description of the problem

The following first-order SPVDIDE is considered:

$$\begin{cases} \mathcal{L}_\varepsilon u := \varepsilon u' + a(t)u + \int\limits_{t-\tau}^{t} K(t,\xi)u(\xi)d\xi = f(t), \quad t \in \Omega = (0,T], \\ u(t) = \varphi(t), \quad t \in \Omega_0 = [-\tau, 0], \end{cases} \tag{8.1}$$

where $\tau > 0$ is a constant delay. Moreover, $0 < \varepsilon \ll 1$, $\bar{\Omega} = [0,T]$,

$$\Omega = \bigcup_{r=1}^{p} \Omega_r, \quad \Omega_r = \{t : (r-1)\tau < t \le r\tau\}, \quad 1 \le r \le p.$$

$a(t), f(t)(t \in \bar{\Omega}), \varphi(t)(t \in \Omega_0)$ and $K(t,\xi)((t,\xi) \in \bar{\Omega} \times \bar{\Omega})$ are assumed to be twice continuously differentiable functions. It is assumed that the coefficient function satisfies the condition $a(t) > \alpha > 0, \quad \text{for all } t \in \bar{\Omega}$. Under these conditions, the solution of problem (8.1) has an initial layer at $t = 0$ for small values of ε.

8.2 Properties of the exact solution

This section provides a priori estimates for the solution to the problem (8.1). These estimates reveal the asymptotic behavior of the solution and its derivative. The bounds give crucial insights into the solution's behavior across the entire domain and will be instrumental in the error analysis presented in later sections. Guided by these insights, the following results are presented:

Lemma 8.2.1 (Gronwall's Lemma). *Suppose that $f(t)$ and $g(t)$ are continuous real valued functions with $f(t), g(t) \geq 0$ on an interval [a,b]. For $c, k \geq 0$, if*

$$f(t) \leq c + k\int_a^t g(\xi)f(\xi)d\xi, \tag{8.2}$$

then

$$f(t) \leq ce^{\int_a^t kg(\xi)d\xi}. \tag{8.3}$$

Proof. Let

$$G(t) = c + k\int_a^t g(\xi)f(\xi)d\xi. \tag{8.4}$$

This implies $f(t) \leq G(t)$, $G(a) = c$ and

$$G'(t) \leq kg(t)G(t). \tag{8.5}$$

Dividing both sides of the inequality in (8.5) by $G(t)$ and integrating over (a,t) leads to

$$\int_a^t \frac{G'(\xi)}{G(\xi)}d\xi \leq \int_a^t kg(\xi)d\xi.$$

This yields

$$\ln\left(\frac{G(t)}{c}\right) \leq \int_a^t kg(\xi)d\xi.$$

Raising e to the power of both sides of the inequality and noticing that $f(t) \leq G(t)$ gives

$$\frac{f(t)}{c} \leq e^{\int_a^t kg(\xi)d\xi}. \tag{8.6}$$

It follows that

$$f(t) \leq c e^{\int_a^t k g(\xi) d\xi}.$$

This completes the proof. $\square$

Lemma 8.2.2. *Let $a, \Phi \in C[0,T]$ such that $a(t) \geq \alpha > 0$. Then, for a nonincreasing continuous function $F(t)$, with $|\Phi(t)| \leq F(t)$, the solution of the initial value problem*

$$\varepsilon \nu' + a(t)\nu = \Phi(t), \quad t \in \Omega, \tag{8.7}$$

$$\nu(0) = \mu, \tag{8.8}$$

satisfies

$$|\nu(t)| \leq |\mu| + \alpha^{-1} F(t), \quad t \in \Omega. \tag{8.9}$$

Proof. Problem (8.7)-(8.8) has the exact solution

$$\nu(t) = e^{-\frac{1}{\varepsilon}\int_0^t a(\xi)d\xi} \nu(0) + \frac{1}{\varepsilon}\int_0^t e^{-\frac{1}{\varepsilon}\int_\xi^t a(\xi)d\xi} \Phi(\xi) d\xi. \tag{8.10}$$

Taking the absolute value of both sides and applying triangle inequality

$$|\nu(t)| \leq \left| e^{-\frac{1}{\varepsilon}\int_0^t a(\xi)d\xi} \nu(0) \right| + \left| \frac{1}{\varepsilon}\int_0^t e^{-\frac{1}{\varepsilon}\int_\xi^t a(\xi)d\xi} \Phi(\xi) d\xi \right|. \tag{8.11}$$

Using integral inequality and simplifying

$$\begin{aligned}
|\nu(t)| \leq & e^{-\frac{1}{\varepsilon}\int_0^t a(\xi)d\xi} |\mu| + \frac{1}{\varepsilon}\int_0^t e^{-\frac{1}{\varepsilon}\int_\xi^t a(\xi)d\xi} |\Phi(\xi)| d\xi \\
\leq & e^{-\frac{1}{\varepsilon}\int_0^t \alpha d\xi} |\mu| + \frac{1}{\varepsilon}\int_0^t e^{-\frac{1}{\varepsilon}\int_\xi^t \alpha d\xi} |\Phi(\xi)| d\xi \\
= & e^{-\frac{\alpha}{\varepsilon}t} |\mu| + \frac{1}{\varepsilon}\int_0^t e^{-\frac{\alpha(t-\xi)}{\varepsilon}} |\Phi(\xi)| d\xi \\
\leq & e^{-\frac{\alpha}{\varepsilon}t} |\mu| + \alpha^{-1} \|\Phi\|_\infty (1 - e^{-\frac{\alpha t}{\varepsilon}}).
\end{aligned}$$

Observe that $0 \leq 1 - e^{-\frac{\alpha t}{\varepsilon}}, e^{-\frac{\alpha t}{\varepsilon}} \leq 1$, and hence

$$|\nu(t)| \leq |\mu| + \alpha^{-1} \|\Phi\|_\infty, \tag{8.12}$$

which leads to (8.9). $\square$

Lemma 8.2.3. *(Amiraliyev et al., 2019; Yapman & Amiraliyev, 2021) For* $a, f \in C^2[0,T]$, $\varphi \in C^2(\Omega_0)$ *and* $\frac{\partial^m K}{\partial t^m}, \frac{\partial^n K}{\partial s^n} \in C^2([0,T]^2)$, *m,n=0,1,2, the solution of (8.1) satisfies*

$$|u^k(t)| \leq C\left(1+\varepsilon^{-k}e^{-\frac{\alpha t}{\varepsilon}}\right), \qquad t \in \bar{\Omega},\ k=0,1, \tag{8.13}$$

$$|u''(t)| \leq \begin{cases} C\left(1+(t-\tau)^{r-1}\varepsilon^{-2}e^{-\frac{\alpha(t-(r-1)\tau)}{\varepsilon}}\right), & t \in \Omega_r,\ r=1,2, \\ C, & t \in \Omega_r,\ r \geq 3. \end{cases} \tag{8.14}$$

Proof. The proof of this lemma can be achieved using Gronwall's inequality and Lemma 8.2.2. To prove (8.13), note that

$$\left| f(t) - \int\limits_{t-\tau}^{t} K(t,\xi)u(\xi)d\xi \right| \leq ||f||_\infty + K_0 \begin{cases} \int\limits_{t-\tau}^{0} |\varphi(\xi)|d\xi + \int\limits_{0}^{t} |u(\xi)|d\xi, & \text{for } t<\tau \\ \int\limits_{t-\tau}^{t} |u(\xi)|d\xi, & \text{for } t>\tau, \end{cases}$$

where $K_0 = \max\limits_{\bar{\Omega}\times\bar{\Omega}} |K(t,\xi)|$. Let $||\varphi||_{1,0} = \int\limits_{-\tau}^{0} |\varphi(\xi)|d\xi$, then write the inequality in the form

$$\left| f(t) - \int\limits_{t-\tau}^{t} K(t,\xi)u(\xi)d\xi \right| \leq K_0||\varphi||_{1,0} + ||f||_\infty + K_0 \int\limits_{0}^{t} |u(\xi)|d\xi, \quad t>0.$$

Applying Lemma 8.2.2 to (8.1) gives

$$|u(t)| \leq |\varphi(0)| + \alpha^{-1}K_0||\varphi||_{1,0} + \alpha^{-1}||f||_\infty + \alpha^{-1}K_0 \int\limits_{0}^{t} |u(\xi)|d\xi, \quad t \in \bar{\Omega}. \tag{8.15}$$

An application of Gronwall's inequality on (8.15) yields

$$|u(t)| \leq \left(|\varphi(0)| + \alpha^{-1}K_0||\varphi||_{1,0} + \alpha^{-1}||f||_\infty\right)e^{\alpha^{-1}K_0 t},$$

which completes the proof of (8.13) for $k=0$. For $k=1$, differentiating (8.1) gives

$$\varepsilon v' + a(t)v = \Phi(t), \quad t>0, \tag{8.16}$$

with $v(t) = u'(t)$ and

$$\Phi(t) = f'(t) - a'(t)u(t) - \int\limits_{t-\tau}^{t} \frac{\partial}{\partial t}K(t,\xi)u(\xi)d\xi - K(t,t)u(t) + K(t,t-\tau)u(t-\tau).$$

It follows that

$$|\Phi(t)| \leq ||f'||_\infty + ||a'||_\infty ||u||_\infty + C\left(||\varphi||_{1,0} + ||u||_\infty\right) + K_0\left(||u||_\infty + ||\varphi||_\infty\right), \quad 0 < t < r,$$
$$|\Phi(t)| \leq ||f'||_\infty + ||a'||_\infty ||u||_\infty + C||u||_\infty + 2K_0||u||_\infty, \quad t > r,$$

together with (8.13) for $k = 0$, implies that

$$|\Phi(t)| \leq C, \quad 0 \leq t \leq T. \tag{8.17}$$

An estimate for $u'(0)$ can be derived from (8.1).

$$|u'(0)| \leq \frac{1}{\varepsilon}\left| f(0) - a(0)u(0) - \int\limits_{-\tau}^{0} K(0,\xi)u(\xi)d\xi \right| \leq \frac{1}{\varepsilon}\left(||f||_\infty + ||a||_\infty ||u||_\infty + K_0||\varphi||_{1,0}\right),$$

consequently,

$$|v(0)| \leq \frac{C}{\varepsilon}. \tag{8.18}$$

Based on the results of (8.16) and (8.18), it follows that

$$v(t) = v(0)e^{-\frac{1}{\varepsilon}\int\limits_0^t a(\xi)d\xi} + \frac{1}{\varepsilon}\int\limits_0^t \Phi(\xi)e^{-\frac{1}{\varepsilon}\int\limits_\xi^t a(\eta)d\eta}d\xi.$$

Therefore

$$|v(t)| \leq |v(0)|e^{-\frac{\alpha t}{\varepsilon}} + \frac{1}{\varepsilon}\int\limits_0^t |\Phi(\xi)|e^{-\frac{\alpha(t-\xi)}{\varepsilon}}d\xi$$

and after using (8.17) and (8.18)

$$|v(t)| \leq \frac{C}{\varepsilon}e^{-\frac{\alpha t}{\varepsilon}} + C\alpha^{-1}\left(1 - e^{-\frac{\alpha t}{\varepsilon}}\right)$$

which shows that (8.13) holds for $k = 1$. This completes the proof of (8.13). For the proof of (8.14), see Lemma 1 in (Yapman & Amiraliyev, 2021). □

8.3 Formulation of the numerical scheme

The finite difference scheme will be considered on a uniform mesh on the interval $[0, T]$.

$$\bar{\Omega}_{N_0} = \left\{ t_i = ih,\ h = \frac{\tau}{N} = \frac{T}{N_0},\ 1 \leq i \leq N_0 \right\}.$$

The mesh $\bar{\Omega}_{N_0}$ contains $N_0 = pN$ points, p submeshs $\Omega_{N,p}$ $(1 \le r \le p)$ and N points on each subinterval. The mesh can be organized as

$$\bar{\Omega}_{N_0} = \bigcup_{r=1}^{p} \Omega_{N,r},$$

where

$$\Omega_{N,r} = \{t_i, i = (r-1)N, \ldots, rN\}.$$

To obtain a difference approximation for (8.1), a NSFD is applied to approximate the derivative.

$$u_i' \approx u_{\bar{t},i} = \frac{u_{i+1} - u_i}{\phi_i}, \quad 1 \le i \le N_0, \tag{8.19}$$

where

$$\phi_i = \frac{\varepsilon}{a_i}\left(1 - e^{-\frac{a_i h}{\varepsilon}}\right).$$

The composite trapezoidal rule is applied to approximate the integral.

$$\int_{t_i-\tau}^{t_i} K(t_i,\xi)u(\xi)d\xi \approx \sum_{j=i-N+1}^{i} \frac{h}{2}\left(K_{i,j-1}u_{j-1} + K_{i,j}u_j\right), \quad 1 \le i \le N_0. \tag{8.20}$$

The resulting discrete problem becomes

$$\mathcal{L}_\varepsilon^N u_i := \varepsilon u_{\bar{t},i} + a_i u_i + \sum_{j=i-N+1}^{i} \frac{h}{2}\left(K_{i,j-1}u_{j-1} + K_{i,j}u_j\right) + \mathcal{R}_i = f_i, 1 \le i \le N_0, \tag{8.21}$$

$$u_i = \varphi_i, \quad -N \le i \le 0, \tag{8.22}$$

where

$$\mathcal{R}_i = \varepsilon\left(u_i' - u_{\bar{t},i}\right) + \int_{t_i-\tau}^{t_i} K(t_i,\xi)u(\xi)d\xi - \sum_{j=i-N+1}^{i} \frac{h}{2}\left(K_{i,j-1}u_{j-1} + K_{i,j}u_j\right). \tag{8.23}$$

From (8.21)-(8.22), the following scheme is obtained for approximating (8.1):

$$\mathcal{L}_\varepsilon^N U_i := \varepsilon U_{\bar{t},i} + a_i U_i + \sum_{j=i-N+1}^{i} \frac{h}{2}\left(K_{i,j-1}U_{j-1} + K_{i,j}U_j\right) = f_i,\ 1 \le i \le N_0, \tag{8.24}$$

$$U_i = \varphi_i, \quad -N \le i \le 0. \tag{8.25}$$

8.4 Stability and uniform convergence

In the present section, the stability and uniform convergence of the scheme are investigated. The Lemmas in this section are a slight variant of a result in (Amiraliyev & Şevgin, 2006) and the proof follows their argument closely.

Lemma 8.4.1. *Assume the difference operator*

$$\mathcal{L}_\varepsilon^N U_i = A_i U_{i+1} - B_i U_i, \qquad 1 \le i \le N_0, \tag{8.26}$$

is given with $A_i, B_i > 0$. *Then,*

i. *For the difference operator (8.26), the discrete minimum principle holds: If* $\mathcal{L}_\varepsilon^N U_i \le 0, i \ge 1$ *and* $U_0 \ge 0$, *then* $U_i \ge 0$, *for all* $i \ge 0$.

ii. *If* $|A_i - B_i| \ge \alpha > 0$, *then the solution of the difference initial value problem*

$$\mathcal{L}_\varepsilon^N U_i = F_i, \quad i \ge 1, \tag{8.27}$$

$$U_0 = \mu, \tag{8.28}$$

satisfies the estimate

$$\|U\|_\infty \le |\mu| + \alpha^{-1} \max_{1 \le i \le N_0} |F_i|. \tag{8.29}$$

iii. *If* $F_i \ge 0$ *is nonincreasing and* $|A_i - B_i| \ge \alpha > 0$, *then*

$$|U_i| \le |\mu| + \alpha^{-1} F_i. \tag{8.30}$$

Proof.

i. The proof is by contradiction. Consider a mesh function ψ. Suppose ψ takes its minimum at the index s; $0 \le s \le N_0$; $\psi_s = \min_{1 \le i \le N_0} \psi_i$ and that $\psi_s < 0$. Clearly, $s \ne 0$ and $\psi_{s+1} - \psi_s > 0$,

$$\begin{aligned}\mathcal{L}_\varepsilon^N \psi_s =& A_s \psi_{s+1} - B_s \psi_s \\ =& A_s \psi_{s+1} - A_s \psi_s + A_s \psi_s - B_s \psi_s \\ =& A_s(\psi_{s+1} - \psi_s) + (A_s - B_s)\psi_s > 0, \quad \text{provided that } A_s - B_s < 0.\end{aligned}$$

This is a contradiction and therefore $\psi_i \geq 0$ for all $i, 0 \leq i \leq N_0$.

ii. The bound on U is an immediate consequence of the minimum principle. Consider the two mesh functions

$$\psi_i^{\pm} = |\mu| + \alpha^{-1} \max_{1 \leq i \leq N_0} |F_i| \pm U_i.$$

For $i = 0$,

$$\psi_0^{\pm} = |\mu| + \alpha^{-1} \max_{1 \leq i \leq N_0} |F_i| \pm U_0 \geq 0,$$

and that for $i \geq 1$,

$$\begin{aligned}
\mathcal{L}_\varepsilon^N \psi_i^{\pm} &= A_i(|\mu| + \alpha^{-1} \max_{1 \leq i \leq N_0} |F_{i+1}| \pm U_{i+1}) - B_i(|\mu| + \alpha^{-1} \max_{1 \leq i \leq N_0} |F_i| \pm U_i) \\
&= (A_i - B_i)|\mu| + (A_i - B_i)\alpha^{-1} \max_{1 \leq i \leq N_0} |F_i| \pm (A_i U_{i+1} - B_i U_i) \\
&= (A_i - B_i)|\mu| + (A_i - B_i)\alpha^{-1} \max_{1 \leq i \leq N_0} |F_i| \pm F_i \leq 0.
\end{aligned}$$

Applying the discrete minimum principle then gives $\psi_i^{\pm} \geq 0$, and so

$$|U_i| \leq |\mu| + \alpha^{-1} \max_{1 \leq i \leq N_0} |F_i|, \tag{8.31}$$

which leads to (8.29).

iii. Similarly consider the two mesh functions

$$\psi_i^{\pm} = |\mu| + \alpha^{-1} F_i \pm U_i.$$

For $i = 0$, it follows that

$$\psi_0^{\pm} = |\mu| + \alpha^{-1} F_i \pm U_0 \geq 0,$$

and that for $i \geq 1$,

$$\begin{aligned}
\mathcal{L}_\varepsilon^N \psi_i^{\pm} &= A_i \left(|\mu| + \alpha^{-1} F_{i+1} \pm U_{i+1}\right) - B_i \left(|\mu| + \alpha^{-1} F_i \pm U_i\right) \\
&= (A_i - B_i)|\mu| + \alpha^{-1}(A_i F_{i+1} - B_i F_i) \pm (A_i U_{i+1} - B_i U_i) \\
&\leq (A_i - B_i)|\mu| + (A_i - B_i)\alpha^{-1} F_i \pm F_i \leq 0.
\end{aligned}$$

Applying the discrete minimum principle then gives $\psi_i^{\pm} \geq 0$, and so

$$|U_i| \leq |\mu| + \alpha^{-1} F_i,$$

as required.

$\square$

Lemma 8.4.2. *Under the assumption*

$$\left| a_i + \frac{K_{i,i} h}{2} \right| \geq \alpha_* > 0, \quad 1 \leq i \leq N_0, \tag{8.32}$$

the difference operator

$$\mathcal{L}_\varepsilon^N U_i = \varepsilon U_{\bar{t},i} + a_i U_i + \frac{h}{2} K_{i,i} U_i, \tag{8.33}$$

satisfies

$$\|U\|_\infty \leq |U_0| + \alpha_*^{-1} \max_{1 \leq i \leq N} |\mathcal{L}_\varepsilon^N U_i|. \tag{8.34}$$

Proof. Difference expression (8.33) can be rewritten as

$$\mathcal{L}_\varepsilon^N U_i = A_i U_{i+1} - B_i U_i,$$

with

$$A_i = \frac{\varepsilon}{\phi_i} \quad \text{and} \quad B_i = \frac{\varepsilon}{\phi_i} - a_i - \frac{h}{2} K_{i,i}.$$

It is easy to see that

$$\begin{aligned} A_i =& \frac{\varepsilon}{\phi_i} = \frac{\varepsilon}{\frac{1-e^{-\frac{a_i h}{\varepsilon}}}{\frac{a_i}{\varepsilon}}} = \frac{a_i}{1-e^{-\frac{a_i h}{\varepsilon}}} > 0, \\ B_i =& \frac{a_i}{1-e^{-\frac{a_i h}{\varepsilon}}} - \left(a_i + \frac{h}{2} K_{i,i} \right) > 0, \text{ for } a_i + \frac{h}{2} K_{i,i} < 0, \\ & A_i - B_i = a_i + \frac{h}{2} K_{i,i} < 0. \end{aligned}$$

The result follows immediately Lemma (8.4.1). $\square$

In what follows stability of the difference problem (8.24)-(8.25) are considered.

Lemma 8.4.3. *The solution of the difference problem (8.24)-(8.25) satisfies the estimate*

$$\|U\|_{\infty,\bar{\Omega}_{N_0}} \leq \left(|\varphi_0| + \alpha_*^{-1}(\|f\|_\infty + K_0\|\varphi\|_{1,0})\right) e^{\alpha_*^{-1}K_0 t_i}, \quad 1 \leq i \leq N_0. \tag{8.35}$$

Proof. From (8.24) it follows that

$$\begin{aligned}
\mathcal{L}_\varepsilon^N U_i =& f_i - \sum_{j=i-N+1}^{i-1} \frac{h}{2}(K_{i,j-1}U_{j-1} + K_{i,j}U_j) - \frac{h}{2}K_{i,i-1}U_{i-1} \\
\leq& |f_i| + \left| \sum_{j=i-N+1}^{i-1} \frac{h}{2}(K_{i,j-1}U_{j-1} + K_{i,j}U_j) \right| + \left| \frac{h}{2}K_{i,i-1}U_{i-1} \right| \\
\leq& \|f\|_\infty + K_0 \sum_{j=i-N+1}^{i} h|U_{j-1}| \\
\leq& \|f\|_\infty + K_0 \begin{cases} \sum\limits_{j=-N+1}^{0} h|\varphi_j|, & i=1, \\ \sum\limits_{j=i-N+1}^{0} h|\varphi_j| + \sum\limits_{j=1}^{i-1} h|U_j|, & 1 < i \leq N-1, \\ \sum\limits_{j=i-N+1}^{i-1} h|U_j|, & i > N-1, \end{cases} \\
\leq& \|f\|_\infty + K_0\|\varphi\|_{1,0} + K_0 \sum_{j=1}^{i} h|U_{j-1}|,
\end{aligned}$$

under the condition (8.32), using Lemma 8.4.1 to (8.24)-(8.25) gives

$$|U_i| \leq |\varphi_0| + \alpha_*^{-1}(\|f\|_\infty + K_0\|\varphi\|_{1,0}) + \alpha_*^{-1}K_0 \sum_{j=1}^{i} h|U_{j-1}|. \tag{8.36}$$

Applying the difference analogue of Gronwall's inequality gives

$$|U_i| \leq \left(|\varphi_0| + \alpha_*^{-1}(\|f\|_\infty + K_0\|\varphi\|_{1,0})\right) e^{\alpha_*^{-1}K_0 t_i},$$

which leads to (8.35). □

It is now convenient to estimate the error associated with the discretization process. Let $e_i = u_i - U_i$. From (8.21)-(8.22) and (8.24)-(8.25), for the error of the approximate solution e_i,

$$\mathcal{L}_\varepsilon^N e_i = \mathcal{R}_i, \quad 1 \leq i \leq N_0, \tag{8.37}$$

$$e_i = 0, \qquad -N \leq i \leq 0. \tag{8.38}$$

Lemma 8.4.4. *The error of the approximate solution e_i satisfies*

$$\|e\|_{\infty,\bar{\Omega}} \leq \alpha_*^{-1} e^{\alpha_*^{-1} K_0 T} \|\mathcal{R}\|_{\infty,\bar{\Omega}}.$$

Proof. It follows immediately from (8.35) by taking $\varphi = 0$ and $f = \mathcal{R}$. $\square$

Lemma 8.4.5. *Let the assumptions of Lemma 8.2.3 be fulfilled. Then, for the truncation error $\mathcal{R}_i$, the following estimate holds*

$$\|\mathcal{R}\|_{\infty,\bar{\Omega}} \leq Ch. \tag{8.39}$$

Proof. From (8.23), it follows that

$$\mathcal{R}_i = \varepsilon\left(u_i' - u_{\bar{t},i}\right) + \left(\int\limits_{t_i-\tau}^{t_i} K(t_i,\xi)u(\xi)d\xi - \sum_{j=i-N+1}^{i} \frac{h}{2}\left(K_{i,j-1}u_{j-1} + K_{i,j}u_j\right)\right).$$

Applying the Taylor series on the terms of $u_{\bar{t},i}$ and considering the error in the composite trapezoidal rule,

$$\begin{aligned}
\mathcal{R}_i =& \varepsilon\left(u_i' - \left(\frac{1}{h} + \frac{a_i}{2\varepsilon} + \cdots\right)\left(hu_i' + \frac{h^2}{2}u_i'' + \cdots\right)\right) \\
&- \sum_{j=i-N+1}^{i} \frac{h^3}{12}\left(\frac{\partial^2 K}{\partial s^2}(t_i,t_{j-1})u_{j-1} + 2\frac{\partial K}{\partial s}(t_i,t_{j-1})u_{j-1}' + K_{i,j-1}u_{j-1}''\right) + \cdots \\
=& -\left(\frac{\varepsilon}{2}u'' + \frac{a_i}{2}u'\right)h - \frac{a_i}{4}u_i''h^2 - \cdots \\
&- \sum_{j=i-N+1}^{i} \frac{h^3}{12}\left(\frac{\partial^2 K}{\partial s^2}(t_i,t_{j-1})u_{j-1} + 2\frac{\partial K}{\partial s}(t_i,t_{j-1})u_{j-1}' + K_{i,j-1}u_{j-1}''\right) + \cdots
\end{aligned}$$

Then, using the result in Lemma 8.2.3 and observing that the exponential terms tend to zero when $\varepsilon \to 0$ (For proof, see (Patidar, 2005)),

$$\begin{aligned}
|\mathcal{R}_i| \leq& Ch + Ch^2 + \cdots + C\sum_{j=i-N+1}^{i} h^3 + \cdots \\
=& Ch + Ch^2 + \cdots + C\tau h^2 + \cdots
\end{aligned}$$

In turn, this leads to (8.39). $\square$

Finally, using Lemma 8.4.4 and 8.4.5, the following main result is obtained:

Theorem 8.1. *Let u be the solution of (8.1) and U be its approximation by the scheme (8.24)-(8.25). The solution of (8.24)-(8.25) converges to the solution of (8.1) and* *satisfies the following $\varepsilon-$uniform error estimate*

$$\|u-U\|_{\infty,\bar{\Omega}} \leq Ch.$$

Results obtained so far can be extended to Shishkin-type meshes. In the following section, the scheme (8.24)-(8.25) will be implemented on the Shishkin-type mesh.

8.5 The proposed scheme on a Shishkin-type mesh

In this section, the Shishkin-type mesh from (Amiraliyev & Yapman, 2019) is considered. Let N be an even positive integer. The mesh $\bar{\Omega}_{N_0}$ is defined as a union of p sub-meshes $\Omega_{N,r}$ $(1 \leq r \leq p)$,

$$\Omega_{N,r} = \begin{cases} t_i = ih_i,\ 1 \leq i \leq \frac{N}{2}; \quad t_i = \sigma + \left(i - \frac{N}{2}\right) h_i,\ \frac{N}{2}+1 \leq i \leq \frac{3N}{2},\ r=1, \\ t_i = (r-1)\tau + \left(i-(r-\frac{1}{2})N\right) h_i, rN - \frac{N}{2}+1 \leq i \leq rN + \frac{N}{2}, r \geq 2, \end{cases}$$

where $\sigma = \alpha^{-1}\varepsilon \ln N$ is the transition point and

$$h_i = \begin{cases} (2\alpha^{-1}\varepsilon \ln N)N^{-1}, & 1 \leq i \leq \frac{N}{2}, \\ (\tau - \alpha^{-1}\varepsilon \ln N)N^{-1}, & \frac{N}{2} \leq i \leq \frac{3N}{2}, \\ \tau N^{-1}, & i \geq \frac{3N}{2} \end{cases}$$

is the piecewise-uniform mesh spacing. The mesh $\bar{\Omega}_{N_0}$ contains $N_0 = (m+\frac{1}{2})N$ points, $\frac{3N}{2}$ on $\Omega_{N,1}$ and N points on each submesh. Applying this Shishkin type mesh in (8.24)-(8.25), the scheme becomes

$$\mathcal{L}_\varepsilon^N U_i := \varepsilon U_{\bar{t},i} + a_i U_i + \sum_{j=i-\bar{N}+1}^{i} \frac{h_j}{2}\left(K_{i,j-1}U_{j-1} + K_{i,j}U_j\right) = f_i,\ 1 \leq i \leq N_0, \tag{8.40}$$

$$U_i = \varphi_i, \quad -\frac{3N}{2} \leq i \leq 0, \tag{8.41}$$

where

$$\bar{N} = \begin{cases} \frac{3N}{2}, 1 \leq i \leq \frac{3N}{2}, \\ N,\ \frac{3N}{2} < i \leq N_0. \end{cases}$$

Lemma 8.5.1. *Let the assumptions of Lemma 8.2.3 be satisfied. Then, the truncation* *error $\mathcal{R}_i$ of the difference scheme (8.40)-(8.41) satisfy the estimate*

$$\|\mathcal{R}_i\|_{\infty,\bar{\Omega}} \le CN^{-1}. \tag{8.42}$$

Proof. In the approximation by the scheme (8.40)-(8.41), the truncation error is

$$\mathcal{R}_i = \varepsilon\left(u_i' - u_{\bar{t},i}\right) + \left(\int_{t_i-\tau}^{t_i} K(t_i,\xi)u(\xi)d\xi - \sum_{j=i-\bar{N}+1}^{i} \frac{h_j}{2}\left(K_{i,j-1}u_{j-1} + K_{i,j}u_j\right)\right).$$

Applying the Taylor series on the terms of $u_{\bar{t},i}$ and taking the error in composite trapezoidal rule approximation, gives

$$\begin{aligned}
\mathcal{R}_i =& \varepsilon\left(u_i' - \left(\frac{1}{h_i} + \frac{a_i}{2\varepsilon} + \cdots\right)\left(h_i u_i' + \frac{h_i^2}{2}u_i'' + \cdots\right)\right) \\
& - \sum_{j=i-\bar{N}+1}^{i} \frac{h_j^3}{12}\left(\frac{\partial^2 K}{\partial s^2}(t_i,t_{j-1})u_{j-1} + 2\frac{\partial K}{\partial s}(t_i,t_{j-1})u_{j-1}' + K_{i,j-1}u_{j-1}''\right) + \cdots \\
=& -\left(\frac{\varepsilon}{2}u'' + \frac{a_i}{2}u'\right)h_i - \frac{a_i}{4}u_i'' h_i^2 - \cdots \\
& - \sum_{j=i-\bar{N}+1}^{i} \frac{h_j^3}{12}\left(\frac{\partial^2 K}{\partial s^2}(t_i,t_{j-1})u_{j-1} + 2\frac{\partial K}{\partial s}(t_i,t_{j-1})u_{j-1}' + K_{i,j-1}u_{j-1}''\right) + \cdots
\end{aligned}$$

By the same argument in the proof of Lemma 8.4.5, it follows that

$$|\mathcal{R}_i| \le Ch_i + Ch_i^2 + \cdots + C\sum_{j=i-\bar{N}+1}^{i} h_j^3 + \cdots$$

Taking $\max_{1\le i\le N_0} h_i = \tau N^{-1}$ then gives

$$|\mathcal{R}_i| \le CN^{-1} + CN^{-2} + \cdots + CN^{-2} + \cdots$$

which leads to (8.42). □

Now combining Lemma 8.4.4 and 8.5.1, the following theorem holds.

Theorem 8.2. *Let u be the solution of (8.1) and U be its approximation by the scheme (8.40)-(8.41). The solution of (8.40)-(8.41) converges to the solution of (8.1) and satisfies the following $\varepsilon-$uniform error estimate*

$$\|u - U\|_{\infty,\bar{\Omega}} \le CN^{-1}.$$

8.6 Numerical results and discussion

This section presents two numerical examples to confirm the theoretical analysis. The accuracy and efficiency of the proposed scheme are also compared with those already available in the literature for solving SPVDIDEs.

Example 8.1. *Consider the Volterra delay-integro-differential equation,*

$$\varepsilon u' + 2u - \int_{t-1}^{t} u(\xi)d\xi = -1 + t - \frac{\varepsilon}{2}(1 - e^{-\frac{2t}{\varepsilon}}), \quad t \in (0,2],$$
$$u(t) = 1, \quad -1 \leq t \leq 0.$$

The exact solution is given by

$$u(t) = \begin{cases} e^{-\frac{2t}{\varepsilon}}, & 0 \leq t \leq 1, \\ \dfrac{e^{(\frac{1-\sqrt{1+\varepsilon}}{\varepsilon})(t-1)} - e^{(\frac{1+\sqrt{1+\varepsilon}}{\varepsilon})(t-1)}}{\sqrt{1+\varepsilon}} - 1 + e^{-\frac{2t}{\varepsilon}} + e^{-\frac{2(t-1)}{\varepsilon}}, & 1 \leq t \leq 2. \end{cases}$$

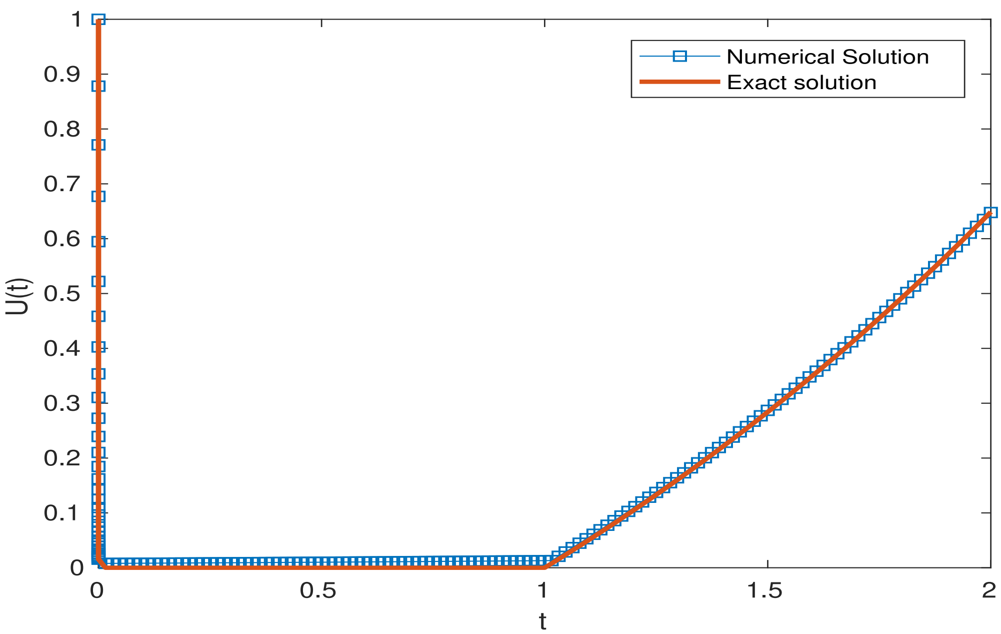

Figure 8.1: Comparison between the exact and numerical solution for $\varepsilon = 2^{-24}$, $N = 64$.

Table 8.1: Max error and rates of convergence of the proposed scheme for various values of ε and N for Example 8.1.

ε	N=32	N=64	N=128	N=256	N=512	N=1024
2^0	2.1873E-03	1.1006E-03	5.5203E-04	2.7645E-04	1.3833E-04	6.9192E-05
	0.99	1.00	1.00	1.00	1.00	
2^{-6}	1.1578E-02	4.9760E-03	2.2042E-03	1.0240E-03	4.9193E-04	2.4090E-04
	1.22	1.17	1.11	1.06	1.03	
2^{-12}	1.3856E-02	7.1315E-03	3.6185E-03	1.8227E-03	9.1328E-04	4.4119E-04
	0.96	0.98	0.99	1.00	1.05	
2^{-18}	1.3857E-02	7.1317E-03	3.6186E-03	1.8227E-03	9.1475E-04	4.5822E-04
	0.96	0.98	0.99	0.99	1.00	
2^{-24}	1.3857E-02	7.1317E-03	3.6186E-03	1.8227E-03	9.1475E-04	4.5822E-04
	0.96	0.98	0.99	0.99	1.00	
e^N	1.3857E-02	7.1317E-03	3.6186E-03	1.8227E-03	9.1475E-04	4.5822E-04
r^N	0.96	0.98	0.99	0.99	1.00	

Table 8.2: Max error and rates of convergence of the proposed scheme on the Shishkin type mesh for various values of ε and N for Example 8.1.

ε	N=32	N=64	N=128	N=256	N=512	N=1024
2^0	4.7014E-03	2.4094E-03	1.2196E-03	6.1354E-04	3.0771E-04	1.5409E-04
	0.96	0.98	0.99	1.00	1.00	
2^{-6}	1.5951E-02	6.7698E-03	2.9081E-03	1.3180E-03	6.2373E-04	3.0294E-04
	1.24	1.22	1.14	1.08	1.04	
2^{-12}	1.8293E-02	9.3985E-03	4.7639E-03	2.3983E-03	1.2029E-03	5.9183E-04
	0.96	0.98	0.99	1.00	1.00	
2^{-18}	1.8295E-02	9.3996E-03	4.7645E-03	2.3986E-03	1.2034E-03	6.0274E-04
	0.96	0.98	0.99	1.00	1.00	
2^{-24}	1.8295E-02	9.3997E-03	4.7645E-03	2.3986E-03	1.2034E-03	6.0274E-04
	0.96	0.98	0.99	1.00	1.00	
e^N	1.8295E-02	9.3997E-03	4.7645E-03	2.3986E-03	1.2034E-03	6.0274E-04
r^N	0.96	0.98	0.99	1.00	1.00	

Example 8.2. *Consider the Volterra delay-integro-differential equation,*

$$\varepsilon u' + u + \int_{t-1}^{t} s u(\xi) d\xi = 5t^2 - 1, \quad t \in (0,2],$$
$$u(t) = 5 + t, \quad -1 \le t \le 0.$$

The double mesh principle is employed to calculate the maximum pointwise error and rate of convergence since the exact solution is not readily available for this problem.

Table 8.3: Max error and rates of convergence of the proposed scheme for various values of ε and N of Example 8.2.

ε	N=32	N=64	N=128	N=256	N=512	N=1024
2^0	3.4787E-02	1.7207E-02	8.5568E-03	4.2667E-03	2.1304E-03	1.0645E-03
	1.02	1.01	1.00	1.00	1.00	
2^{-6}	4.5959E-02	1.9750E-02	9.0285E-03	4.3002E-03	2.0966E-03	1.0349E-03
	1.22	1.13	1.07	1.04	1.02	
2^{-12}	6.5916E-02	3.2512E-02	1.6143E-02	8.0304E-03	3.8577E-03	1.6689E-03
	1.02	1.01	1.01	1.06	1.21	
2^{-18}	6.5916E-02	3.2512E-02	1.6143E-02	8.0437E-03	4.0149E-03	2.0057E-03
	1.02	1.01	1.01	1.00	1.00	
2^{-24}	6.5916E-02	3.2512E-02	1.6143E-02	8.0437E-03	4.0149E-03	2.0057E-03
	1.02	1.01	1.01	1.00	1.00	
e^N	6.5916E-02	3.2512E-02	1.6143E-02	8.0437E-03	4.0149E-03	2.0057E-03
r^N	1.02	1.01	1.01	1.00	1.00	

Table 8.4: Max error and rates of convergence of the proposed scheme on the Shishkin type mesh for various values of ε and N of Example 8.2.

ε	N=32	N=64	N=128	N=256	N=512	N=1024
2^0	4.1090E-02	2.0252E-02	1.0053E-02	5.0079E-03	2.4994E-03	1.2485E-03
	1.02	1.01	1.01	1.00	1.01	
2^{-6}	6.3526E-02	2.6750E-02	1.1982E-02	5.6505E-03	2.7536E-03	1.3675E-03
	1.25	1.16	1.08	1.04	1.01	
2^{-12}	8.2876E-02	4.0738E-02	2.0197E-02	1.0060E-02	4.9342E-03	2.2122E-03
	1.02	1.01	1.01	1.03	1.16	
2^{-18}	8.2947E-02	4.0779E-02	2.0214E-02	1.0063E-02	5.0207E-03	2.5076E-03
	1.02	1.01	1.01	1.00	1.00	
2^{-24}	8.2948E-02	4.0780E-02	2.0214E-02	1.0063E-02	5.0208E-03	2.5077E-03
	1.02	1.01	1.01	1.00	1.00	
e^N	8.2948E-02	4.0780E-02	2.0214E-02	1.0063E-02	5.0208E-03	2.5077E-03
r^N	1.02	1.01	1.01	1.00	1.00	

From Tables 8.1 and 8.2, and Tables 8.3 and 8.4, it can be observed that the results on the uniform mesh are slightly accurate than those obtained on the Shishkin-type mesh. It can also be noted that the numerical results of the proposed scheme approximations are more accurate than those obtained in (Amiraliyev & Yapman, 2019), as shown in table 8.5. Moreover, the results show that the convergence rate of the difference scheme is essentially in agreement with the theoretical analysis.

Table 8.5: Comparison of numerical results for Example 8.2 at $\varepsilon = 2^{-24}$.

Scheme		N=64	N=128	N=256	N=512
Scheme in	e^N	6.6203E-02	3.7500E-02	2.0096E-02	1.0621E-02
(Amiraliyev & Yapman, 2019)	r^N	0.82	0.90	0.92	0.97
Proposed	e^N	3.2512E-02	1.6143E-02	8.0437E-03	4.0149E-03
Scheme	r^N	1.01	1.01	1.00	1.00

8.7 Summary

In this chapter, a nonstandard finite difference scheme in combination with a composite trapezoidal rule is considered for solving linear first-order singularly perturbed Volterra delay-integro-differential equation. The scheme was implemented on a uniform and Shishkin-type meshes. The stability and convergence analysis of the proposed scheme was studied. Numerical experiments are performed and results are presented to validate the theoretical error estimates. In experiments, it is observed that despite their simple structure and ease of analysis, Shishkin-type meshes give numerical results that are inferior to those obtained on uniform meshes. It is also shown that the scheme exhibits uniform convergence independent of the perturbation parameter in the discrete maximum norm, and it is first-order uniformly accurate.

CONCLUSIONS AND RECOMMENDATIONS

This section provides a summary of the important results related to the initial research objectives and discusses their significance and contribution. In addition, it highlights the limitations of the study and provides recommendations for further research.

Conclusions

This study aimed to formulate numerical schemes for a class of singularly perturbed integro-differential equations. Five distinct problems were examined, each belonging to one of three categories of integro-differential equations. The first three problems are singularly perturbed Fredholm integro-differential equations which fall in the first category. The fourth problem belonged to the second category, characterized by singularly perturbed Volterra-Fredholm integro-differential equations. The fifth problem belonged to the third category, which encompasses singularly perturbed Volterra delay integro-differential equations.

The five problems that were chosen had different challenges. Out of the five problems under consideration, a duo of them signify solely singularly perturbed problems, while another two problems are not only singularly perturbed but also possess a discontinuous source term. Additionally, one of the problems encompasses a singular perturbation accompanied by a delay. By studying these cases in detail, the goal was to develop schemes to handle all the different complexities in equations with singularly perturbed integro-differential equations.

In this dissertation, the principal technique employed for devising the numerical scheme is a fusion of a finite difference method and a composite trapezoidal rule, both operating on an adaptive mesh generated through the equidistribution principle. The literature review has revealed a conspicuous dearth of $\varepsilon-$uniform numerical methods for certain problems. Furthermore, the existing numerical schemes used for the remaining problems suffer from inadequate precision. By bridging this research gap, $\varepsilon-$uniform numerical schemes have been devised for problems that previously lacked such approaches, while for problems where only low-accuracy schemes existed, a more precise solution has been furnished.

When developing an efficient numerical scheme, accuracy and computational cost are the key factors taken into consideration. Within this dissertation, the focus is solely on evaluating the efficiency of the numerical scheme through its accuracy, which is evident in its ability to yield low error and demonstrate a high convergence rate. The computational cost is not investigated in this study, which is a weakness of the study.

Recommendations

Drawing upon the study's insights and acknowledging its limitations, the following key areas are proposed for future exploration:

- The use of Algorithm 2 (presented in Chapter 5) is highly recommended for allocating mesh points in problems with discontinuous source terms, particularly those involving singular perturbations. This algorithm is efficient and effective, ensuring an optimal point distribution near both the boundary and interior layers, resulting in high accuracy. Researchers working on similar problems are strongly encouraged to explore and adopt Algorithm 2.

- In this dissertation, the sole metric employed to evaluate the efficiency of a numerical scheme is its numerical accuracy. This singular focus, while valuable, hinders holistic comprehension of its effectiveness. Consequently, future research focusing on the computational cost of the scheme is strongly recommended to provide a more comprehensive assessment.

Building on this study, future research directions include delving deeper into singularly perturbed integro-differential equations with fractional and partial derivatives.

REFERENCES

Amiraliyev, G. M., & Cakir, M. (2000). A uniformly convergent difference scheme for a singularly perturbed problem with convective term and zeroth order reduced equation. *International Journal of Applied Mathematics*, *2*(12), 1407–1420.

Amiraliyev, G. M., Durmaz, M. E., & Kudu, M. (2018). Uniform convergence results for singularly perturbed fredholm integro-differential equation. *J. Math. Anal*, *9*(6), 55–64.

Amiraliyev, G. M., Durmaz, M. E., & Kudu, M. (2021). A numerical method for a second order singularly perturbed fredholm integro-differential equation. *Miskolc Mathematical Notes*. doi: doi:10.18514/MMN.2021.2930

Amiraliyev, G. M., & Şevgin, S. (2006). Uniform difference method for singularly perturbed volterra integro-differential equations. *Applied Mathematics and Computation*, *179*(2), 731–741. doi: doi:10.1016/j.amc.2005.11.155

Amiraliyev, G. M., & Yapman, Ö. (2019). On the volterra delay-integro-differential equation with layer behavior and its numerical solution. *Miskolc Mathematical Notes*. Retrieved from https://api.semanticscholar.org/CorpusID:201255760

Amiraliyev, G. M., Yapman, Ö., & Mustafa, K. (2019). A fitted approximate method for a volterra delay-integro-differential equation with initial layer. *Hacettepe Journal of Mathematics and Statistics*, *48*(5), 1417–1429. doi: doi:10.15672/HJMS.2018.582

Andreev, V. B. (2004). On the theory of difference schemes for singularly perturbed equations. *Differential Equations*, *40*, 959–970. doi: doi:10.1023/B:DIEQ.0000047027.16299.38

Angell, J., & Olmstead, W. E. (1985). Singular perturbation analysis of an integrodifferential equation modelling filament stretching. *Zeitschrift für angewandte*

Mathematik und Physik ZAMP, *36*(3), 487–490.

Badeye, S. R., Woldaregay, M. M., & Dinka, T. G. (2023). Solving singularly perturbed fredholm integro-differential equation using exact finite difference method. *BMC Research Notes*, *16*(1), 233. doi: doi:10.1186/s13104-023-06488-8

Beckett, G., & Mackenzie, J. (2000). Convergence analysis of finite difference approximations on equidistributed grids to a singularly perturbed boundary value problem. *Applied Numerical Mathematics*, *35*(2), 87–109. doi: doi:https://doi.org/10.1016/S0168-9274(99)00065-3

Beckett, G., & Mackenzie, J. (2001). On a uniformly accurate finite difference approximation of a singularly perturbed reaction–diffusion problem using grid equidistribution. *Journal of computational and applied mathematics*, *131*(1-2), 381–405. doi: doi:10.1016/S0377-0427(00)00260-0

Bocharov, G. A., & Rihan, F. A. (2000). Numerical modelling in biosciences using delay differential equations. *Journal of Computational and Applied Mathematics*, *125*(1-2), 183–199. doi: doi:10.1016/s0377-0427(00)00468-4

Brunner, H., & Zhang, W. (1999). Primary discontinuities in solutions for delay integro-differential equations. *Methods and Applications of Analysis*, *6*(4), 525–534.

Burton, T. A. (2005). *Volterra integral and differential equations* (Vol. 202). Elsevier.

Cakir, M., & Gunes, B. (2022). A fitted operator finite difference approximation for singularly perturbed volterra–fredholm integro-differential equations. *Mathematics*, *10*(19), 3560. doi: doi:10.3390/math10193560

Cakir, M., & Güneş, B. (2022). A new difference method for the singularly perturbed volterra-fredholm integro-differential equations on a shishkin mesh. *Hacettepe Journal of Mathematics and Statistics*, *51*(3), 787–799. doi: doi:10.15672/hujms.950075

Chadha, N. M., & Kopteva, N. (2011). A robust grid equidistribution method for a one-dimensional singularly perturbed semilinear reaction-diffusion problem. *IMA journal of numerical analysis*, *31*(1), 188–211. doi: doi:10.1093/imanum/drp033

De Boor, C. (2006). Good approximation by splines with variable knots. ii. In *Conference on the numerical solution of differential equations: Dundee 1973* (pp.

12–20). doi: doi:10.1007/BFb0069121

Durmaz, M. E. (2023). A numerical approach for singularly perturbed reaction diffusion type volterra-fredholm integro-differential equations. *Journal of Applied Mathematics and Computing*, *69*(5), 3601–3624. doi: doi:10.1007/s12190-023-01895-3

Durmaz, M. E., & Amiraliyev, G. M. (2021). A robust numerical method for a singularly perturbed fredholm integro-differential equation. *Mediterranean Journal of Mathematics*, *18*(1), 24. doi: doi:10.1007/s00009-020-01693-2

Durmaz, M. E., Yapman, Ö., Mustafa, K., & Amirali, G. (2023). An efficient numerical method for a singularly perturbed volterra-fredholm integro-differential equation. *Hacettepe Journal of Mathematics and Statistics*, *52*(2), 326–339. doi: doi:10.15672/hujms.1050505

Farrell, P., Miller, J., & Shishkin, G. (2000). Singularly perturbed differential equations with discontinuous source terms. *Analytical and numerical methods for convection-dominated and singularly perturbed problems*, 23–32.

Gaetano, A. D., & Arino, O. (2000). Mathematical modelling of the intravenous glucose tolerance test. *Journal of mathematical biology*, *40*(2), 136–168. doi: doi:10.1007/s002850050007

Hamoud, A., Mohammed, N., & Ghadle, K. (2020). Existence and uniqueness results for volterra-fredholm integro differential equations. *Advances in the Theory of Nonlinear Analysis and its Application*, *4*(4), 361–372.

Horvat, V., & Rogina, M. (2002). Tension spline collocation methods for singularly perturbed volterra integro-differential and volterra integral equations. *Journal of Computational and Applied Mathematics*, *140*(1-2), 381–402. doi: doi:10.1016/s0377-0427(01)00517-9

Huang, W., & Russell, R. D. (2010). *Adaptive moving mesh methods* (Vol. 174). Springer Science & Business Media.

Hunter, J. K. (2004). Asymptotic analysis and singular perturbation theory. *Department of Mathematics, University of California at Davis*, 1–3.

Jackiewicz, Z., Rahman, M., & Welfert, B. (2006). Numerical solution of a fredholm integro-differential equation modelling neural networks. *Applied Numerical*

Mathematics, *56*(3-4), 423–432. doi: doi:10.1016/j.apnum.2005.04.020

Jackiewicz, Z., Rahman, M., & Welfert, B. D. (2008). Numerical solution of a fredholm integro-differential equation modelling θ-neural networks. *Applied Mathematics and Computation*, *195*(2), 523–536. doi: doi:10.1016/j.amc.2007.05.031

Kadalbajoo, M. K., & Gupta, V. (2010). A brief survey on numerical methods for solving singularly perturbed problems. *Applied mathematics and computation*, *217*(8), 3641–3716. doi: doi:10.1016/j.amc.2010.09.059

Kadalbajoo, M. K., & Patidar, K. C. (2002). A survey of numerical techniques for solving singularly perturbed ordinary differential equations. *Applied Mathematics and Computation*, *130*(2-3), 457–510. doi: doi:10.1016/S0096-3003(01)00112-6

Kadalbajoo, M. K., & Reddy, Y. (1989). Asymptotic and numerical analysis of singular perturbation problems: a survey. *Applied Mathematics and computation*, *30*(3), 223–259. doi: doi:10.1016/0096-3003(89)90054-4

Kauthen, J.-P. (1997). A survey of singularly perturbed volterra equations. *Applied numerical mathematics*, *24*(2-3), 95–114. doi: doi:10.1016/S0168-9274(97)00014-7

Kopteva, N. (2001). Maximum norm a posteriori error estimates for a one-dimensional convection-diffusion problem. *SIAM Journal on numerical analysis*, *39*(2), 423–441. doi: doi:10.1137/S0036142900368642

Kopteva, N. (2007). Maximum norm a posteriori error estimates for a 1d singularly perturbed semilinear reaction–diffusion problem. *IMA journal of numerical analysis*, *27*(3), 576–592. doi: doi:10.1093/imanum/drl020

Kopteva, N., Madden, N., & Stynes, M. (2005). Grid equidistribution for reaction-diffusion problems in one dimension. *Numerical Algorithms*, *40*, 305–322. doi: doi:10.1007/s11075-005-7079-6

Kopteva, N., & O'Riordan, E. (2010). Shishkin meshes in the numerical solution of singularly perturbed differential equations. *Int. J. Numer. Anal. Model*, *7*(3), 393–415. doi: doi:hdl.handle.net/10344/5612

Kopteva, N., & Stynes, M. (2001). A robust adaptive method for a quasi-linear one-dimensional convection-diffusion problem. *SIAM Journal on Numerical Analysis*, *39*(4), 1446–1467. doi: doi:10.1137/S003614290138471X

Lakshmikantham, V. (1995). *Theory of integro-differential equations* (Vol. 1). CRC press.

Linß, T. (2001). Uniform pointwise convergence of finite difference schemes using grid equidistribution. *Computing*, *66*(1), 27–39. doi: doi:10.1007/s006070170037

Liseikin, V. D. (2010). Dynamic adaptation. *Grid Generation Methods*, 195–226. doi: doi:10.1007/978-90-481-2912-6_7

Manning, P. M., & Margrave, G. F. (2006). Introduction to non-standard finite-difference modelling. *CREWES Research Report*(18).

Marino, S., Beretta, E., & Kirschner, D. E. (2007). The role of delays in innate and adaptive immunity to intracellular bacterial infection. *Mathematical Biosciences & Engineering*, *4*(2), 261. doi: doi:10.3934/mbe.2007.4.261

Mbroh, N. A., Noutchie, S. C. O., & Massoukou, R. Y. M. (2020). A second order finite difference scheme for singularly perturbed volterra integro-differential equation. *Alexandria Engineering Journal*, *59*(4), 2441–2447. doi: doi:10.1016/j.aej.2020.03.007

Mickens, R. E. (2002). Nonstandard finite difference schemes for differential equations. *Journal of Difference Equations and Applications*, *8*(9), 823–847. doi: doi:10.1080/1023619021000000807

Miller, J. J. H., O'riordan, E., & Shishkin, G. I. (1996). *Fitted numerical methods for singular perturbation problems: error estimates in the maximum norm for linear problems in one and two dimensions.* World scientific.

Miller, J. J. H., O'Riordan, E., & Shishkin, G. I. (2012). *Fitted numerical methods for singular perturbation problems.* World Scientific Publishing Company.

O'Malley, R. E. (2012). *Singular perturbation methods for ordinary differential equations* (Vol. 89). Springer Science & Business Media.

Parand, K., & Rad, J. (2011). An approximation algorithm for the solution of the singularly perturbed volterra integro-differential and volterra integral equations. *Int. J. of Nonlinear Science*, *12*(4), 430–441.

Patidar, K. C. (2005). High order fitted operator numerical method for self-adjoint singular perturbation problems. *Applied mathematics and computation*, *171*(1), 547–566. doi: doi:10.1016/j.amc.2005.01.069

Pereyra, V., & Sewell, E. (1974). Mesh selection for discrete solution of boundary problems in ordinary differential equations. *Numerische Mathematik*, *23*, 261–268. doi: doi:10.1007/BF01400309

Ramos, J. I. (2007). Piecewise-quasilinearization techniques for singularly perturbed volterra integro-differential equations. *Applied mathematics and computation*, *188*(2), 1221–1233. doi: doi:10.1016/j.amc.2006.10.076

Ramos, J. I. (2008). Exponential techniques and implicit runge kutta methods for singularly perturbed volterra integro differential equations. *Neural, Parallel and Scientific Computations*, *16*(3), 387.

Rathore, A. S., Shanthi, V., & Ramos, H. (2023). A fitted numerical method for a singularly perturbed fredholm integro-differential equation with discontinuous source term. *Applied Numerical Mathematics*, *185*, 88–100. doi: doi:10.1016/j.apnum.2022.11.019

Rihan, F. A. (2021). *Delay differential equations and applications to biology.* Springer.

Roos, H.-G., Stynes, M., & Tobiska, L. (2008). *Robust numerical methods for singularly perturbed differential equations, volume 24 of springer series in computational mathematics.* Springer-Verlag, Berlin,.

Russell, R., & Christiansen, J. (1978). Adaptive mesh selection strategies for solving boundary value problems. *SIAM Journal on Numerical Analysis*, *15*(1), 59–80. doi: doi:10.1137/0715004

Salama, A., & Bakr, S. (2007). Difference schemes of exponential type for singularly perturbed volterra integro-differential problems. *Applied Mathematical Modelling*, *31*(5), 866–879. doi: doi:10.1016/j.apm.2006.02.007

Salama, A., & Evans, D. (2001). Fourth order scheme of exponential type for singularly perturbed volterra integro-differential equations. *International Journal of Computer Mathematics*, *77*(1), 153–164. doi: doi:10.1080/00207160108805058

Samarskii, A. A. (2001). *The theory of difference schemes* (Vol. 240). CRC Press.

Şevgin, S. (2014). Numerical solution of a singularly perturbed volterra integro-differential equation. *Advances in Difference Equations*, *2014*(1), 1–15. doi: doi:10.1186/1687-1847-2014-171

Shishkin, G. I., & Shishkina, L. P. (2008). *Difference methods for singular perturbation* *problems*. Chapman and Hall/CRC.

Tao, X., & Zhang, Y. (2019). The coupled method for singularly perturbed volterra integro-differential equations. *Advances in Difference Equations*, *2019*(1). doi: doi:10.1186/s13662-019-2139-8

Tikhonov, A., & Samarskii, A. (1963). Homogeneous difference schemes on non-uniform nets. *USSR Computational Mathematics and Mathematical Physics*, *2*(5), 927-953. doi: doi:10.1016/0041-5553(63)90505-6

Vasil'Eva, A. B., Butuzov, V. F., & Kalachev, L. V. (1995). *The boundary function method for singular perturbation problems*. SIAM.

Wazwaz, A.-M. (2011). *Linear and nonlinear integral equations* (Vol. 639). Springer. doi: doi:10.1007/978-3-642-21449-3

White, A. B., Jr. (1979). On selection of equidistributing meshes for two-point boundary-value problems. *SIAM Journal on Numerical Analysis*, *16*(3), 472–502. doi: doi:10.1137/0716038

Wu, S., & Gan, S. (2009). Errors of linear multistep methods for singularly perturbed volterra delay-integro-differential equations. *Mathematics and Computers in Simulation*, *79*(10), 3148–3159. doi: doi:10.1016/j.matcom.2009.03.006

Yapman, Ö., & Amiraliyev, G. M. (2021). Convergence analysis of the homogeneous second order difference method for a singularly perturbed volterra delay-integro-differential equation. *Chaos, Solitons & Fractals*, *150*, 111100. doi: doi:10.1016/j.chaos.2021.111100

Ömer Yapman, & Amiraliyev, G. M. (2019). A novel second-order fitted computational method for a singularly perturbed volterra integro-differential equation. *International Journal of Computer Mathematics*, *97*(6), 1293–1302. doi: doi:10.1080/00207160.2019.1614565

APPENDIX A
LIST OF PUBLICATIONS

The contributions of this dissertation have been disseminated through publication or submission to esteemed international peer-reviewed journals, which are listed as follows:

Published papers

1. Manebo, W., Woldaregay, M., Dinka, T. & Duressa, G. An equidistributed grid-based second-order scheme for a singularly perturbed Fredholm integro-differential equation with an interior layer. Applied Mathematics And Computation. 464 pp. 128398 (2024), https://doi:10.1016/j.amc.2023.128398.

2. Manebo, W., Woldaregay, M., Dinka, T. & Duressa, G. A computational approach to solving a second-order singularly perturbed Fredholm integro-differential equation with discontinuous source term. Numerical Algorithms. pp. 1-16 (2024) https://doi.org/10.1007/s11075-024-01756-5

Submitted papers

1. Manebo, W., Woldaregay, M., Dinka, T. & Duressa, G. Grid equidistribution for numerical solutions to a class of singularly perturbed integro-differential equations. International Journal of Computer Mathematics.

2. Manebo, W., Woldaregay, M., Dinka, T. & Duressa, G. An efficient numerical scheme for solving second-order singularly perturbed Volterra-Fredholm integro-differential equations. Intl. Journal of Applied and Computational Mathematics.

3. Manebo, W., Duressa, G., Woldaregay, M.,& Dinka, T. Investigating a non-standard finite difference scheme for singularly perturbed Volterra delay-integro-differential equations. Research in mathematics.